HDL-TR-2168

April 1990

The Normal Mode E- and H-Field Distribution in the Concentric Spherical Cavity

by Louis F. Libelo and Guy E. Pisane

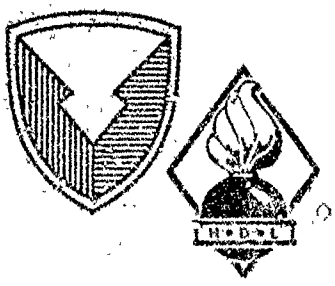

U.S. Army Laboratory Command
Harry Diamond Laboratories
Adelphi, MD 20783-1197

The findings in this report are not to be construed as an official Department of the Army position unless so designated by other authorized documents.

Citation of manufacturers' or trade names does not constitute an official endorsement or approval of the use thereof.

Destroy this report when it is no longer needed. Do not return it to the originator.

UNCLASSIFIED

SECURITY CLASSIFICATION OF THIS PAGE

REPORT DOCUMENTATION PAGE

Form Approved OMB No. 0704-0188

1a. REPORT SECURITY CLASSIFICATION Unclassified	1b. RESTRICTIVE MARKINGS
2a. SECURITY CLASSIFICATION AUTHORITY	3. DISTRIBUTION/AVAILABILITY OF REPORT Approved for public release; distribution unlimited.
2b. DECLASSIFICATION/DOWNGRADING SCHEDULE	
4. PERFORMING ORGANIZATION REPORT NUMBER(S) HDL-TR-2168	5. MONITORING ORGANIZATION REPORT NUMBER(S)
6a. NAME OF PERFORMING ORGANIZATION Harry Diamond Laboratories 6b. OFFICE SYMBOL (if applicable) SLCHD-NW-TN	7a. NAME OF MONITORING ORGANIZATION
6c. ADDRESS (City, State, and ZIP Code) 2800 Powder Mill Road Adelphi, MD 20783-1197	7b. ADDRESS (City, State, and ZIP Code)
8a. NAME OF FUNDING/SPONSORING ORGANIZATION U.S. Army Laboratory Command 8b. OFFICE SYMBOL (if applicable) AMSLC	9. PROCUREMENT INSTRUMENT IDENTIFICATION NUMBER
8c. ADDRESS (City, State, and ZIP Code) 2800 Powder Mill Road Adelphi, MD 20783-1145	10. SOURCE OF FUNDING NUMBERS PROGRAM ELEMENT NO. 6.37.37A; PROJECT NO. 9790400; TASK NO.; WORK UNIT ACCESSION NO.
11. TITLE (Include Security Classification) The Normal Mode E- and H-Field Distribution in the Concentric Spherical Cavity	
12. PERSONAL AUTHOR(S) Louis F. Libelo and Guy E. Pisane	
13a. TYPE OF REPORT Final 13b. TIME COVERED FROM Dec 87 TO Dec 88	14. DATE OF REPORT (Year, Month, Day) April 1990 15. PAGE COUNT 116
16. SUPPLEMENTARY NOTATION AMS code: 623737.0000, HDL project: FE79B9	
17. COSATI CODES FIELD / GROUP / SUB-GROUP	18. SUBJECT TERMS (Continue on reverse if necessary and identify by block number) Concentric spherical cavity, eigenfields

19. ABSTRACT (Continue on reverse if necessary and identify by block number)

The eigenfields of the concentric spherical cavity are investigated in this report. This simple cavity structure serves as a foundation toward understanding a number of important practical problems. The fields are developed mathematically, and extensive computer-generated graphs are presented. A thorough exposition accompanies the graphs explaining how the fields vary with the cavity parameters in a systematic fashion, and how they relate to the corresponding eigenvalue mode charts.

20. DISTRIBUTION/AVAILABILITY OF ABSTRACT ☒ UNCLASSIFIED/UNLIMITED ☐ SAME AS RPT. ☐ DTIC USERS	21. ABSTRACT SECURITY CLASSIFICATION Unclassified
22a. NAME OF RESPONSIBLE INDIVIDUAL Louis F. Libelo	22b. TELEPHONE (Include Area Code) (202) 394-4144 22c. OFFICE SYMBOL SLCHD-NW-TN

DD Form 1473, JUN 86 *Previous editions are obsolete.* SECURITY CLASSIFICATION OF THIS PAGE

UNCLASSIFIED

Contents

Contents (cont'd)

Page

Figures

Figures (cont'd)

Figures (cont'd)

Figures (cont'd)

Figures (cont'd)

Figures (cont'd)

Figures (cont'd)

Figures (cont'd)

Page

Figures (cont'd)

Figures (cont'd)

Figures (cont'd)

Figures (cont'd)

Figures (cont'd)

Figures (cont'd)

Figures (cont'd)

1. Introduction

In a previous report[1] we presented the theoretical development for the eigenvalue problem of the concentric spherical cavity, homogeneously filled with dielectric. This report — the companion publication — contains the corresponding electric and magnetic field distributions within that cavity. Again we should like to emphasize that this report is merely another in a sequence of publications that is forthcoming; each report elaborates on some physical characteristics of loaded spherical cavities that are of practical significance.

Section 2 of this report contains a brief presentation of the geometry involved and the necessary formal treatment for understanding the analytic results. Section 3 consists of the transverse electric (TE) normal mode cavity field distributions. In section 4 the field distributions for the transverse magnetic (TM) cavity modes are presented. Finally, in section 5, the preceding field results are summarized and discussed. Before proceeding it should be pointed out that in this report only a pure lossless dielectric medium will be considered within the cavity.

2. Cavity Geometry and Formal Field Expressions

2.1 Cavity Geometry

We shall repeat in figure 1 the illustration of the previous, related report[1] that displays the intrinsic geometry for the concentric spherical cavity filled with a homogeneous dielectric. The outer radius is "a" and the inner radius is "b." The fields will be displayed below for the region contained between the two conducting spheres.

2.2 The Eigenfields

We showed in the earlier publication[1] that the cavity eigenfields could be derived from two Debye potentials. The TE potentials are obtained from potential functions of the form

$$\Phi^{(e)}_{nmp}\left(\vec{r}\right) \equiv \phi_{np}\left(\gamma^{(1)}_{np} r\right) P_{nm}(\cos\Theta)\cos m\phi \qquad (1a)$$

[1] *L. Libelo and M. Campi, The Concentric Spherical Cavity TE and TM Eigenvalues, Harry Diamond Laboratories, HDL-TR-2034 (July 1984).*

Figure 1. Geometry of the concentric spherical cavity.

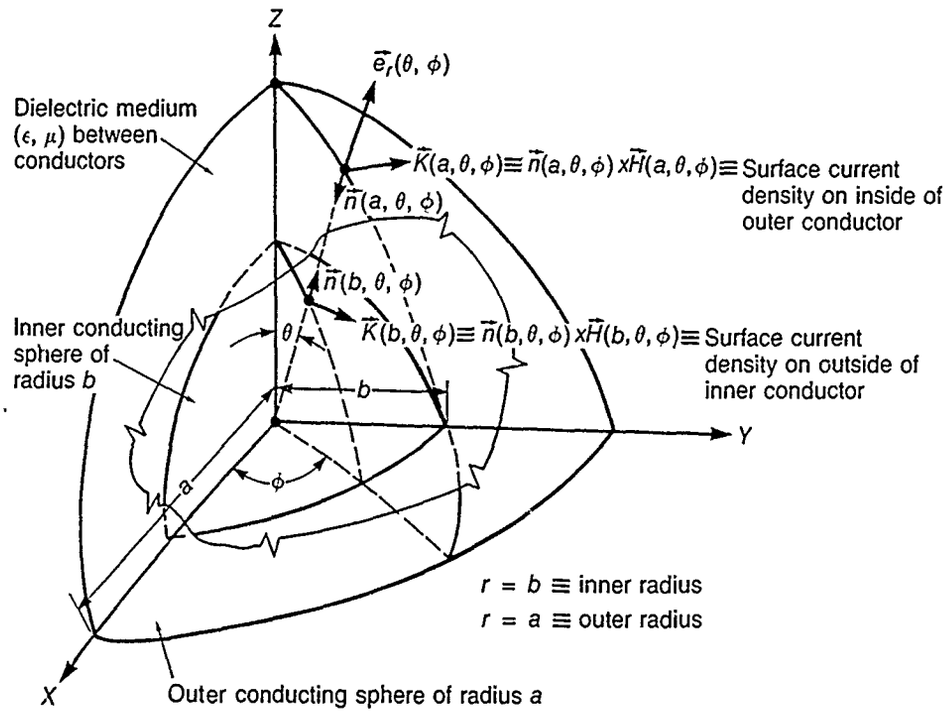

and

$$\Phi^{(o)}_{nmp}\left(\vec{r}\right) \equiv \phi_{np}\left(\gamma^{(1)}_{np} r\right) P_{nm}(\cos\Theta) \sin m\phi \qquad (1b)$$

and the TM eigenfields from the potentials

$$\Psi^{(e)}_{nmp}\left(\vec{r}\right) \equiv \psi_{np}\left(\gamma^{(2)}_{np} r\right) P_{nm}(\cos\Theta) \cos m\phi \qquad (2a)$$

and

$$\Psi^{(o)}_{nmp}\left(\vec{r}\right) \equiv \psi_{np}\left(\gamma^{(2)}_{np} r\right) P_{nm}(\cos\Theta) \sin m\phi \ , \qquad (2b)$$

where the values $\gamma^{(1)}_{np} a$ and $\gamma^{(2)}_{np} a$ are, respectively, the TE and TM eigenvalues, and where a is the radius of the outer conductor, as mentioned earlier. More explicitly, the radially dependent factors are

$$\Phi_{np}\left(\gamma^{(1)}_{np} r\right) = i_n\left(\gamma^{(1)}_{np} r\right) k_n\left(\gamma^{(1)}_{np} b\right) - i_n\left(\gamma^{(1)}_{np} b\right) k_n\left(\gamma^{(1)}_{np} r\right) \equiv \Lambda^{(1)}_{np}(r,b) \qquad (3)$$

and

$$\psi_{np}\left(\gamma_{np}^{(2)} r\right) = i_n\left(\gamma_{np}^{(2)} r\right)\left[\gamma_{np}^{(2)} b\, k_n\left(\gamma_{np}^{(2)} b\right)\right]' - k_n\left(\gamma_{np}^{(2)} r\right)\left[\gamma_{np}^{(2)} b\, i_n\left(\gamma_{np}^{(2)} b\right)\right]' \equiv \Upsilon_{np}^{(2)}(r,b) \quad , \tag{4}$$

where b is the radius of the inner conducting sphere, $i_n(\,)$ and $k_n(\,)$ are the modified spherical Bessel functions, and $[xf(x)]'$ denotes differentiation with respect to the argument x. We have also introduced Λ_{np} and Υ_{np} as notation for later convenience.

The field components are derived directly from the Debye potentials of equations (1) and (2). Thus the eigenfield components are, for the TE modes,

$$E_{r;nmp}^{(1;\substack{e\\o})}\left(\vec{r}\right) = 0 \tag{5a}$$

$$E_{\theta;nmp}^{(1;\substack{e\\o})}\left(\vec{r}\right) = -\frac{1}{r\sin\theta}\frac{\partial}{\partial\phi}\left[r\,\phi_{nmp}^{\binom{e}{o}}\left(\vec{r}\right)\right] , \tag{5b}$$

$$E_{\phi;nmp}^{(1;\substack{e\\o})}\left(\vec{r}\right) = \frac{1}{r}\frac{\partial}{\partial\theta}\left[r\,\phi_{nmp}^{\binom{e}{o}}\left(\vec{r}\right)\right] , \tag{5c}$$

$$H_{r;nmp}^{(1;\substack{e\\o})}\left(\vec{r}\right) = \frac{1}{j\omega\mu}\left(\frac{\partial^2}{\partial r^2} - \left[\gamma_{np}^{(1)}\right]^2\right)\left[r\,\phi_{nm\phi}^{\binom{e}{o}}\left(\vec{r}\right)\right] = \frac{n(n+1)}{j\omega\mu}\,\phi_{nmp}^{\binom{e}{o}}\left(\vec{r}\right) , \tag{5d}$$

$$H_{\theta;nmp}^{(1;\substack{e\\o})}\left(\vec{r}\right) = \frac{1}{j\omega\mu}\frac{1}{r}\frac{\partial^2}{\partial r\partial\theta}\left[r\,\phi_{nmp}^{\binom{e}{o}}\left(\vec{r}\right)\right] , \tag{5e}$$

and

$$H_{\phi;nmp}^{(1;\substack{e\\o})}\left(\vec{r}\right) = \frac{1}{j\omega\mu}\frac{1}{r\sin\theta}\frac{\partial^2}{\partial r\partial\phi}\left[r\,\phi_{nmp}^{\binom{e}{o}}\left(\vec{r}\right)\right] . \tag{5f}$$

For the TM modes, the eigenfield components are

$$E^{(2;\substack{e\\o})}_{r;nmp}(\vec{r}) = \frac{1}{j\omega\varepsilon}\left(\frac{\partial^2}{\partial r^2} - \left[\gamma^{(2)}_{np}\right]^2\right)\left[r\,\psi^{(\substack{e\\o})}_{nmp}(\vec{r})\right] = \frac{n(n+1)}{j\omega\varepsilon}\,\frac{1}{r}\,\psi^{(\substack{e\\o})}_{nmp}(\vec{r})\ , \tag{6a}$$

$$E^{(2;\substack{e\\o})}_{\theta;nmp}(\vec{r}) = \frac{1}{j\omega\varepsilon}\,\frac{1}{r}\,\frac{\partial^2}{\partial r\partial\theta}\left[r\,\psi^{(\substack{e\\o})}_{nmp}(\vec{r})\right]\ , \tag{6b}$$

$$E^{(2;\substack{e\\o})}_{\phi;nmp}(\vec{r}) = \frac{1}{j\omega\varepsilon}\,\frac{1}{r\sin\theta}\,\frac{\partial^2}{\partial r\partial\phi}\left[r\,\psi^{(\substack{e\\o})}_{nmp}(\vec{r})\right]\ , \tag{6c}$$

$$H^{2;\substack{e\\o}}_{r;nmp}(\vec{r}) = 0\ , \tag{6d}$$

$$H^{(2;\substack{e\\o})}_{\theta;nmp}(\vec{r}) = \frac{1}{r\sin\theta}\,\frac{\partial}{\partial\phi}\left[r\psi^{(\substack{e\\o})}_{nmp}(\vec{r})\right]\ ,\ \text{and} \tag{6e}$$

$$H^{(2;\substack{e\\o})}_{\phi;nmp}(\vec{r}) = -\frac{1}{r}\,\frac{\partial}{\partial\theta}\left[r\,\psi^{(\substack{e\\o})}_{nmp}(\vec{r})\right]\ . \tag{6f}$$

Here we define j to be the square root of -1, and recall that the eigenvalues $\gamma^{(1)}_{np}a$ and $\gamma^{(2)}_{np}a$ are purely imaginary when the cavity is filled with lossless material.

The components in equations (5) and (6) can be written as products of an angular function depending on θ and ϕ, and a function depending solely on the radius variable, r. Thus we write the components in the more convenient factored form. For the TE case:

$$E^{(1;\substack{e\\o})}_{r;nmp}(\vec{r}) = 0\ , \tag{7a}$$

$$E^{(1;\epsilon_o)}_{\theta;nmp}(\vec{r}) = E^{(1;\epsilon_o)}_{\theta;nm}(\theta,\phi)\,E^{(1)}_{\theta;np}(r) \quad , \tag{7b}$$

$$E^{(1;\epsilon_o)}_{\phi;nmp}(\vec{r}) = E^{(1;\epsilon_o)}_{\phi;nm}(\theta,\phi)\,E^{(1)}_{\phi;np}(r) \quad , \tag{7c}$$

$$H^{(1;\epsilon_o)}_{r;nmp}(\vec{r}) = H^{(1;\epsilon_o)}_{r;nm}(\theta,\phi)\,H^{(1)}_{r;np}(r) \quad , \tag{7d}$$

$$H^{(1;\epsilon_o)}_{\theta;nmp}(\vec{r}) = H^{(1;\epsilon_o)}_{\theta;nm}(\theta,\phi)\,H^{(1)}_{\theta;np}(r) \quad , \text{ and} \tag{7e}$$

$$H^{(1;\epsilon_o)}_{\phi;nmp}(\vec{r}) = H^{(1;\epsilon_o)}_{\phi;nm}(\theta,\phi)\,H^{(1)}_{\phi;np}(r) \quad . \tag{7f}$$

And for the TM case:

$$E^{(2;\epsilon_o)}_{r;nmp}(\vec{r}) = E^{(2;\epsilon_o)}_{r;nm}(\theta,\phi)\,E^{(2)}_{r;np}(r) \quad , \tag{8a}$$

$$E^{(2;\epsilon_o)}_{\theta;nmp}(\vec{r}) = E^{(2;\epsilon_o)}_{\theta;nm}(\theta,\phi)\,E^{(2)}_{\theta;np}(r) \quad , \tag{8b}$$

$$E^{(2;\epsilon_o)}_{\phi;nmp}(\vec{r}) = E^{(2;\epsilon_o)}_{\phi;nmp}(\theta,\phi)\,E^{(2)}_{\theta;np}(r) \quad , \tag{8c}$$

$$H^{(2;\epsilon_o)}_{r;nmp}(\vec{r}) = 0 \quad , \tag{8d}$$

$$H^{(2;\epsilon_o)}_{\theta;nmp}(\vec{r}) = H^{(2;\epsilon_o)}_{\theta;nm}(\theta,\phi)\,H^{(2)}_{\theta;np}(r) \quad , \text{ and} \tag{8e}$$

$$H^{(2;\epsilon_o)}_{\phi;nmp}(\vec{r}) = H^{(2;\epsilon_o)}_{\phi;nm}(\theta,\phi)\,H^{(2)}_{\phi;np}(r) \quad . \tag{8f}$$

If we examine the factors in (7) and (8) that depend only on the radius, r, we find further helpful simplifications. We obtain for the TE modes,

$$E^{(1)}_{\theta;np}(r) = E^{(1)}_{\phi;np}(r) = \Lambda^{(1)}_{np}(r,b) \quad , \tag{9}$$

$$H^{(1)}_{r;np}(r) = \frac{\Lambda^{(1)}_{np}(r,b)}{\gamma^{(1)}_{np}\,r} \quad , \text{ and} \tag{10}$$

$$H^{(1)}_{\theta;np}(r) = H^{(1)}_{\phi;np}(r) = -\frac{1}{\gamma^{(1)}_{np} r}\,\frac{d}{d\left[\gamma^{(1)}_{np} r\right]}\left[\gamma^{(1)}_{np} r\,\Lambda^{(1)}_{np}(r,b)\right] = \frac{\Upsilon^{(1)}_{np}(r,b)}{\gamma^{(1)}_{np} r} \quad . \tag{11}$$

And for the TM modes,

$$E^{(2)}_{r;np}(r) = \frac{\Upsilon^{(2)}_{np}(r,b)}{\gamma^{(2)}_{np} r} \quad , \tag{12}$$

$$E^{(2)}_{\theta;np}(r) = E^{(2)}_{\phi;np}(r) = \frac{\mathrm{T}^{(2)}_{np}(r;b)}{\gamma^{(2)}_{np} r} \quad , \text{ and} \tag{13}$$

$$H^{(2)}_{\theta;np}(r) = H^{(2)}_{\phi;np}(r) = \Upsilon^{(2)}_{np}(r;b) \quad , \tag{14}$$

where for convenience we have introduced the notation

$$T^{(i)}_{n}(x,y) \equiv \left[\gamma^{(i)}_{np} x\, i_n\left(\gamma^{(i)}_{np} x\right)\right]'\left[\gamma^{(i)}_{np} y\, k_n\left(\gamma^{(i)}_{np} y\right)\right]' - \left[\gamma^{(i)}_{np} y\, i_n\left(\gamma^{(i)}_{np} y\right)\right]'\left[\gamma^{(i)}_{np} x\, k_n\left(\gamma_{np} x\right)\right]' \quad . \tag{15}$$

Examination of equations (9), (10), and (11) clearly reveals that there are only three distinct radial functions required to specify the radial dependence of the TE mode field components. These are the "transverse electric field" functions which we shall denote by $E^{(1)}_{t;np}(r)$, where

$$E^{(1)}_{t;np}(r) \equiv E^{(1)}_{\theta;np}(r) = E^{(1)}_{\phi;np}(r) = \Lambda^{(1)}_{np}(r,b) \quad , \tag{16}$$

the "transverse magnetic field" radial function, $H^{(1)}_{t;np}(r)$, where

$$H^{(1)}_{t;np}(r) \equiv H^{(1)}_{\theta;np}(r) = H^{(1)}_{\phi;np}(r) = \Upsilon^{(1)}_{np}(b,r)/\gamma^{(1)}_{np} r \quad , \tag{17}$$

and finally the "longitudinal magnetic field" radial function, $H^{(1)}_{l;np}(r)$, where

$$H^{(1)}_{l;np}(r) \equiv H^{(1)}_{r;np}(r) = \Lambda^{(1)}_{np}(r,b)/\gamma^{(1)}_{np} r \quad . \tag{18}$$

Note further that the longitudinal magnetic field radial function is easily obtained from the transverse electric field radial function.

Similarly, ror the TM mode field components, only three distinct radial functions are required. The first is the transverse magnetic field radial function, denoted by $H^{(2)}_{t;np}(r)$, where

$$H^{(2)}_{t;np}(r) \equiv H^{(2)}_{\theta;np}(r) = H^{(2)}_{\phi;np}(r) = \Upsilon^{(2)}_{np}(r,b) \quad . \tag{19}$$

The second is the transverse electric field radial function, denoted by $E^{(2)}_{t;np}(r)$, where

$$E^{(2)}_{t;np}(r) \equiv E^{(2)}_{\theta;np}(r) = E^{(2)}_{\phi;np}(r) = T^{(2)}_{np}(r,b)/\gamma^{(2)}_{np} r \quad . \tag{20}$$

And the third is the longitudinal electric field radial function, denoted by $E^{(2)}_{l;np}(r)$, where

$$E^{(2)}_{l;np}(r) \equiv E^{(2)}_{r;np}(r) = \Upsilon^{(2)}_{n}(r,b)/\gamma^{(2)}_{np} r \quad . \tag{21}$$

Again we observe that one of the components, namely the longitudinal electric field radial function, can be obtained readily from another TM component, namely, via the transverse magnetic field radial function. Equations (16) through (21) contain the expressions for the field components that we will determine explicitly in the following paragraphs of this report. The θ and ϕ dependences that accompany the dependence on r are the well-known conventional behaviors and do not require any further elaboration.

2.3 Normalization

We introduced the transverse electric field radial function via equation (16). Since the eigenvalues calculated in the earlier publication[1] were those values of γa that satisfied

$$i_n(\gamma a)\, k_n(\gamma b) - k_n(\gamma a)\, i_n(\gamma b) = 0$$

[1] *L. Libelo and M. Campi, The Concentric Spherical Cavity TE and TM Eigenvalues, Harry Diamond Laboratories, HDL-TR-2034 (July 1984).*

for fixed b, it is more convenient to write

$$\Lambda_{np}^{(1)}(r,b) \equiv i_n\left[\gamma_{np}^{(1)} a\left(\frac{r}{a}\right)\right] k_n\left[\gamma_{np}^{(1)} a\left(\frac{b}{a}\right)\right] - i_n\left[\gamma_{np}^{(1)} a\left(\frac{b}{a}\right)\right] k_n\left[\gamma_{np}^{(1)} a\left(\frac{r}{a}\right)\right] . \tag{22}$$

We also write

$$\begin{aligned}\Upsilon_{np}^{(1)}(b,r) \equiv i_n\left[\gamma_{np}^{(1)} a\left(\frac{b}{a}\right)\right]\left\{\gamma_{np}^{(1)} a\left(\frac{r}{a}\right) k_n\left[\gamma_{np}^{(1)} a\left(\frac{r}{a}\right)\right]\right\}' \\ - k_n\left[\gamma_{np}^{(1)} a\left(\frac{b}{a}\right)\right]\left\{\gamma_{np}^{(1)}\left(\frac{r}{a}\right) i_n\left[\gamma_{np}^{(1)} a\left(\frac{r}{a}\right)\right]\right\}'\end{aligned} \tag{23}$$

which by equation (18) is the function we will need to calculate to obtain the transverse magnetic field radial function. The variable is now r/a, i.e., r scaled by the radius of the outer spherical conductor.

In order to more efficiently display the radial function for the field components we change variables from the normalized radial quantity, r/a, to the variable "d," which we will define as the radial distance from the inner conducting sphere. We will further require d to be normalized to unity at the outer conducting sphere. The relation between the variables d and r is thus

$$d \equiv \frac{\left(\frac{r}{a} - \frac{b}{a}\right)}{\left(1 - \frac{b}{a}\right)} \quad , \text{ where } 0 < d < 1 \ . \tag{24}$$

Clearly, $d = 0$ corresponds to the inner conductor and $d = 1$ corresponds to the outer.

Furthermore, somewhere in the range $0 < d < 1$ (or equivalently, $b < r < a$), the magnitude of each field component radial function will take on its maximum value. We choose to scale each field component by its maximum absolute value. In this manner we have normalized each field component radial function to range between the amplitudes of +1 and −1. We

then have, for the TE eigenfields for a fixed ratio $R = b/a$, the normalized transverse electric field radial function,

$$\frac{E^{(1)}_{t;np}(R;d)}{\left|E^{(1)}_{t;np}(R,d)\right|_{max}} = \frac{\Lambda^{(1)}_{np}(r,b)}{\left|\Lambda^{(1)}_{np}(r,b)\right|_{max}} , \tag{25}$$

the normalized transverse magnetic field radial function,

$$\frac{H^{(1)}_{t;np}(R;d)}{\left|H^{(1)}_{t;np}(R;d)\right|_{max}} = \frac{\dfrac{\Upsilon^{(1)}_{np}(b,r)}{\gamma^{(1)}_{np}\, a\left(\dfrac{r}{a}\right)}}{\left|\dfrac{\Upsilon^{(1)}_{np}(b,r)}{\gamma^{(1)}_{np}\, a\left(\dfrac{r}{a}\right)}\right|_{max}} . \tag{26}$$

and the normalized longitudinal magnetic field radial function,

$$\frac{H^{(1)}_{l;np}(R;d)}{\left|H^{(1)}_{l;np}(R;d)\right|_{max}} = \frac{\dfrac{\Lambda^{(1)}_{np}(r,b)}{\gamma^{(1)}_{np}\, a\left(\dfrac{r}{a}\right)}}{\left|\dfrac{\Lambda^{(1)}_{np}(r,b)}{\gamma^{(1)}_{np}\, a\left(\dfrac{r}{a}\right)}\right|_{max}} . \tag{27}$$

The TM eigenfields have been similarly normalized.

In what follows, computer plots are shown for the TE field component radial functions, equations (16) to (18), as normalized in equations (25) to (27), and the TM expressions, equations (19) to (21), similarly normalized, as functions of the normalized distance from the inner conducting sphere. For each eigenmode the dependence of these eigenfield component distributions on the size of the inner conductor is shown. The variable $R = b/a$ is the quantity representing the size of the inner sphere.

The field plots are in three-dimensional form, with the field strength plotted on the vertical axis against both $R = b/a$ and the normalized distance from the inner sphere, d. These surfaces have been embellished by

asterisk markers at the maximum value for each *b/a* plotted. Also, a coordinate box has been added as a background to better understand the surface in relation to its coordinate axes.

We recall that each eigenvalue is a function of R, i.e.,

$$\gamma_{np}^{(1)} a \equiv \left[\gamma_{np}^{(1)}(R)\right] a \ .$$

These eigenvalues also form a doubly infinite set, indicated by the subscripts n and p. The subscript n denotes the order of the eigenvalue, i.e., the order of the Bessel equation from which the resonance equation was derived. The subscript p connotes family, indicating groupings into which modes with similar behavior patterns fall. The concept of families of modes was quite evident in the previous report[1] on the eigenvalues, where the various trajectories as functions of *b/a* were shown to be so grouped. These groupings are seen to extend into the behavior of the actual electromagnetic field distributions.

Because the eigenvalues can increase *ad infinitum*, we have chosen to limit those fields plotted to have eigenvalues less than 20. However, it is possible to plot the fields of the higher modes using the same techniques described in this document.

[1] *L. Libelo and M. Campi, The Concentric Spherical Cavity TE and TM Eigenvalues, Harry Diamond Laboratories, HDL-TR-2034 (July 1984)*

3. Radial Distribution for TE Field Components

3.1 Transverse Electric Field Component for TEnp Modes

3.1.1 The p = 1 E-Transverse TEnp Eigenfields for n = 1 to 5

Perhaps the easiest field component of this investigation to understand is the E-transverse for the TE11 mode. This component must vanish on the two conducting walls ($d = 0$ and $d = 1$), and reaches a single maximum in between. The surface therefore resembles a tunnel, as shown in figure 2. Examining this surface reveals that the maximum value occurs at slightly different values of d for each b/a computed. As n is increased from 1, the same basic pattern exists, except for changes in the position of the maxima. When b/a is large, these changes are minute. However, when b/a is small, there is a significant shift of the maximum values to larger values of d, so that the "tunnel" becomes somewhat altered for small b/a. See figures 3 to 6.

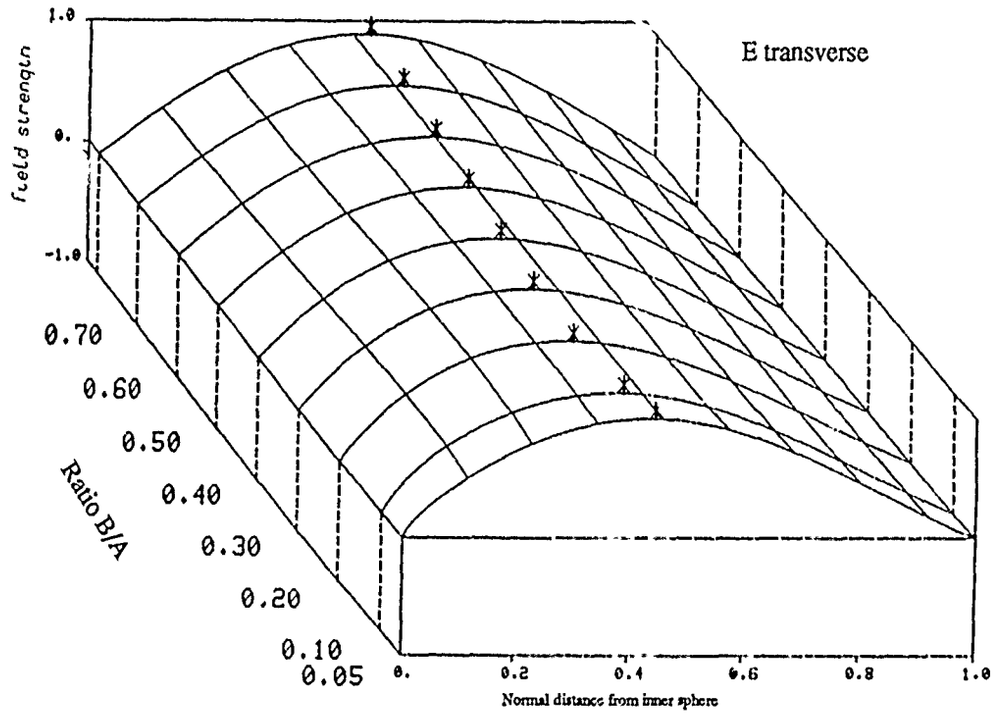

Figure 2. Distribution of the normalized transverse electric field component in the concentric spherical cavity as a function of the inner to outer conductor radii, $R = b/a$, for the TE11 mode. Asterisk indicates peak value of field with d.

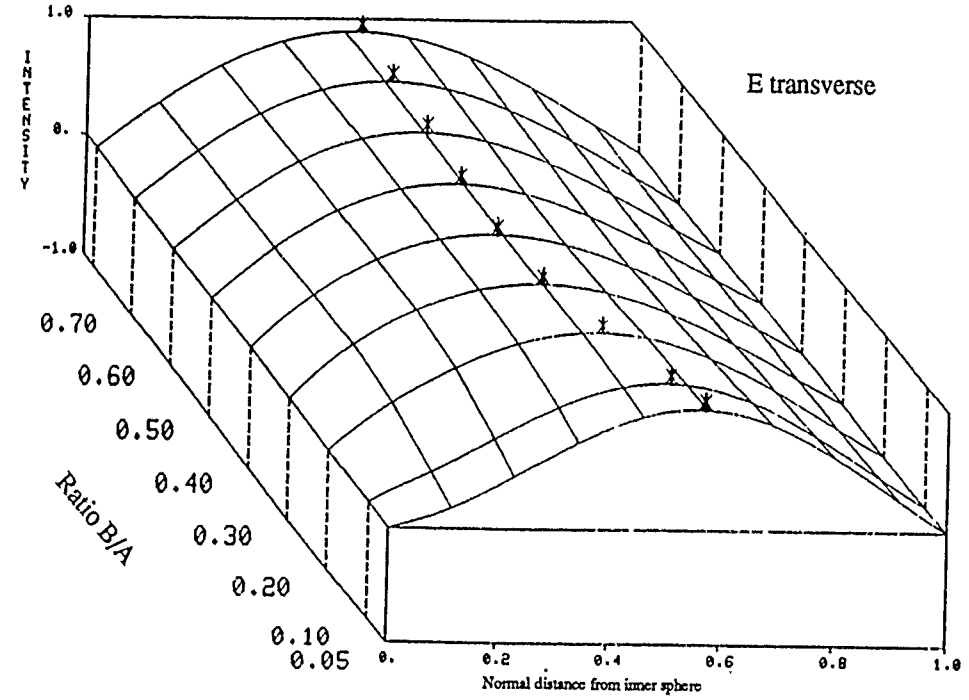

Figure 3. Distribution of the normalized transverse electric field component in the concentric spherical cavity as a function of the inner to outer conductor radii, $R = b/a$, for the TE21 mode. Asterisk indicates peak value of field with d.

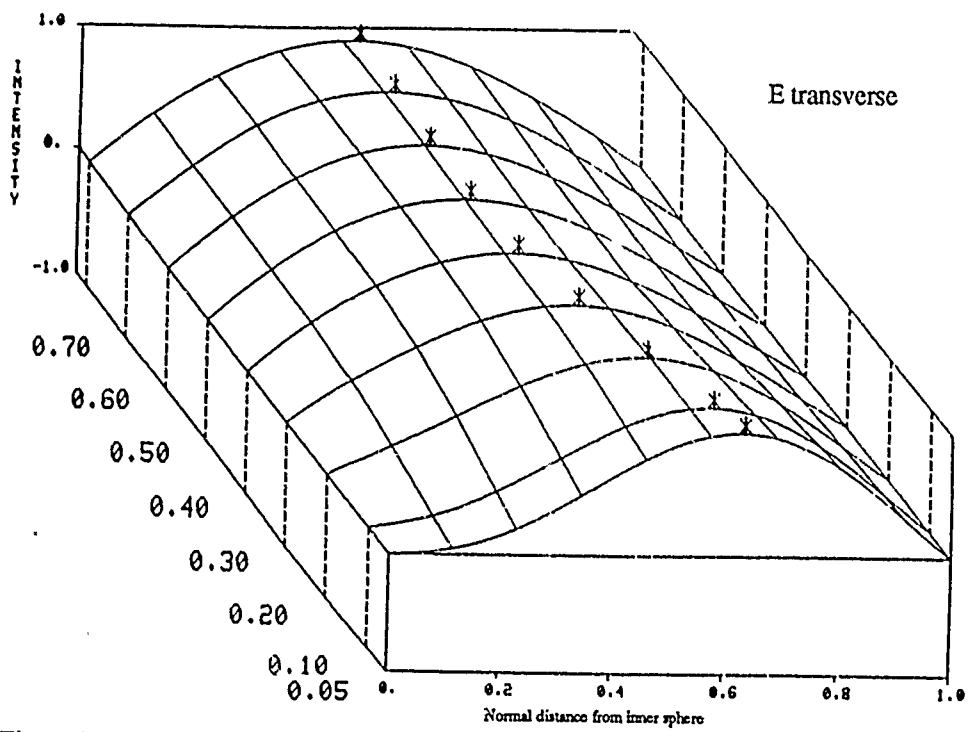

Figure 4. Distribution of the normalized transverse electric field component in the concentric spherical cavity as a function of the inner to outer conductor radii, $R = b/a$, for the TE31 mode. Asterisk indicates peak value of field with d.

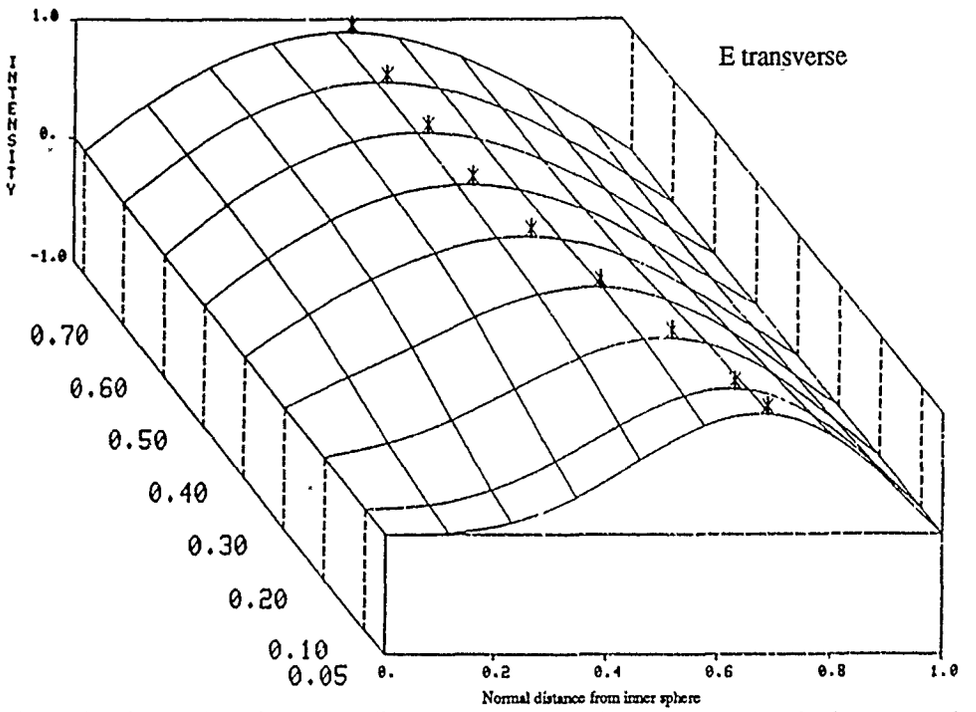

Figure 5. Distribution of the normalized transverse electric field component in the concentric spherical cavity as a function of the inner to outer conductor radii, $R = b/a$, for the TE41 mode. Asterisk indicates peak value of field with d.

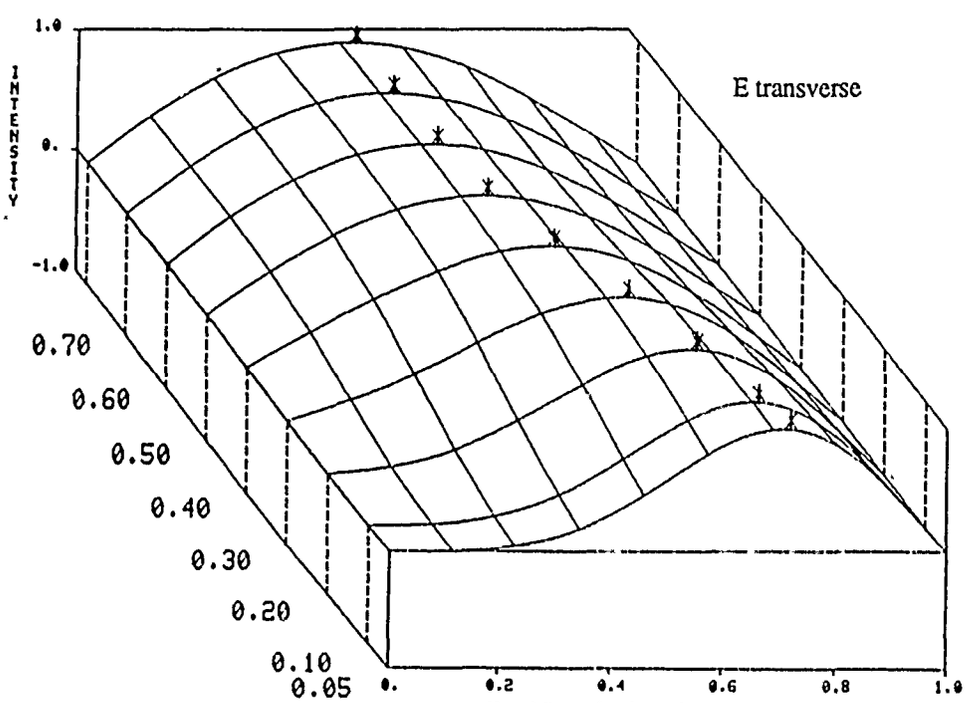

Figure 6. Distribution of the normalized transverse electric field component in the concentric spherical cavity as a function of the inner to outer conductor radii, $R = b/a$, for the TE51 mode. Asterisk indicates peak value of field with d.

3.1.2 *The p = 2 E-Transverse TEnp Eigenfields for n = 1 to 5*

Increasing p (i.e., changing the family) from 1 to 2 has the effect of making the field more oscillatory. This is a general rule of thumb that shall be observed for all field components as we increase p. Thus, instead of having one maximum, the absolute value of the field now has two local maxima between $d = 0$ and $d = 1$. For the combinations of n and b/a that were considered, the local maximum occurring at the smaller value of d is the absolute maximum. Increasing n from 1 to 5 has the effect of changing the position of the maxima. The change is negligible for larger b/a, but for smaller b/a there is once again a significant shift of the maxima to larger d. See figures 7 to 11.

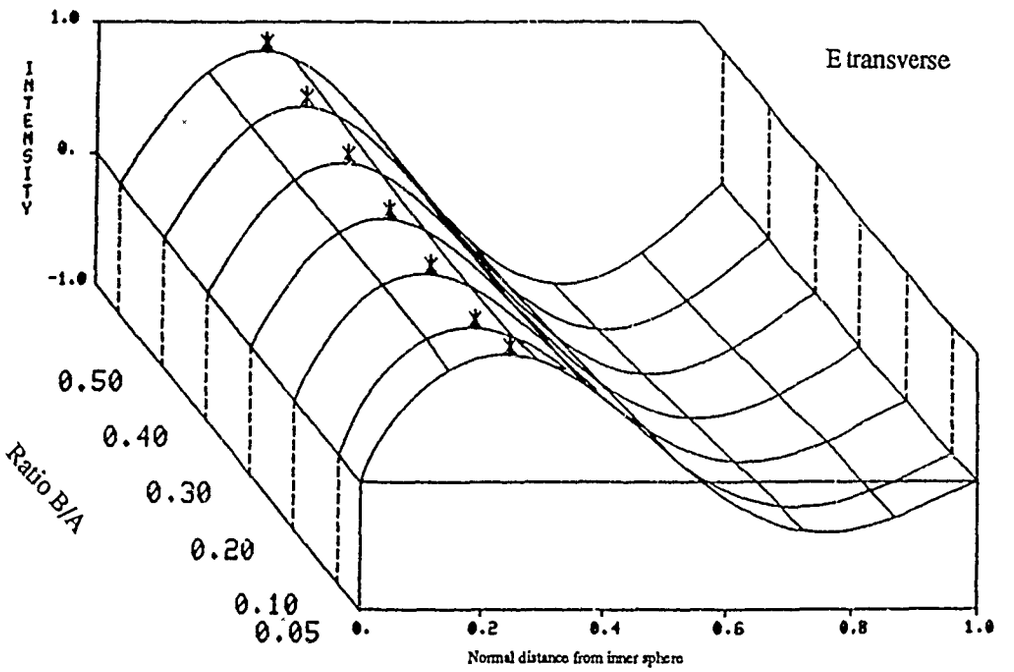

Figure 7. Distribution of the normalized transverse electric field component in the concentric spherical cavity as a function of the inner to outer conductor radii, $R = b/a$, for the TE12 mode. Asterisk indicates peak value of field with d.

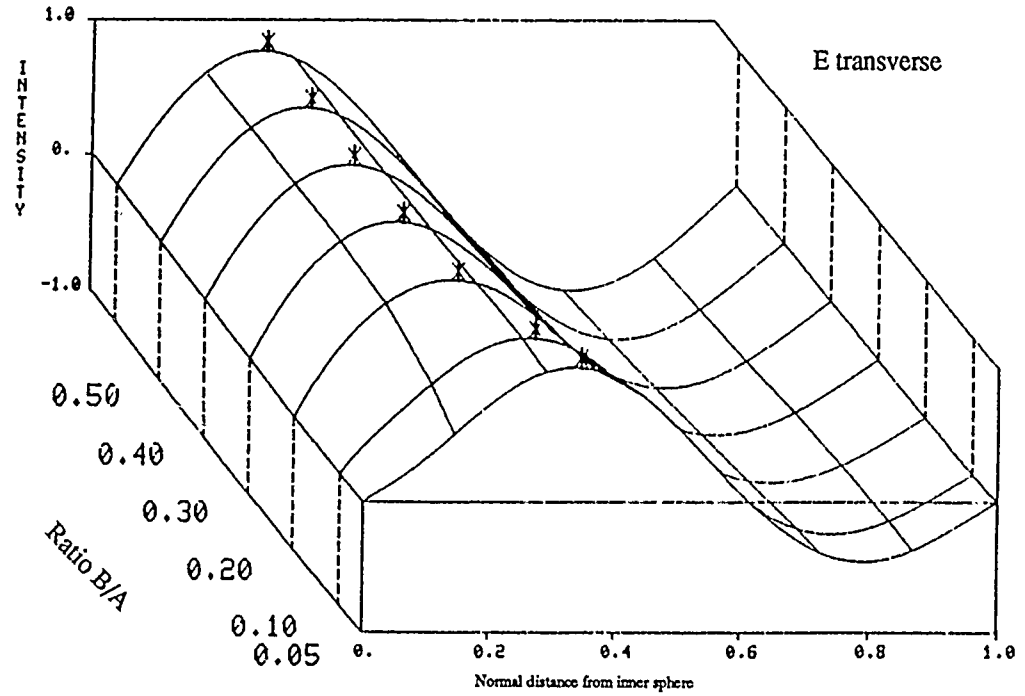

Figure 8. Distribution of the normalized transverse electric field component in the concentric spherical cavity as a function of the inner to outer conductor radii, $R = b/a$, for the TE22 mode. Asterisk indicates peak value of field with d.

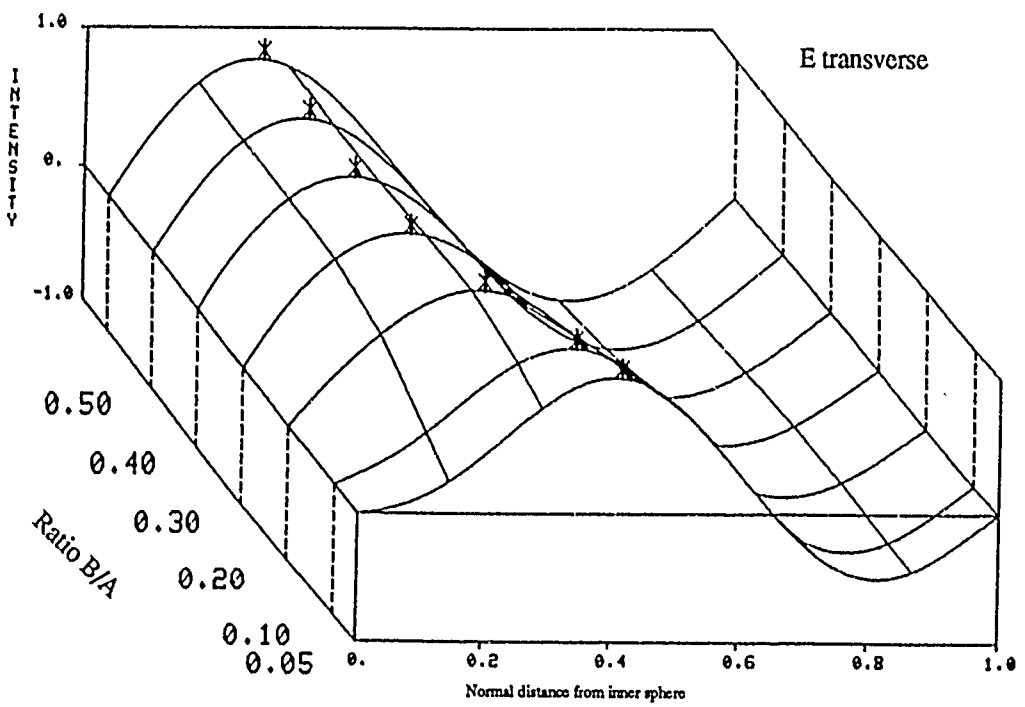

Figure 9. Distribution of the normalized transverse electric field component in the concentric spherical cavity as a function of the inner to outer conductor radii, $R = b/a$, for the TE32 mode. Asterisk indicates peak value of field with d.

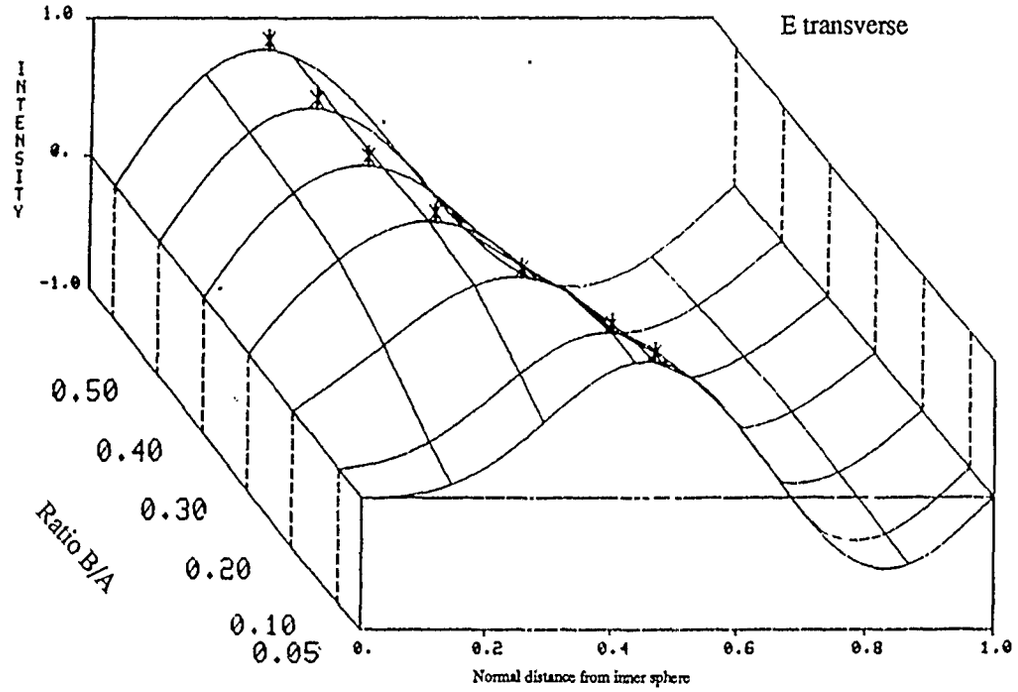

Figure 10. Distribution of the normalized transverse electric field component in the concentric spherical cavity as a function of the inner to outer conductor radii, $R = b/a$, for the TE42 mode. Asterisk indicates peak value of field with d.

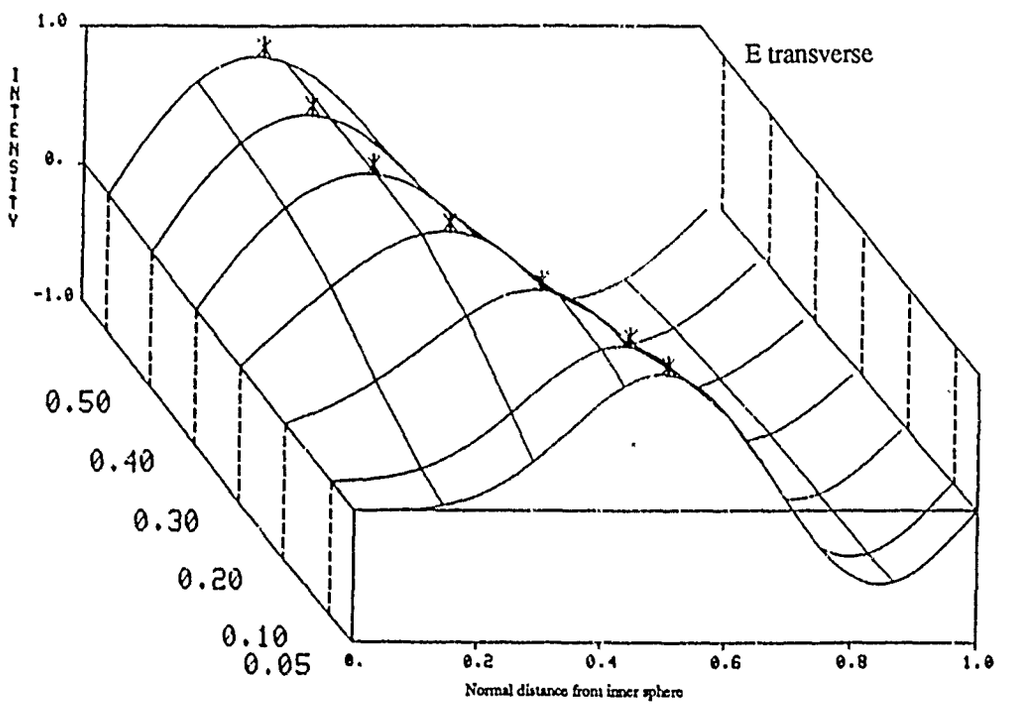

Figure 11. Distribution of the normalized transverse electric field component in the concentric spherical cavity as a function of the inner to outer conductor radii, $R = b/a$, for the TE52 mode. Asterisk indicates peak value of field with d.

3.1.3 *The p = 3 E-Transverse TEnp Eigenfields for n = 1 to 5*

When p is once again increased, from 2 to 3, the fields become still more oscillatory. There are now three local maxima/minima between $d = 0$ (the inner conducting wall) and $d = 1$ (the outer conducting wall). The local maximum at the lower value of d remains the absolute maximum for all cases of n and b/a considered. Increasing n by unity, from 1 to 5, once again changes the position of the maxima negligibly for large b/a, but for each increase produces a noticeable shift to larger d for the smaller values of b/a. See figures 12 to 16.

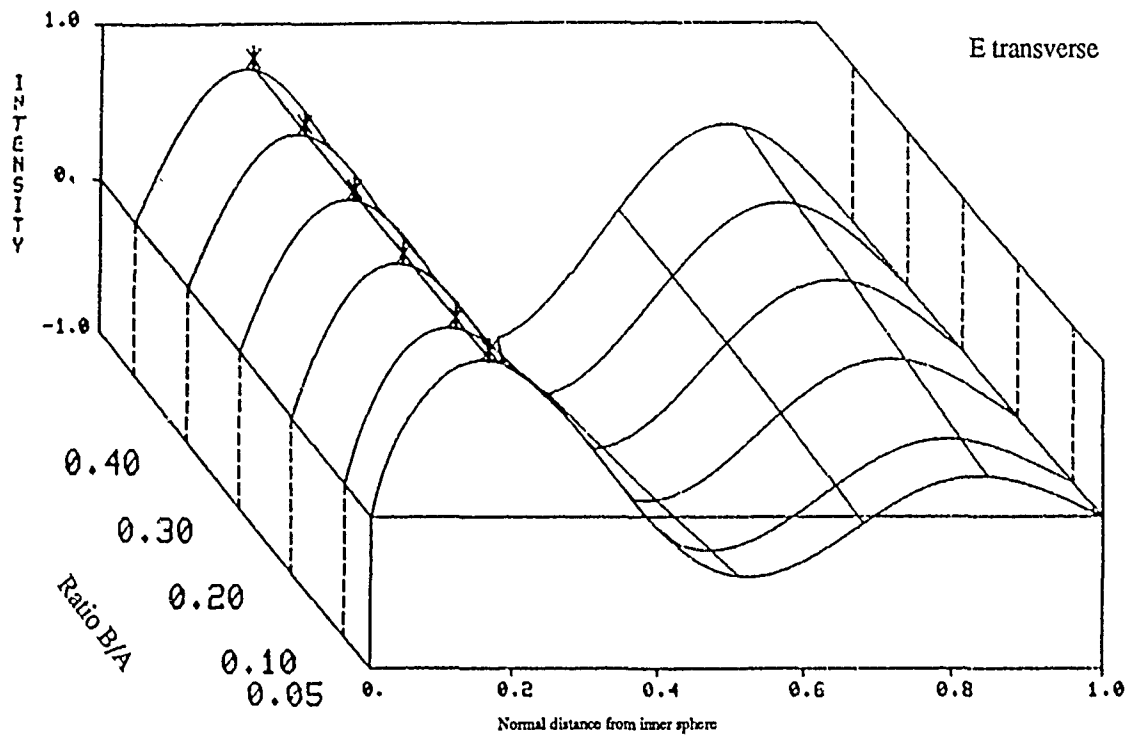

Figure 12. Distribution of the normalized transverse electric field component in the concentric spherical cavity as a function of the inner to outer conductor radii, $R = b/a$, for the TE13 mode. Asterisk indicates peak value of field with d.

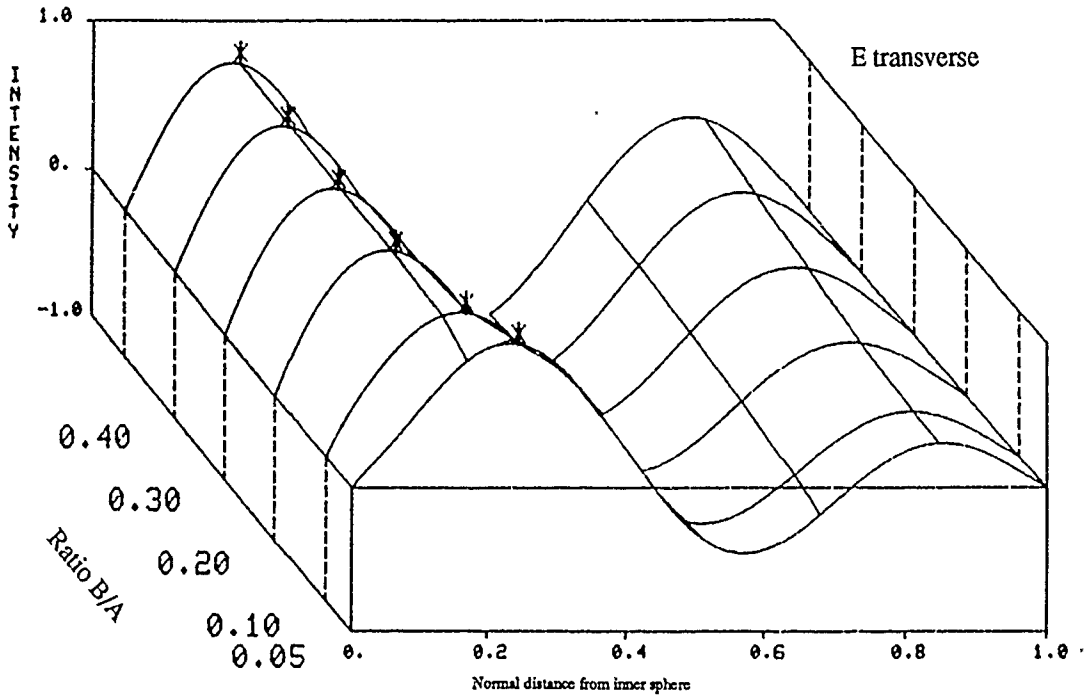

Figure 13. Distribution of the normalized transverse electric field component in the concentric spherical cavity as a function of the inner to outer conductor radii, $R = b/a$, for the TE23 mode. Asterisk indicates peak value of field with d.

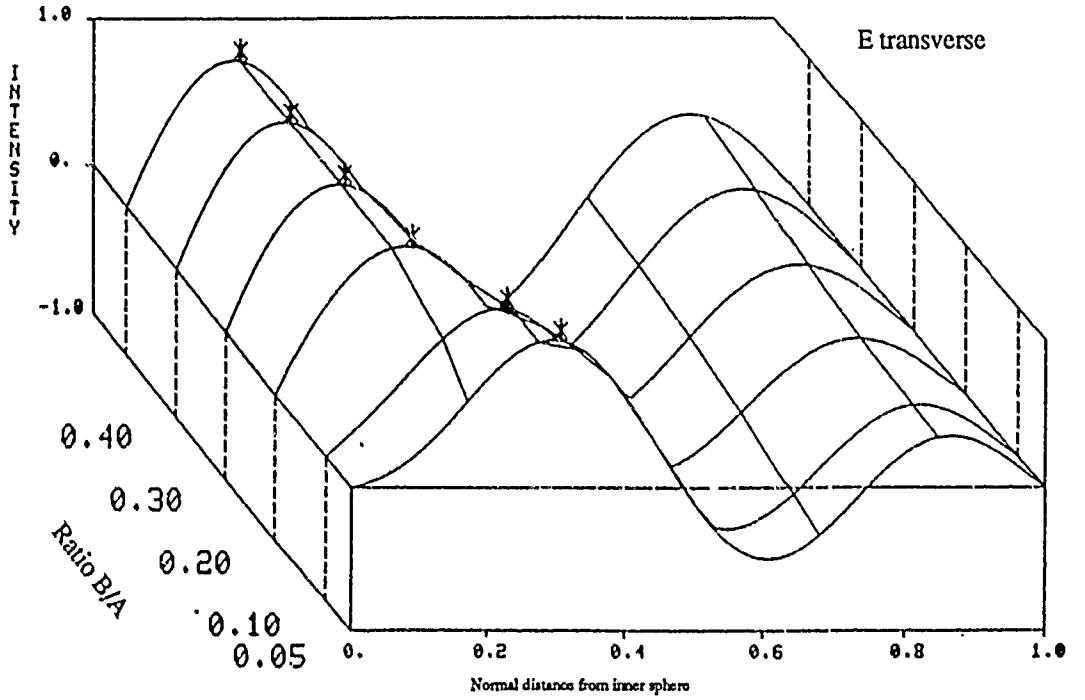

Figure 14. Distribution of the normalized transverse electric field component in the concentric spherical cavity as a function of the inner to outer conductor radii, $R = b/a$, for the TE33 mode. Asterisk indicates peak value of field with d.

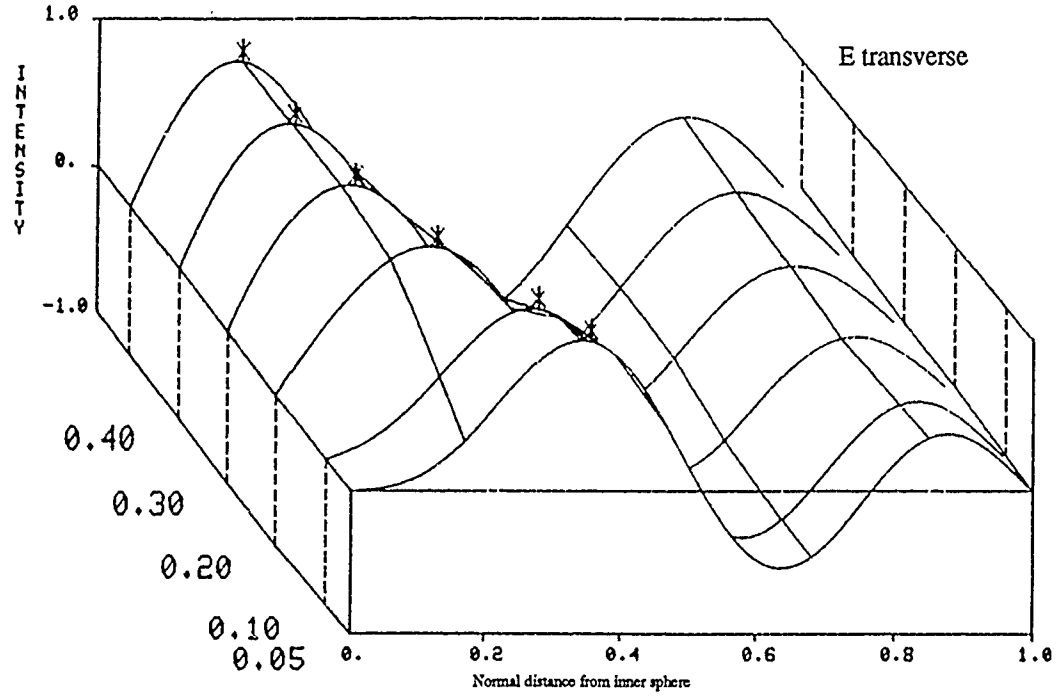

Figure 15. Distribution of the normalized transverse electric field component in the concentric spherical cavity as a function of the inner to outer conductor radii, $R = b/a$, for the TE43 mode. Asterisk indicates peak value of field with d.

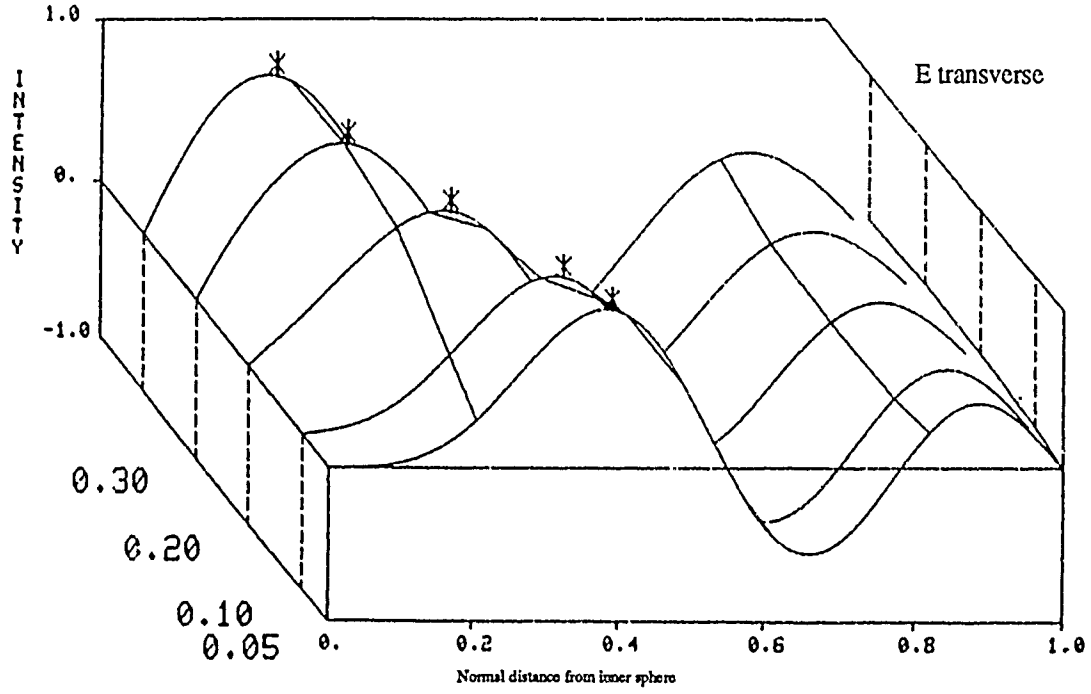

Figure 16. Distribution of the normalized tran .verse electric field component in the concentric spherical cavity as a function of the inner to outer conductor radii, $R = b/a$, for the TE53 mode. Asterisk indicates peak value of field with d.

3.1.4 *The p = 4 E-Transverse TEnp Eigenfields for n = 1 to 5*

A predictable pattern has developed as we increase n and p, and this pattern continues into the final family of TE modes that we will consider. When p is increased from 3 to 4, as expected there are four local maxima in the absolute value of the eigenfields. The local maximum corresponding to the lowest value of d remains the absolute maximum of the field's absolute value for the values of n and b/a that were considered. As before, an increase in n causes a noticeable shift in the location of the maxima to larger values of d for the smaller values of b/a, and much smaller shifts for larger b/a. See figures 17 to 20.

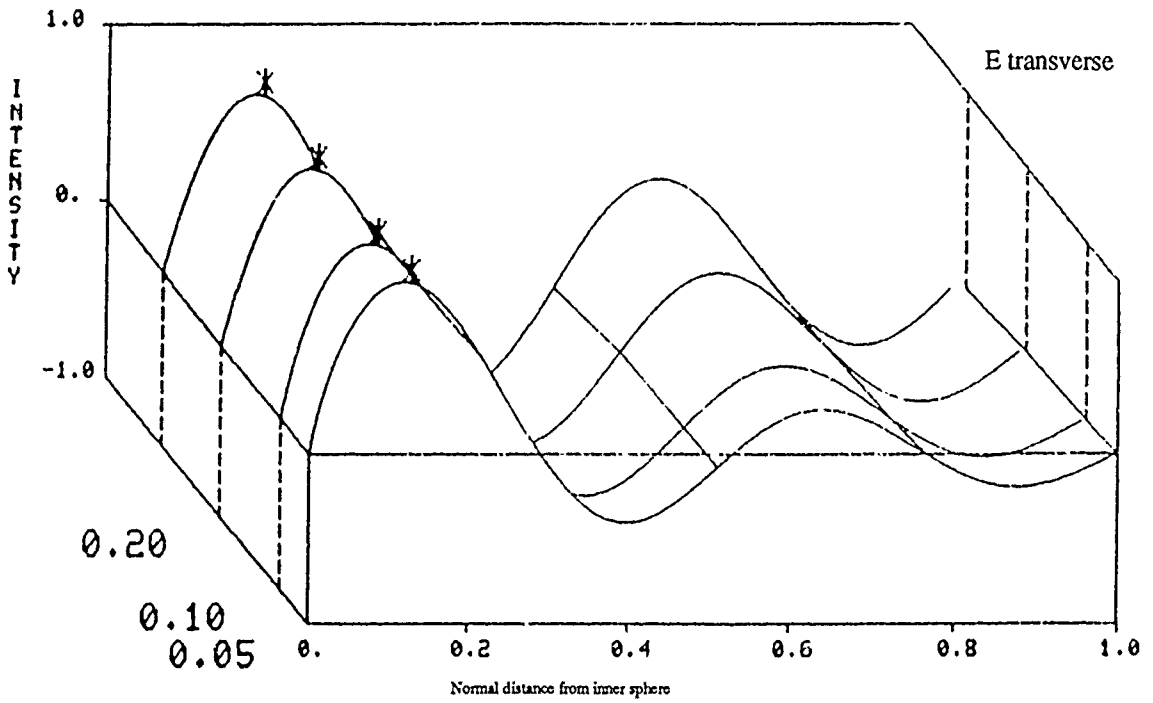

Figure 17. Distribution of the normalized transverse electric field component in the concentric spherical cavity as a function of the inner to outer conductor radii, $R = b/a$, for the TE14 mode. Asterisk indicates peak value of field with d.

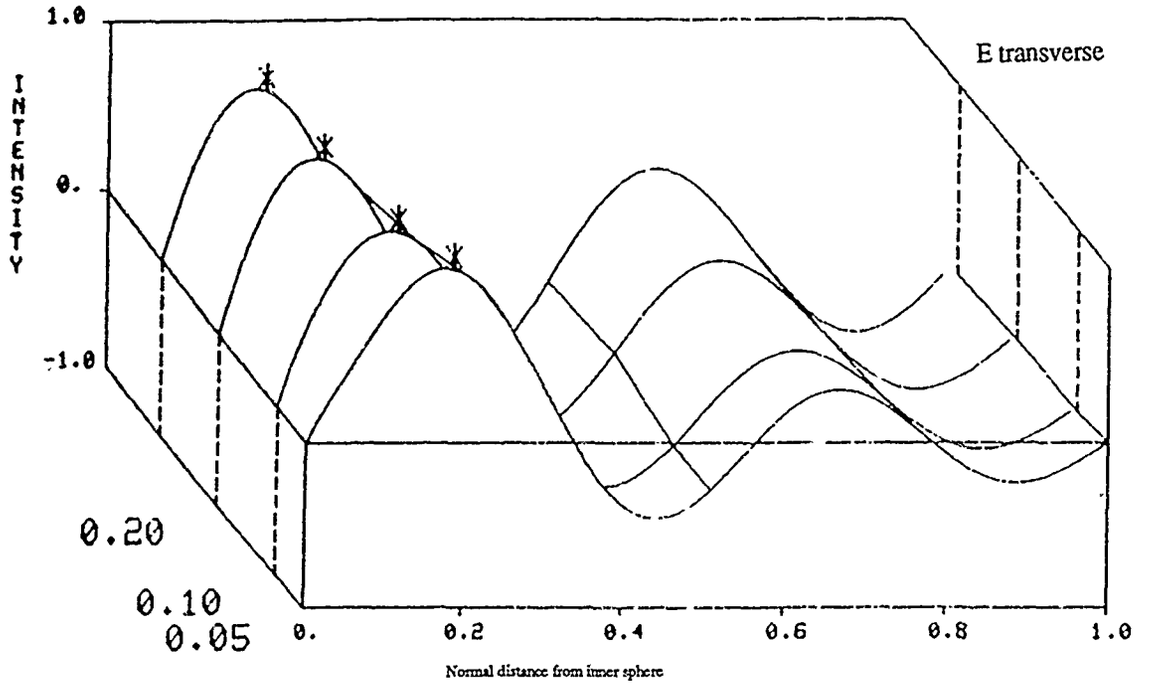

Figure 18. Distribution of the normalized transverse electric field component in the concentric spherical cavity as a function of the inner to outer conductor radii, $R = b/a$, for the TE24 mode. Asterisk indicates peak value of field with d.

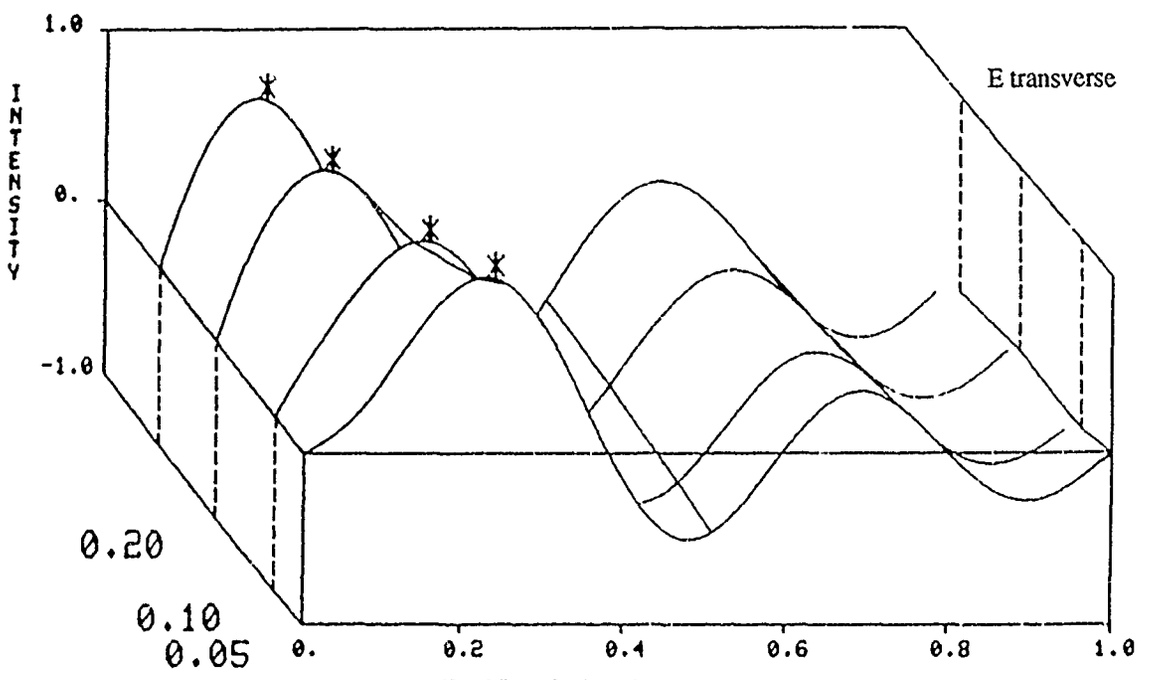

Figure 19. Distribution of the normalized transverse electric field component in the concentric spherical cavity as a function of the inner to outer conductor radii, $R = b/a$, for the TE34 mode. Asterisk indicates peak value of field with d.

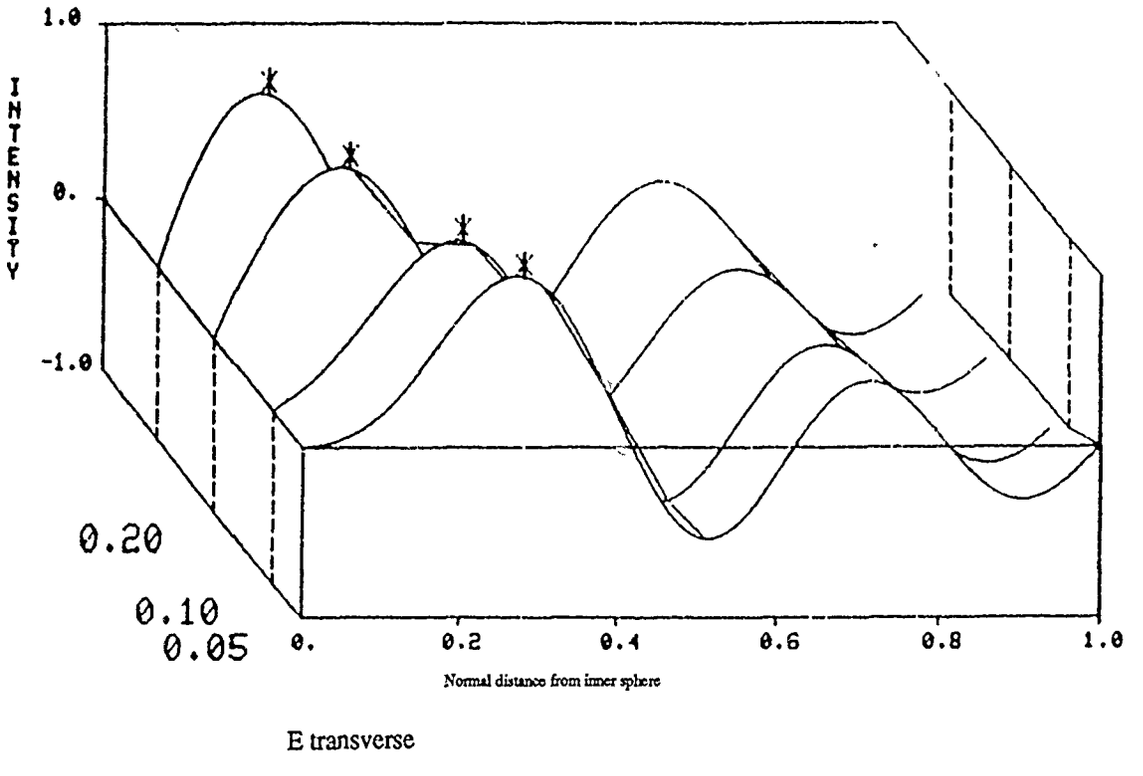

Figure 20. Distribution of the normalized transverse electric field component in the concentric spherical cavity as a function of the inner to outer conductor radii, $R = b/a$, for the TE44 mode. Asterisk indicates peak value of field with d.

3.2 Transverse Magnetic Field Component for TEnp Modes

3.2.1 The p = 1 H-Transverse TEnp Eigenfields for n = 1 to 5

We now turn our attention to the next field component, namely H-transverse for the TE11 mode, as depicted in figure 21. At the metallic boundaries, H-transverse is proportional to the surface current, and is generally nonzero on the walls. For the mode in question, the eigenfield is in fact at its maximum value (has a large surface current) on the inner conductor. The fields then decrease monotonically, including a sign change, until they almost reach the outer conductor, after which they exhibit a very mild increase from somewhere after $d = 0.9$ until reaching the outer conductor at $d = 1$. An exception exists for very small b/a of about 0.001, where this slight upward turn is absent. Monitoring the field at the outer conductor, one notices that its absolute value increases as b/a increases. Also, for very small b/a, there is a very sharp gradient in the decreasing field from its maximum at the inner conductor. Compare figure 21a for b

= 0.001a, figure 21b, for b = 0.01a, and figure 21c for b = 0.05a. And only a hint of the oscillation due to Bessel function dependence is evident in the mildly wavy behavior of the surface plot for $b/a > 0.05$ in figure 21.

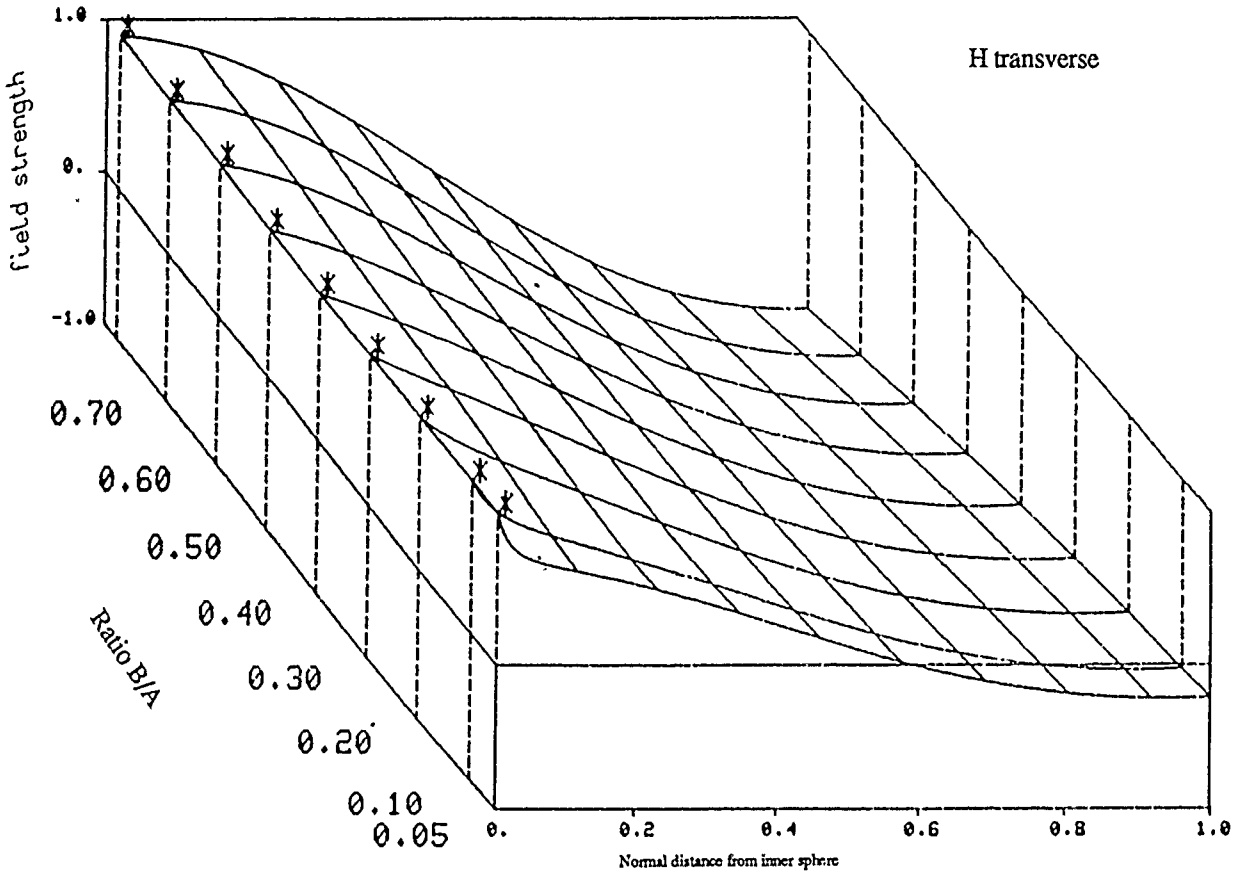

Figure 21. Distribution of the normalized transverse electric field component in the concentric spherical cavity as a function of the inner to outer conductor radii, $R = b/a$, for the TE11 mode. Asterisk indicates peak value of field with d.

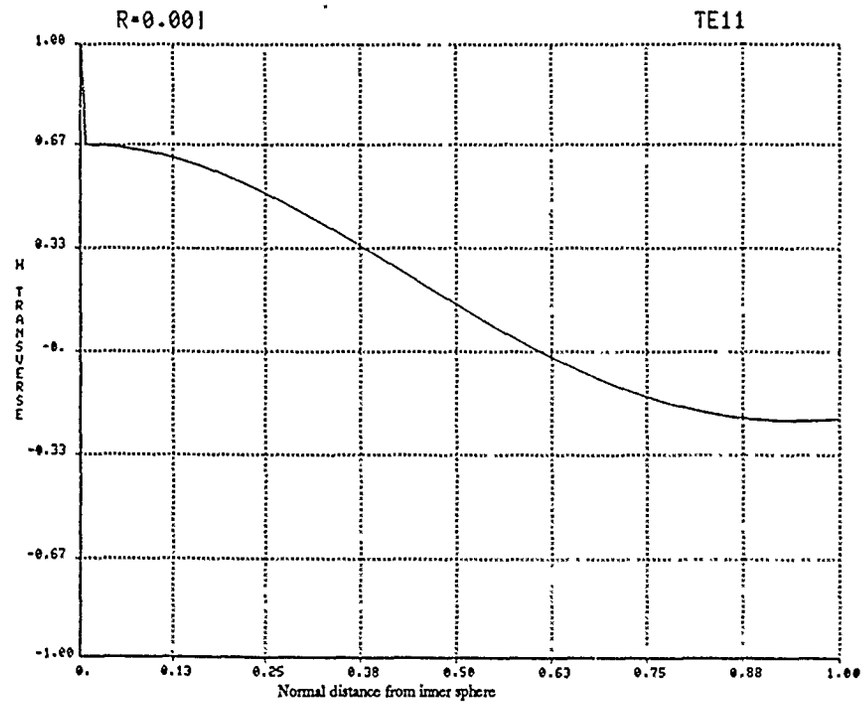

Figure 21a. Distribution of the normalized transverse magnetic field component in the concentric spherical cavity, when the inner to outer conductor radii, $R = b/a$, is 0.001, for the TE11 mode.

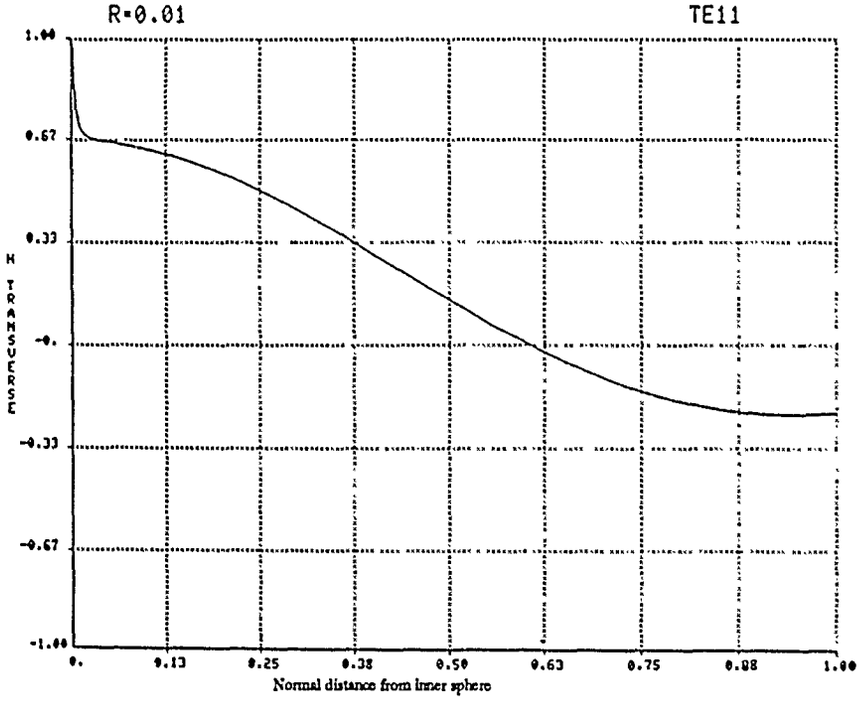

Figure 21b. Distribution of the normalized transverse magnetic field component in the concentric spherical cavity, when the inner to outer conductor radii, $R = b/a$, is 0.01, for the TE11 mode.

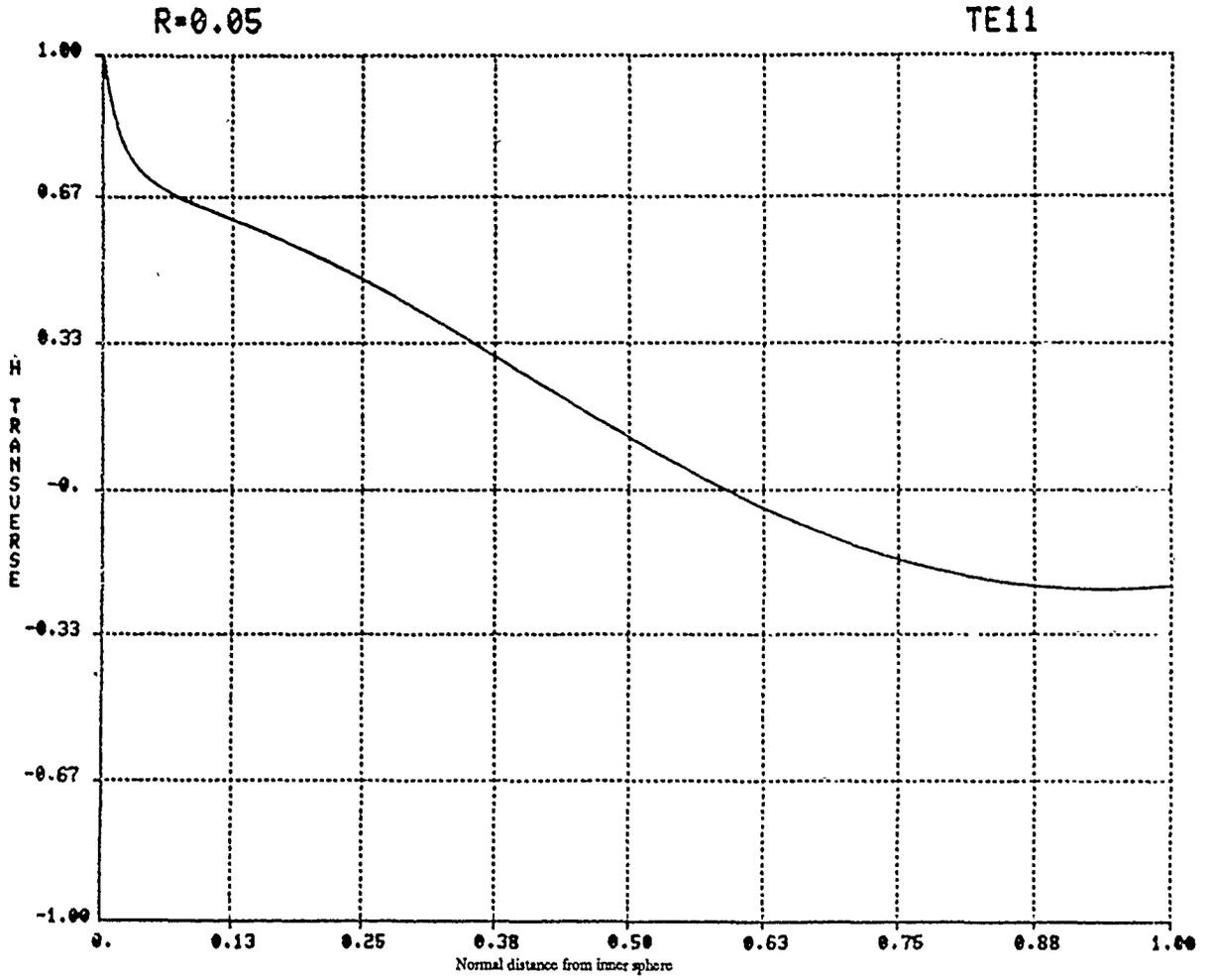

Figure 21c. Distribution of the normalized transverse magnetic field component in the concentric spherical cavity, when the inner to outer conductor radii, $R = b/a$, is 0.05, for the TE11 mode.

When we increase n from 1 to 2, the situation changes with respect to the location of the maxima for small b/a. The change involves the loss of monotonicity in d for small b/a, due to a field fluctuation (i.e., the oscillatory behavior becomes more pronounced), which contains a local maximum somewhere between $d = 0.2$ and $d = 0.3$. There is furthermore a critical value of b/a, somewhere between 0.1 and 0.2, where the absolute field maximum changes from the inner conducting wall for larger b/a to this local peak for smaller b/a. The field then continues to monotonically decrease in d toward the outer conductor as it did before when n equalled 1. At the outer conducting wall, the field intensity is now stronger for smaller b/a than for n =1. See figure 22.

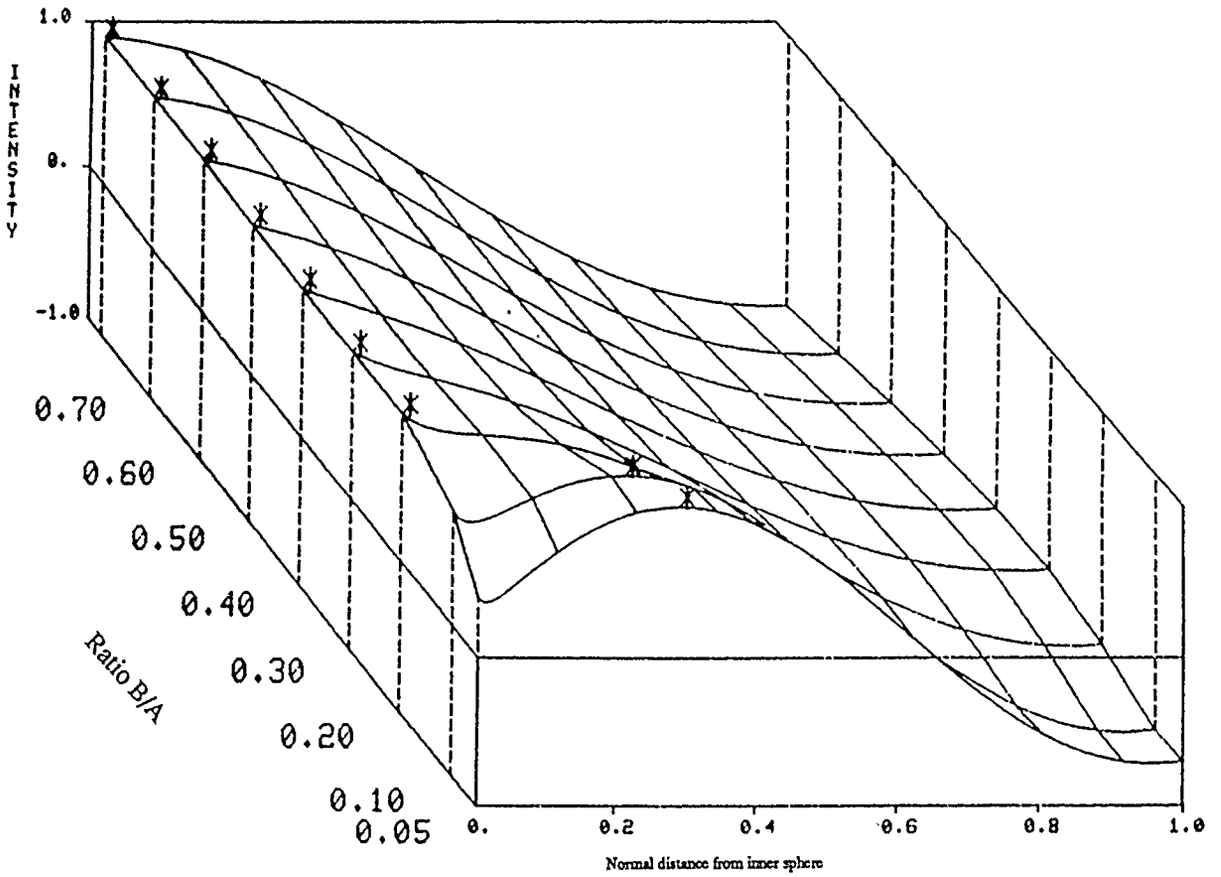

Figure 22. Distribution of the normalized transverse magnetic field component in the concentric spherical cavity as a function of the inner to outer conductor radii, $R = b/a$, for the TE21 mode. Asterisk indicates peak value of field with d.

When n is increased from 2 to 3, the effects described above are enhanced. The critical value, at which the absolute maximum shifts from being at the inner conductor to the local peak, has increased to somewhere between $b/a = 0.2$ and $b/a = 0.3$. Furthermore, these local peaks occur at larger values of d than for $n = 2$. After its absolute maximum, the field decreases in d, including a sign change, until it reaches almost to the outer conductor, and then rises a slight amount as it goes to $d = 1$. The absolute value of the normalized field strength (and hence the surface current) on the outer conductor is becoming large (about 0.9) for the small values of b/a considered ($0.05 < b/a < 0.2$; see fig. 23.)

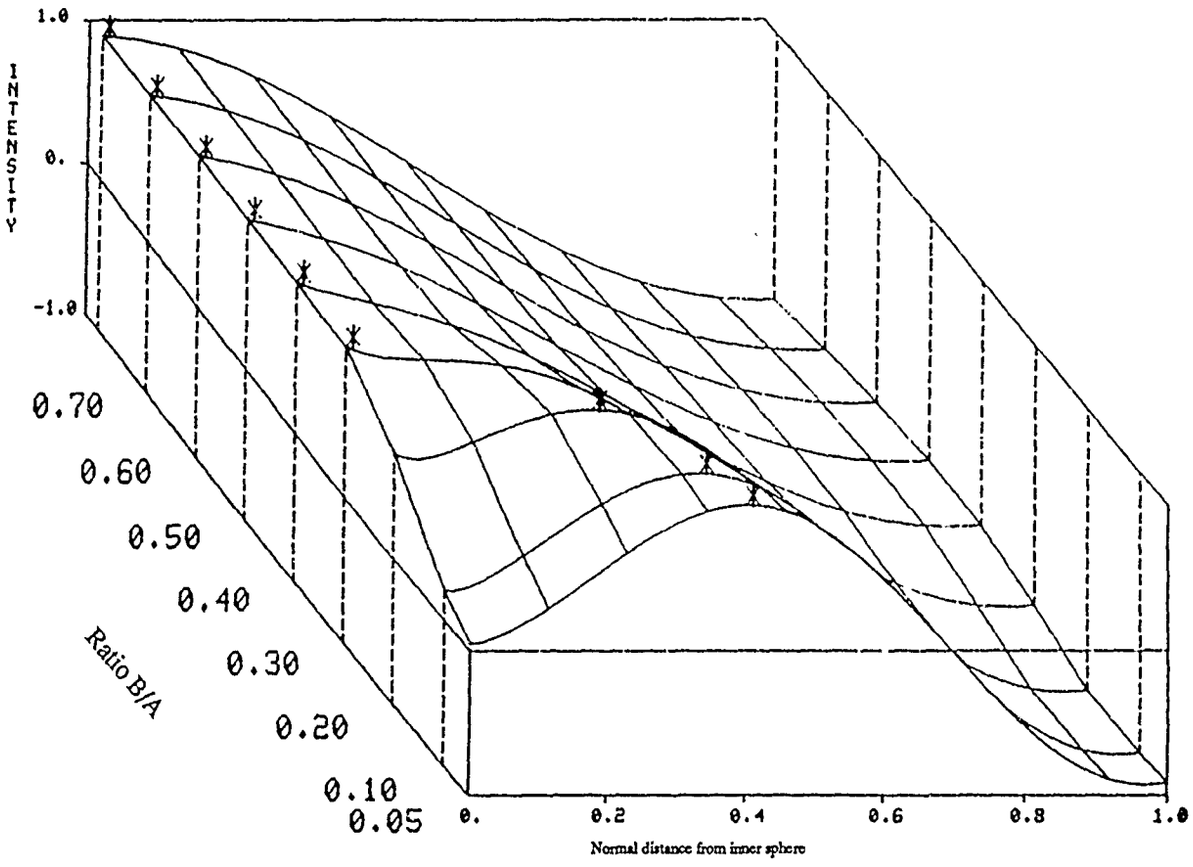

H transverse

Figure 23. Distribution of the normalized transverse magnetic field component in the concentric spherical cavity as a function of the inner to outer conductor radii, $R = b/a$, for the TE31 mode. Asterisk indicates peak value of field with d.

When n is increased to 4, we once again see, in figure 24, that the local peak which caused the field strength to lose its monotonic character in d exists for a still larger range of b/a ($b/a < 0.4$). These peaks furthermore occur at still larger values of d. However, this local peak is no longer the maximum value for smaller b/a, at least for the values computed. For this range ($0.05 < b/a < 0.3$), the absolute maximum (of the absolute value of the field) is on the outer conductor, since the field strength there increased enough to be larger than any other maximum. For $b/a > 0.4$, the absolute maximum remains on the inner conducting wall. A critical value in b/a exists between 0.3 and 0.4.

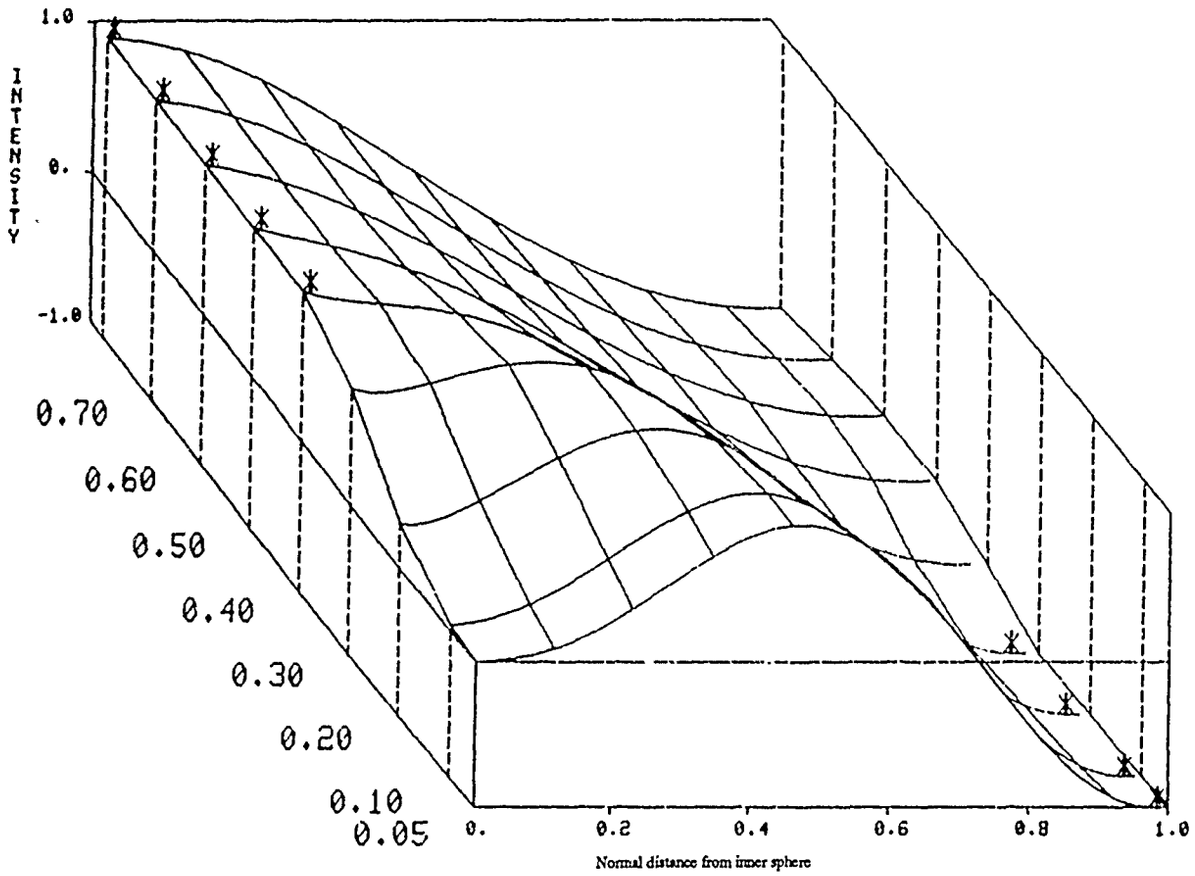

H transverse

Figure 24. Distribution of the normalized transverse magnetic field component in the concentric spherical cavity as a function of the inner to outer conductor radii, $R = b/a$, for the TE41 mode. Asterisk indicates peak value of field with d.

When n is increased to 5, the surface plot of the field strength for H-transverse resembles that of $n = 4$, except for what should now be predictable changes. For $b/a > 0.5$, the absolute maximum remains on the inner wall. Between $b/a = 0.4$ and $b/a = 0.5$, there exists a critical value of b/a, larger than the previous ones, below which the surface loses its monotonic character in d, and develops a local maximum. These local peaks have been shifted to still larger values of d than before. Also between $b/a = 0.4$ and $b/a = 0.5$, the absolute maximum of the absolute value of the field changes from being on the inner conductor for larger b/a, to the outer conductor for smaller b/a (fig. 25). It is worth noting that when n is increased for this $p = 1$ family the component's field strength (surface current) is diminished considerably on the inner conducting wall for smaller b/a.

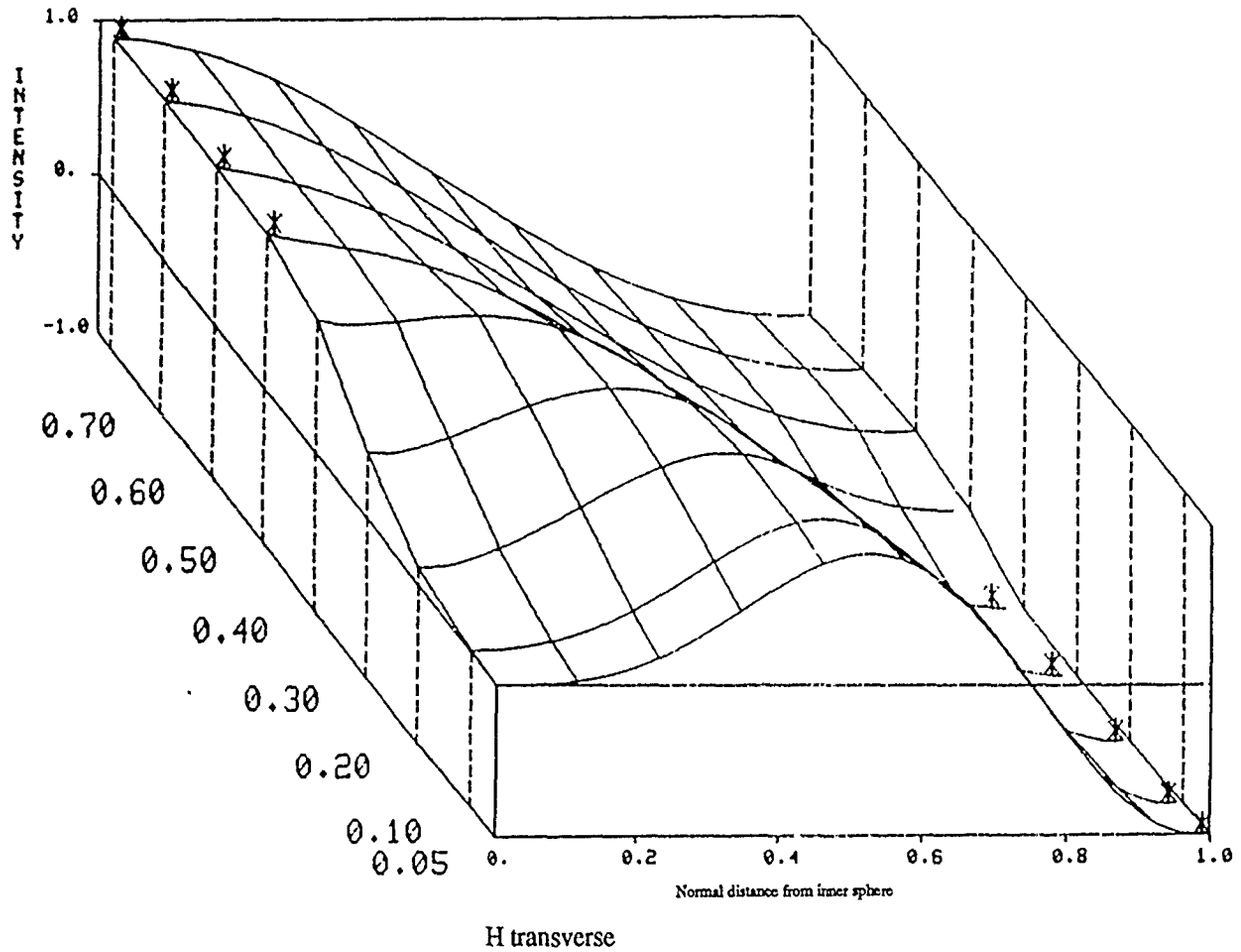

Figure 25. Distribution of the normalized transverse magnetic field component in the concentric spherical cavity as a function of the inner to outer conductor radii, $R = b/a$, for the TE51 mode. Asterisk indicates peak value of field with d.

3.2.2 *The p = 2 H-Transverse TEnp Eigenfields for n = 1 to 5*

When the family index p is increased from 1 to 2, the oscillatory nature of the H-transverse field component is also increased. This is made evident in figure 26 for the TE12 mode. There now exists an additional peak value between $d = 0.45$ and 0.55, indicated as a local minimum in the figure. The component's absolute maximum remains on the inner conductor for all values of b/a that were considered (between 0.05 and 0.6), as it was for the TE11 mode.

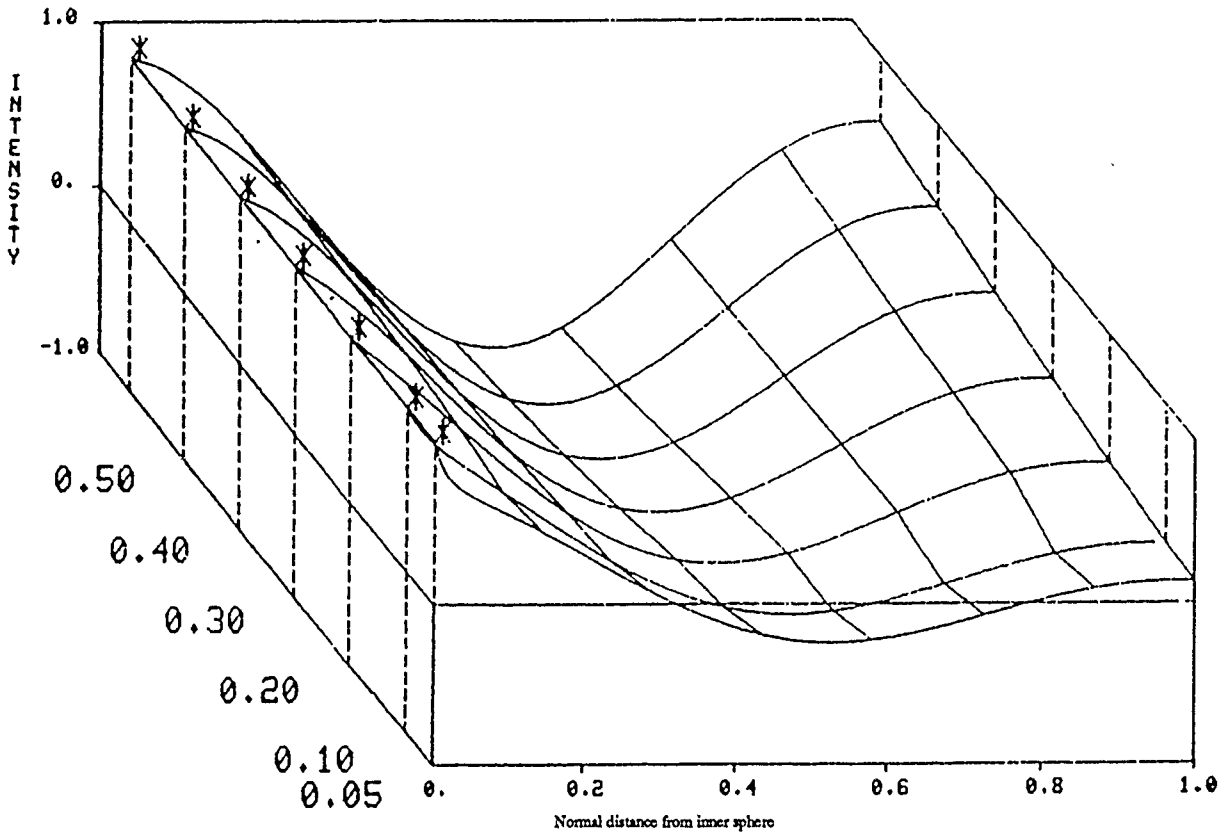

H transverse

Figure 26. Distribution of the normalized transverse magnetic field component in the concentric spherical cavity as a function of the inner to outer conductor radii, $R = b/a$, for the TE12 mode. Asterisk indicates peak value of field with d

Increasing the order index n to 2 has similar effects on the H-transverse field as in the $p = 1$ family. Another local maximum appears at approximately $d = 0.2$, but it exists only for the smaller values of b/a, disappearing somewhere between $b/a = 0.1$ and $b/a = 0.2$. The absolute maximum value of the field component lies on this local peak for a smaller range of b/a than for the $p = 1$ case, with the critical value in b/a somewhere between 0.05 and 0.1, at which the absolute maximum switches from the local peak back to the inner conductor. The other local minimum, which came into being by increasing the family index p to 2, has shifted its position to higher values of d (approximately $d = 0.6$; see fig. 27).

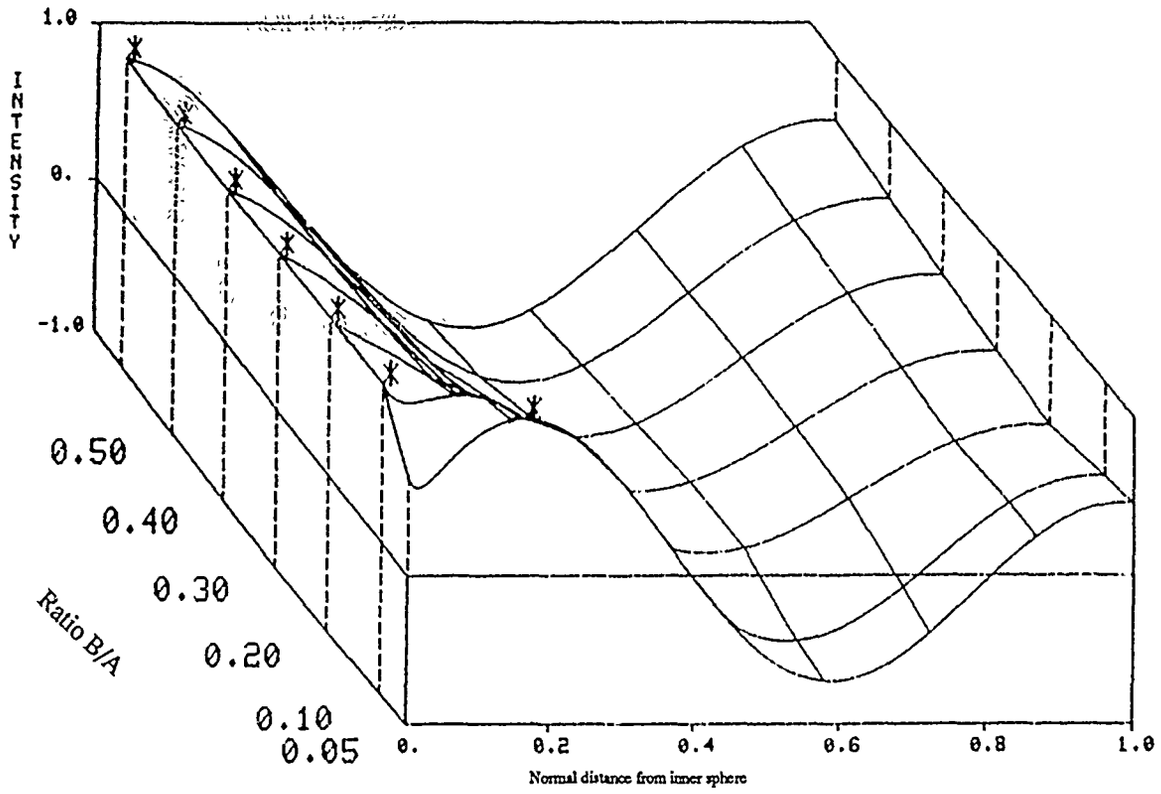

H transverse

Figure 27. Distribution of the normalized transverse magnetic field component in the concentric spherical cavity as a function of the inner to outer conductor radii, $R = b/a$, for the TE22 mode. Asterisk indicates peak value of field with d.

Increasing the order n once more to 3 has the effect of extending the new local peak over a larger range in b/a. The threshold value in b/a is now between 0.2 and 0.3. The local maximum is furthermore the absolute maximum of the absolute value of the field component for small b/a, the cutoff being between $b/a = 0.1$ and $b/a = 0.2$, which is a larger cutoff than for the TE22 mode (fig. 28). There still remain two local peaks; the second, depicted as a minimum, was introduced when p was increased. Above the threshold value of b/a, only the latter (minimum) is present.

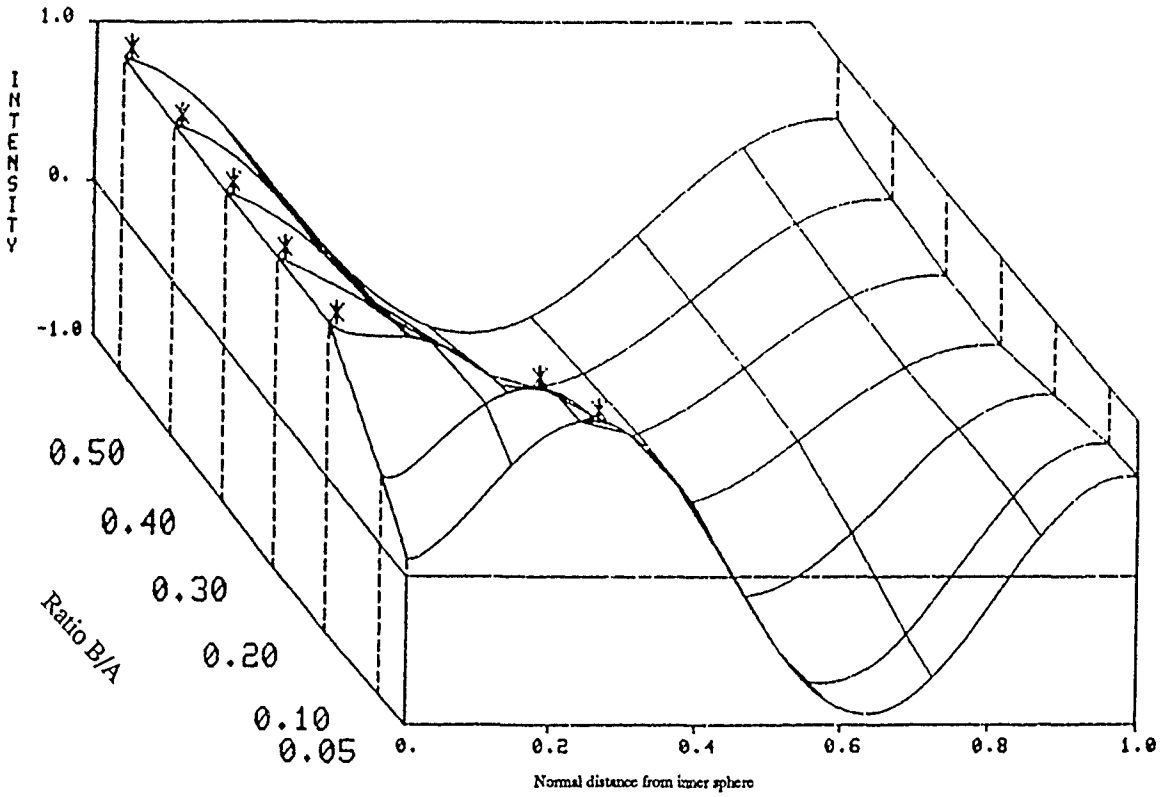

H transverse

Figure 28. Distribution of the normalized transverse magnetic field component in the concentric spherical cavity as a function of the inner to outer conductor radii, $R = b/a$, for the TE32 mode. Asterisk indicates peak value of field with d.

When n is increased from 3 to 4 the changes which occur for $p = 2$ continue to have similarities with those occurring in the $p = 1$ family. The local maximum which appears on the surface when n is increased now exists over still a larger range of b/a. It exists at a slightly larger value of d than for $n = 3$. And, as for the $p = 1$, $n = 4$ case, this local maximum is no longer the absolute maximum of the field component. The absolute maximum in the absolute value of the field is instead at the local minimum which arose from the increased oscillation when p was raised from 1 to 2 (fig. 29).

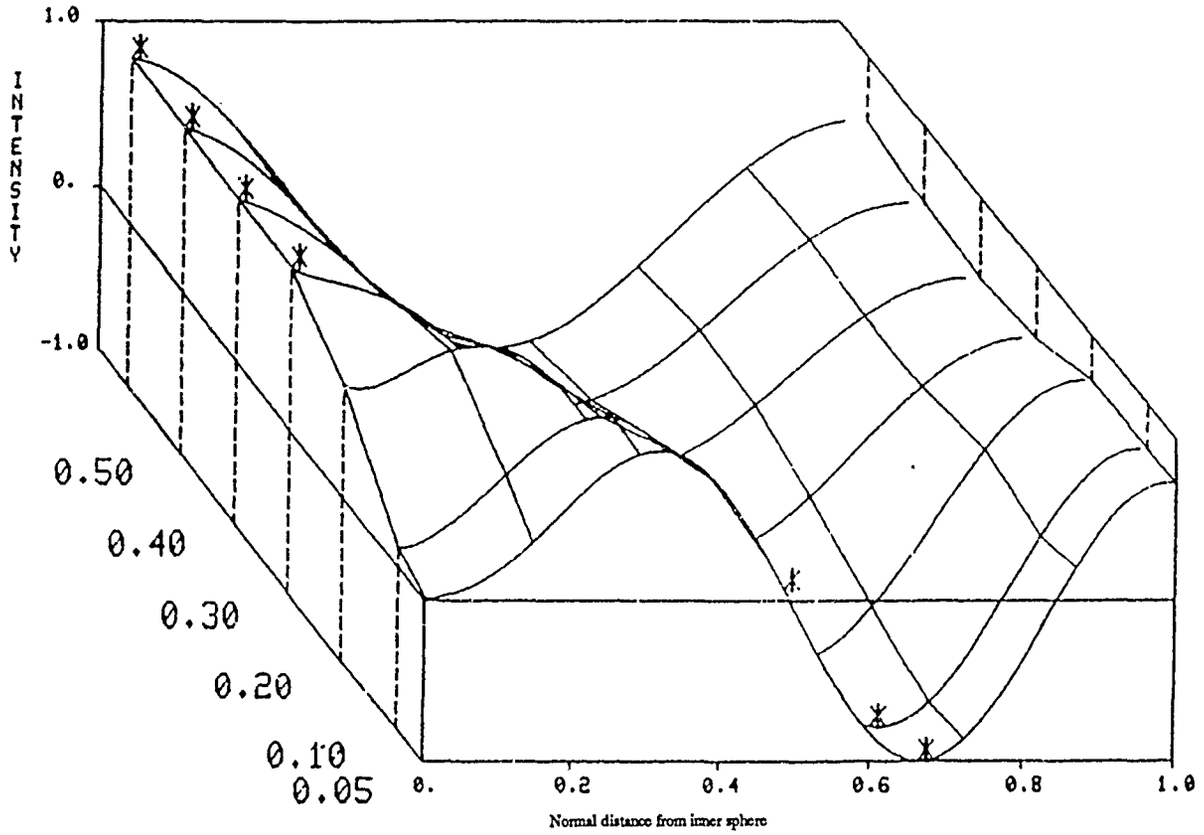

H transverse

Figure 29. Distribution of the normalized transverse magnetic field component in the concentric spherical cavity as a function of the inner to outer conductor radii, $R = b/a$, for the TE42 mode. Asterisk indicates peak value of field with d.

When n is increased from 4 to 5, as expected, the changes which have taken place become enhanced. The range in b/a for which there is a new local maximum due to the increase in n is now still greater. Likewise, the range in b/a is also greater where the absolute maximum of the absolute value of the field component lies on the local minimum which arose from increasing p. Both this local maximum and minimum occur at higher values of d, as expected (fig. 30).

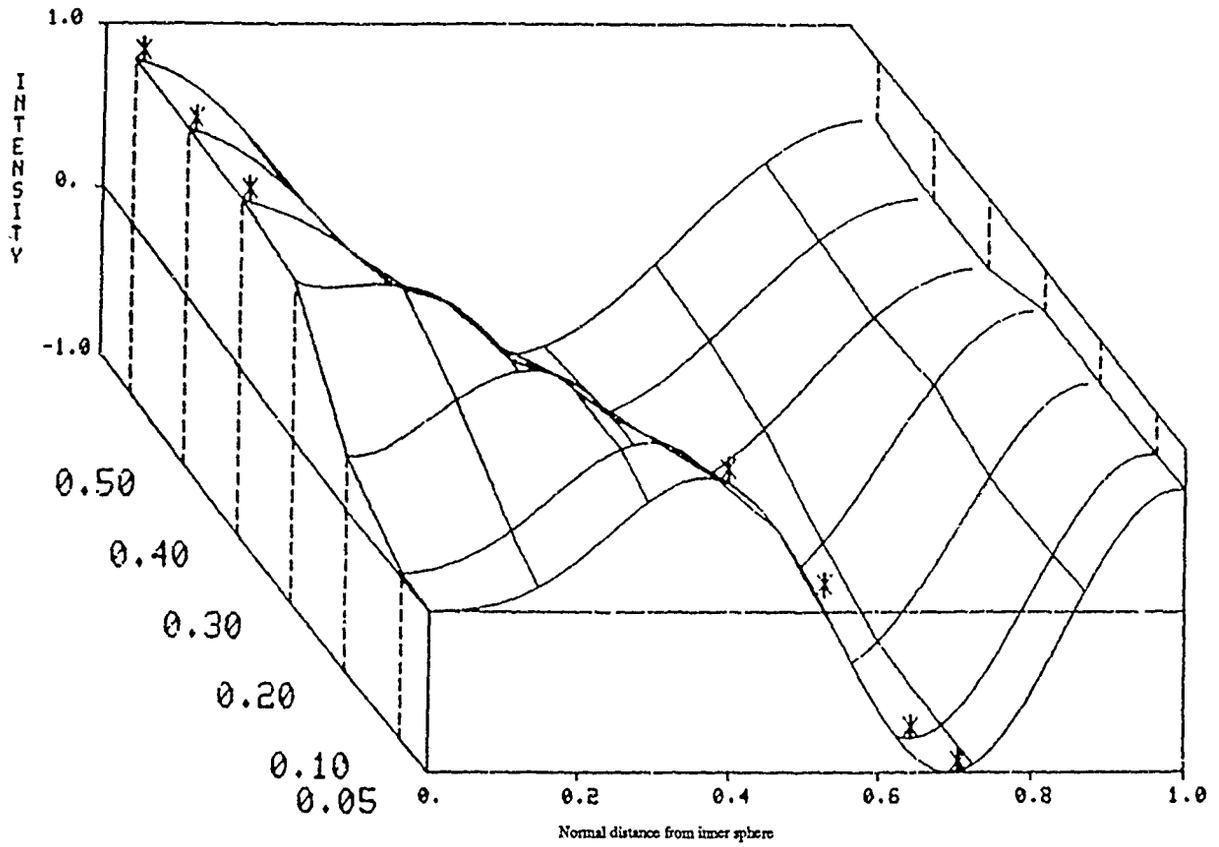

H transverse

Figure 30. Distribution of the normalized transverse magnetic field component in the concentric spherical cavity as a function of the inner to outer conductor radii, $R = b/a$, for the TE52 mode. Asterisk indicates peak value of field with d.

3.2.3 The p = 3 H-Transverse TEnp Eigenfields for n = 1 to 5

Increasing the family index p from 2 to 3 once again increases the oscillatory nature of the fields, so that the TE13 mode exhibits, in addition to the local minimum already present when p equalled 2, an additional local maximum when d is slightly less than 0.7 (fig. 31). As for the TE12 mode, the absolute maximum is on the inner conducting wall for all values of b/a that were calculated ($0.05 < b/a < 0.5$).

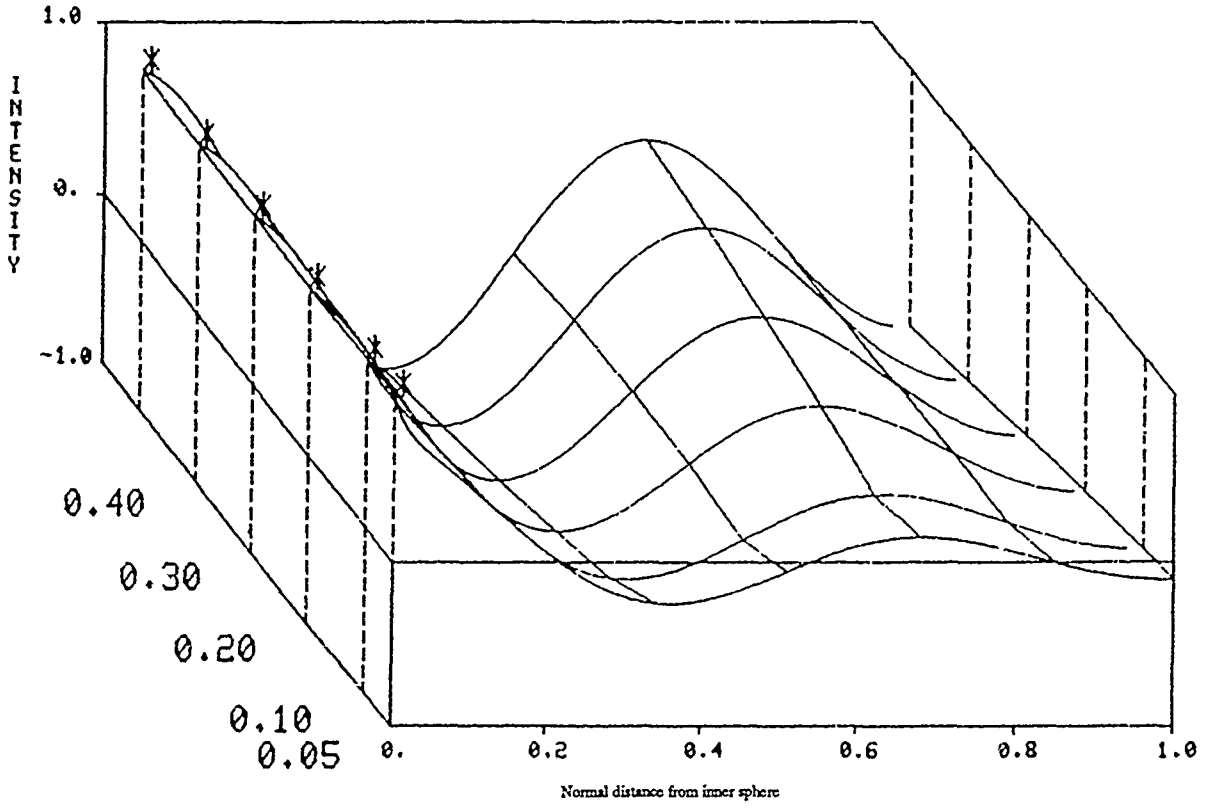

Figure 31. Distribution of the normalized transverse magnetic field component in the concentric spherical cavity as a function of the inner to outer conductor radii, $R = b/a$, for the TE13 mode. Asterisk indicates peak value of field with d.

Increasing n to 2 once again produces a new local maximum only at the smaller values of b/a. Increasing n still further to 3 extends the range of b/a for which this local maximum exists. Moreover, the absolute maximum of the component lies on this new local maximum for smaller values of b/a, as illustrated in fig. 32 and 33. As n is increased to 4 and 5, the new local maximum occurs over still greater ranges of b/a. However, for the $p = 3$ case, the absolute maximum of the absolute value of the field now switches to the next local minimum (illustrated by fig. 34 and 35). Also one may observe from the figures that as n increases, the locations of the local maxima/minima in d increase, as they did for the previous values of p.

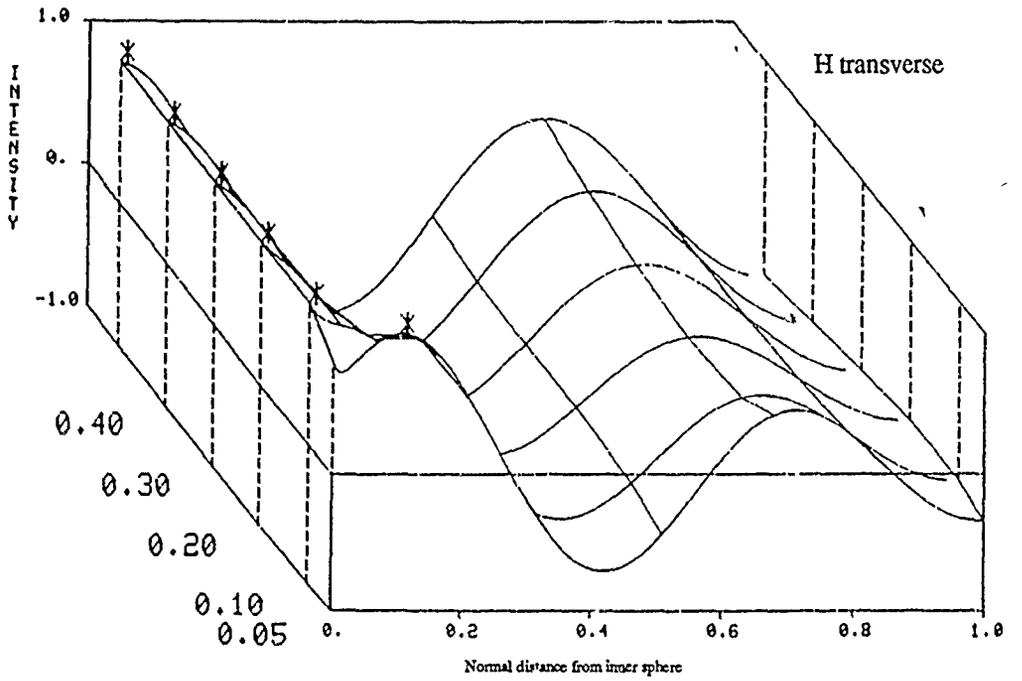

Figure 32. Distribution of the normalized transverse magnetic field component in the concentric spherical cavity as a function of the inner to outer conductor radii, $R = b/a$, for the TE23 mode. Asterisk indicates peak value of field with d.

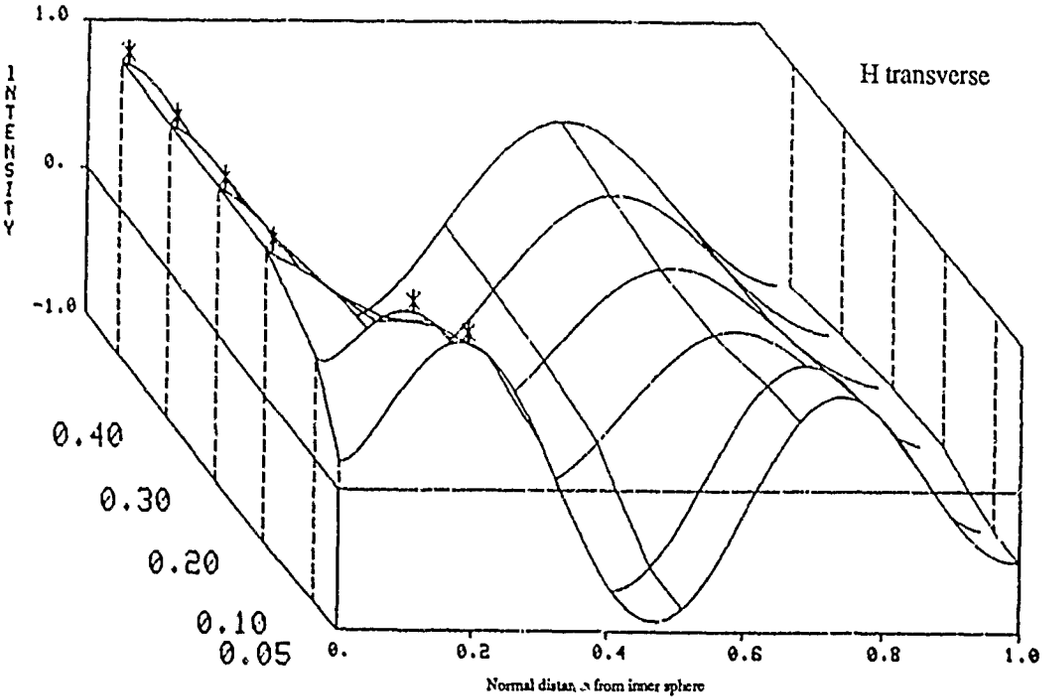

Figure 33. Distribution of the normalized transverse magnetic field component in the concentric spherical cavity as a function of the inner to outer conductor radii, $R = b/a$, for the TE33 mode. Asterisk indicates peak value of field with d.

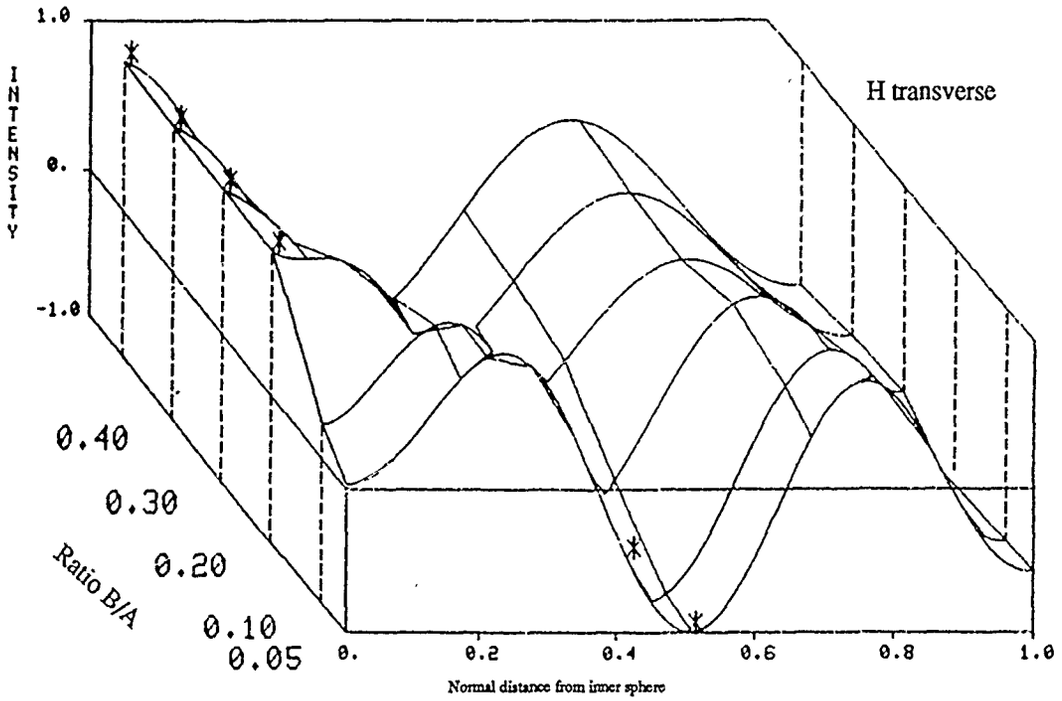

Figure 34. Distribution of the normalized transverse magnetic field component in the concentric spherical cavity as a function of the inner to outer conductor radii, $R = b/a$, for the TE43 mode. Asterisk indicates peak value of field with d.

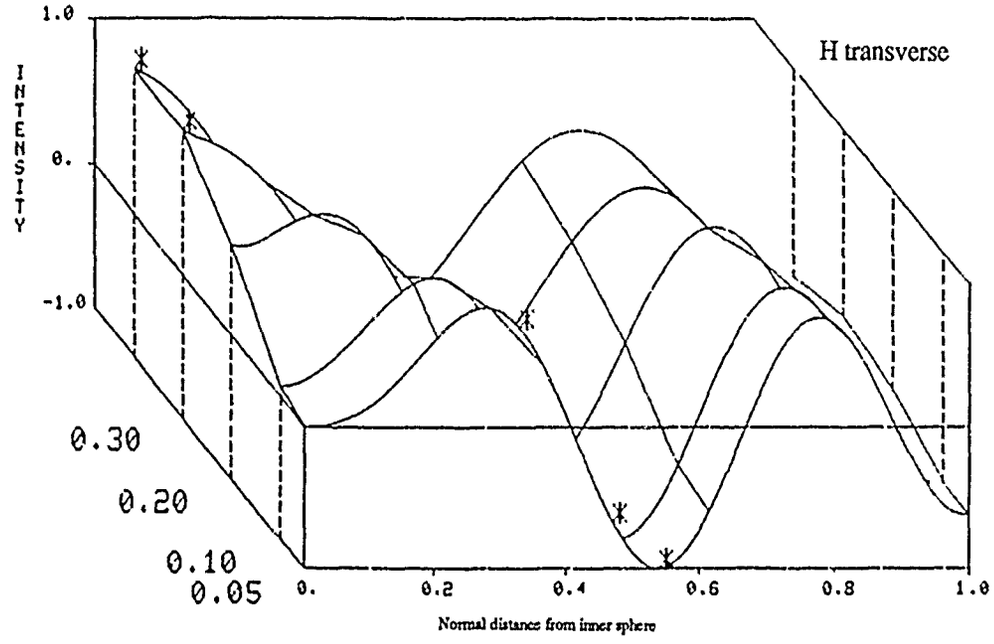

Figure 35. Distribution of the normalized transverse magnetic field component in the concentric spherical cavity as a function of the inner to outer conductor radii, $R = b/a$, for the TE53 mode. Asterisk indicates peak value of field with d.

3.2.4 *The p = 4 H-Transverse TEnp Eigenfields for n = 1 to 4*

Figures 36 to 39 show the H-transverse component for $p = 4$. The patterns we have noticed for $p = 1$, 2, and 3 are continued here, and therefore the behavior of the field patterns is somewhat predictable. The oscillatory nature of the fields has been once again increased. For $n = 1$ the absolute maximum of the field is on the inner conducting wall for all values of b/a computed. For $n = 2$ and 3 another local maximum appears close to the inner conducting wall for smaller values of b/a. The absolute maximum value of the field strength lies on this new local maximum for small b/a. When n is increased to 4, the maximum value of the field strength for smaller b/a switches to the local minimum next closest to the inner conducting wall. And as we increase n from 1 to 4, the location of the local maxima/ minima increases in d.

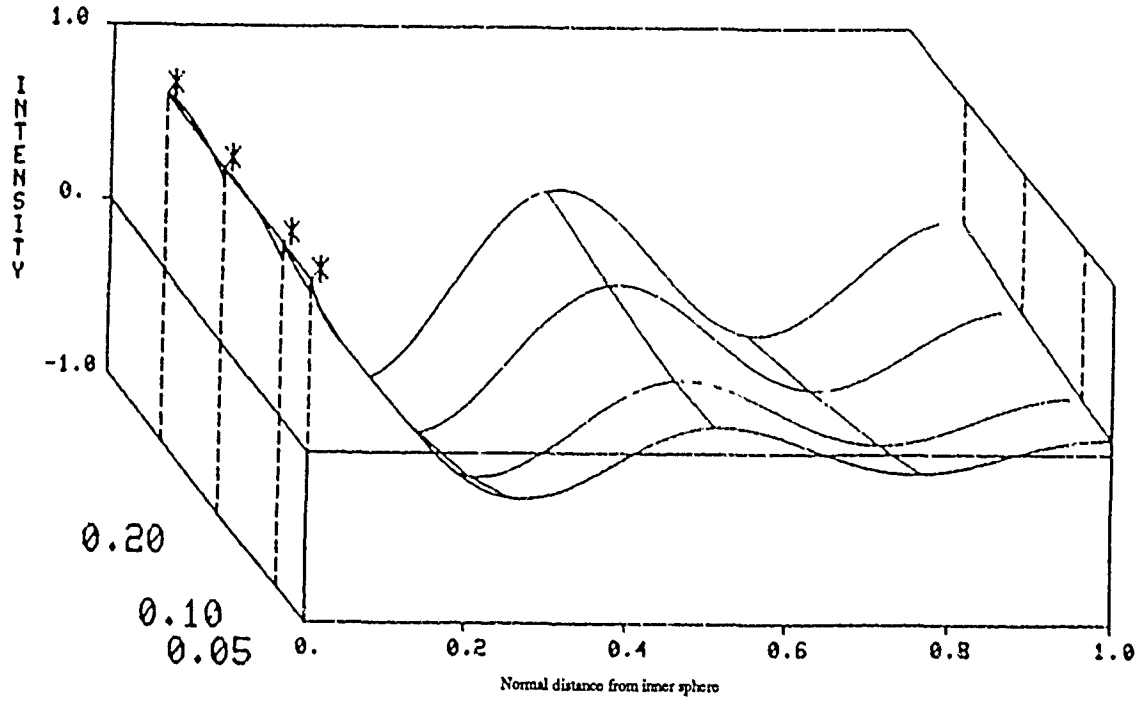

H transverse

Figure 36. Distribution of the normalized transverse magnetic field component in the concentric spherical cavity as a function of the inner to outer conductor radii, $R = b/a$, for the TE14 mode. Asterisk indicates peak value of field with d.

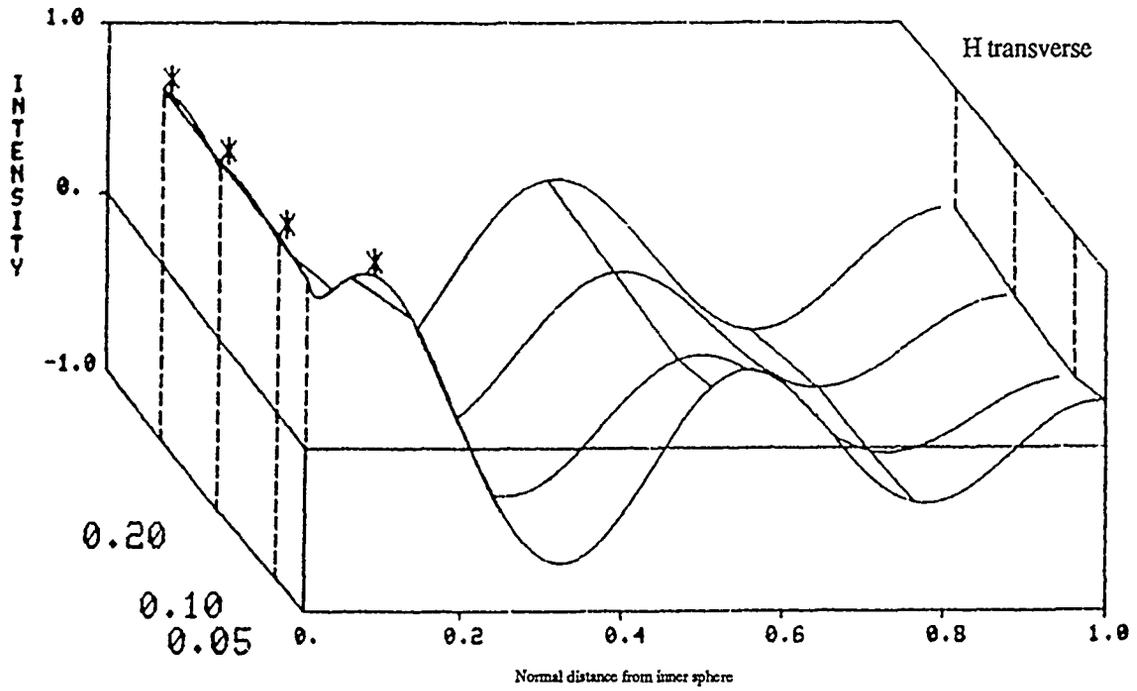

Figure 37. Distribution of the normalized transverse magnetic field component in the concentric spherical cavity as a function of the inner to outer conductor radii, $R = b/a$, for the TE24 mode. Asterisk indicates peak value of field with d.

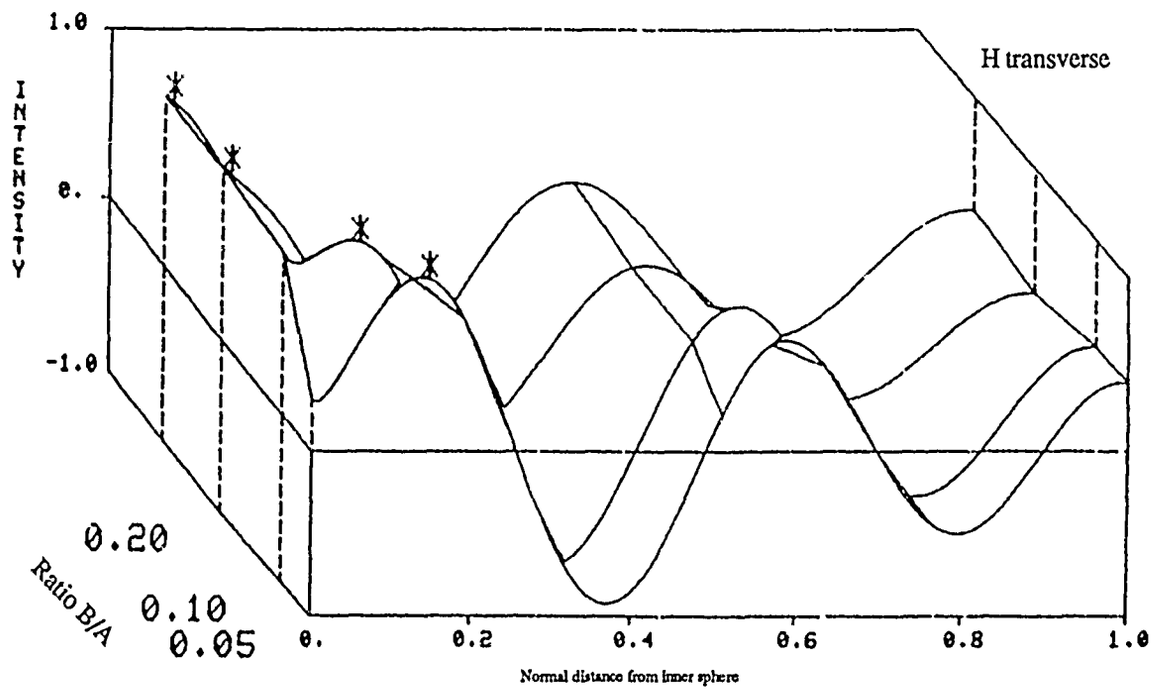

Figure 38. Distribution of the normalized transverse magnetic field component in the concentric spherical cavity as a function of the inner to outer conductor radii, $R = b/a$, for the TE34 mode. Asterisk indicates peak value of field with d.

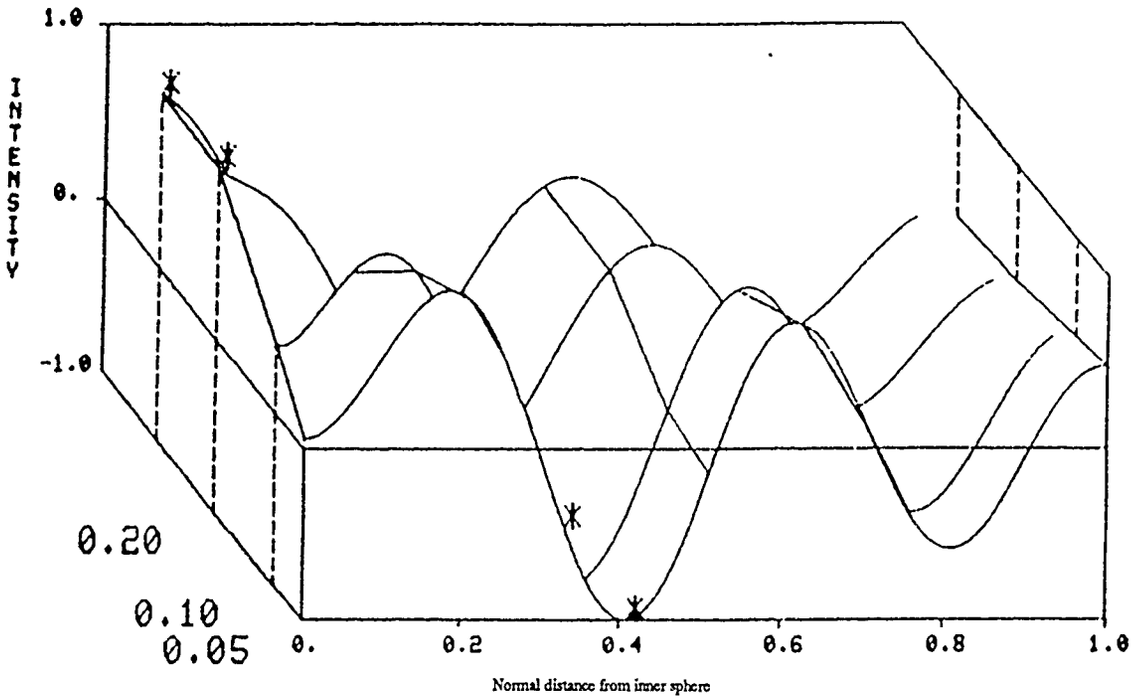

H transverse

Figure 39. Distribution of the normalized transverse magnetic field component in the concentric spherical cavity as a function of the inner to outer conductor radii, $R = b/a$, for the TE44 mode. Asterisk indicates peak value of field with d.

3.3 Radial Magnetic Field Component for TEnp Modes

3.3.1 The p = 1 H-Radial TEnp Eigenfields for n = 1 to 5

As was mentioned in section 2.2, the longitudinal or radial magnetic field component is easily derived from the transverse electric field function. The relationship is basically that the normalized radial H-field can be obtained from the normalized transverse E-field through division by the normalized radius, r/a. Thus, we expect the radial component to resemble the transverse, with the radial H-field strength enhanced from the transverse E, more so for smaller values of r/a than for larger. On the field plots of figures 40 to 44 for $p = 1$, one therefore observes the radial H-field more enhanced for smaller renormalized radial parameter d, and also for smaller b/a because of the way we defined d. Hence the surface plots resemble "tunnels" which are somewhat distorted in shape from those of the transverse E-field. And, due to the a/r multiplicative factor, the peak values of these field components lie on somewhat smaller values of d from the transverse E-field.

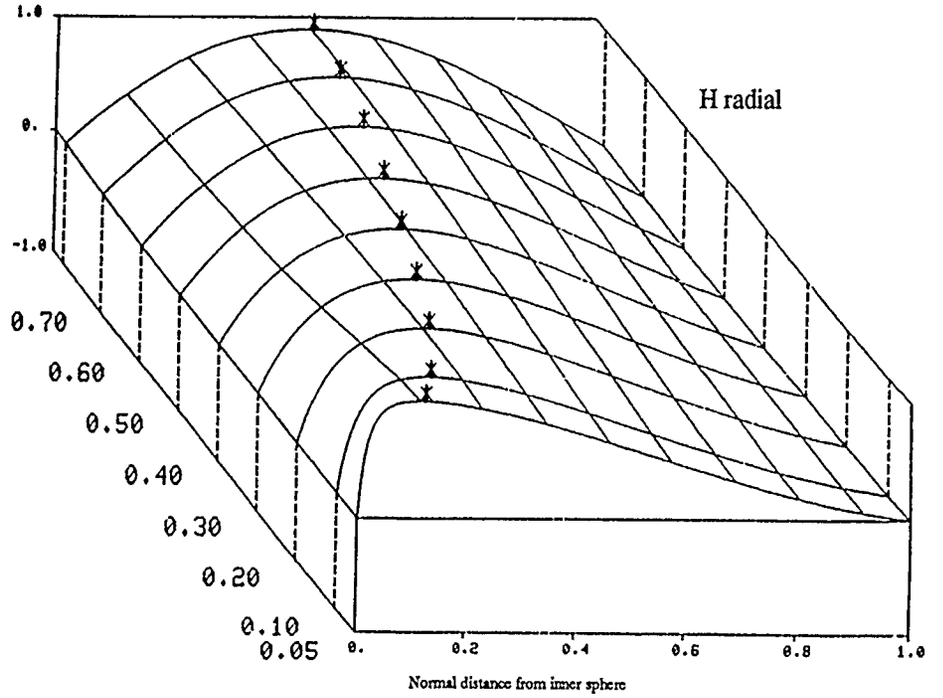

Figure 40. Distribution of the normalized radial magnetic field component in the concentric spherical cavity as a function of the inner to outer conductor radii, $R = b/a$, for the TE11 mode. Asterisk indicates peak value of field with d.

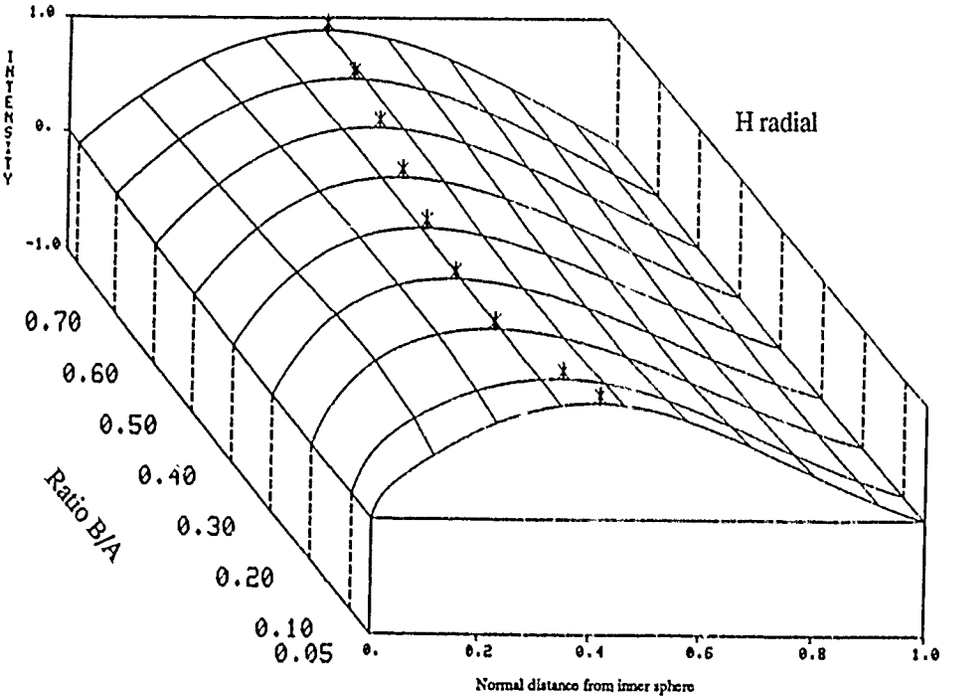

Figure 41. Distribution of the normalized radial magnetic field component in the concentric spherical cavity as a function of the inner to outer conductor radii, $R = b/a$, for the TE21 mode. Asterisk indicates peak value of field with d.

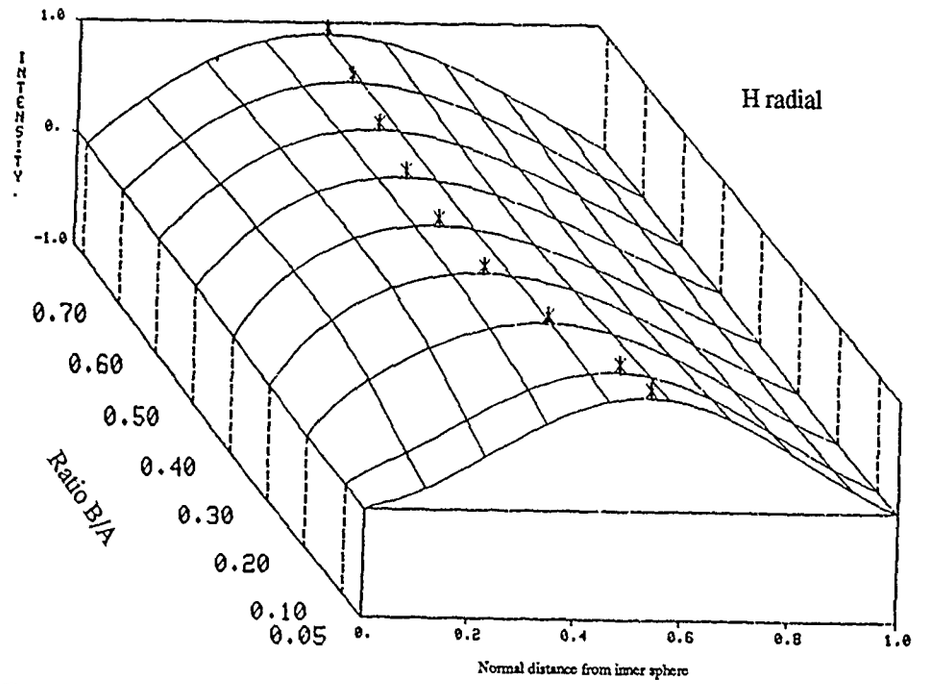

Figure 42. Distribution of the normalized radial magnetic field component in the concentric spherical cavity as a function of the inner to outer conductor radii, $R = b/a$, for the TE31 mode. Asterisk indicates peak value of field with d.

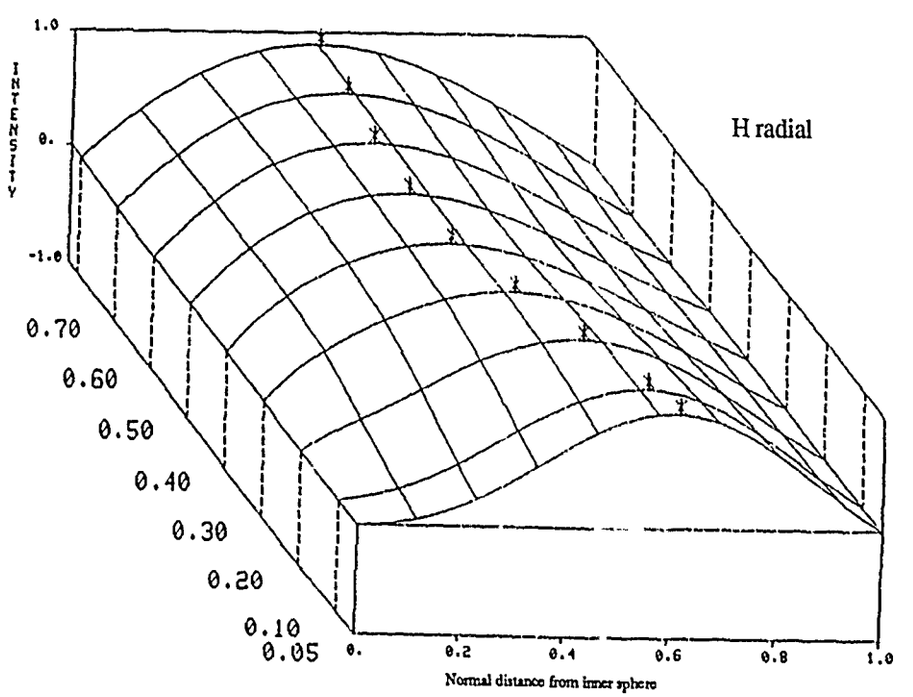

Figure 43. Distribution of the normalized radial magnetic field component in the concentric spherical cavity as a function of the inner to outer conductor radii, $R = b/a$, for the TE41 mode. Asterisk indicates peak value of field with d.

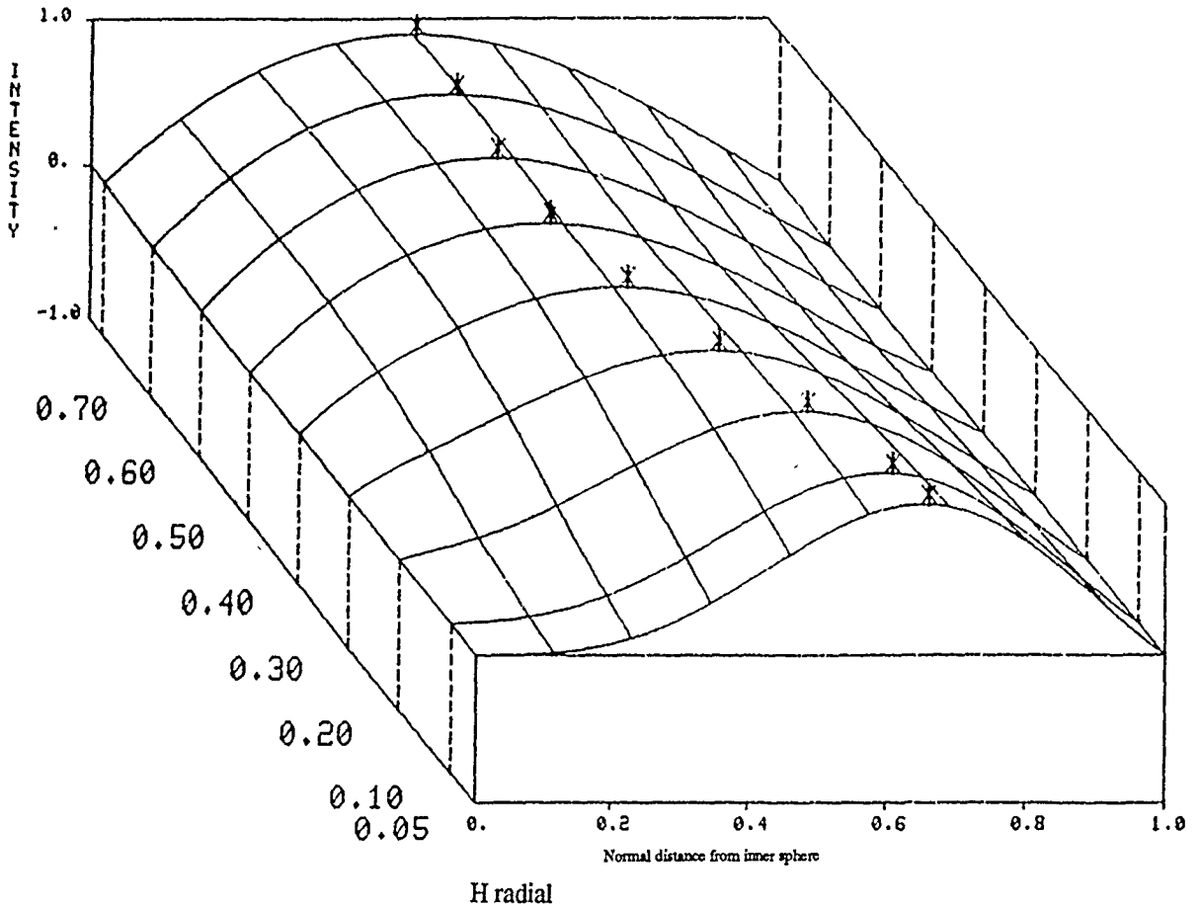

Figure 44. Distribution of the normalized radial magnetic field component in the concentric spherical cavity as a function of the inner to outer conductor radii, $R = b/a$, for the TE51 mode. Asterisk indicates peak value of field with d.

3.3.2 The H-Radial TEnp Eigenfields for Higher Families of Modes

The H-radial field components continue to resemble the transverse E-fields when p is increased by 1, in the same manner and for the same reason. That is, they are related to the latter component by division by r/a, and are therefore enhanced from E-transverse; more for smaller values of d than for larger. These components are more oscillatory than for $p = 1$, as expected, and their peak value with d occurs on the closest local maximum to the inner wall, as it did in E-transverse. The local maxima occur at somewhat lower values of d than in E-transverse, due to the nature of the a/r relationship. Figures 45 through 54 display the H-radial component of the eigenfields for $p = 2$ and 3 and for n between 1 and 5. Figures 55 through 58 show these components for $p = 4$ when n varies between 1 and 4.

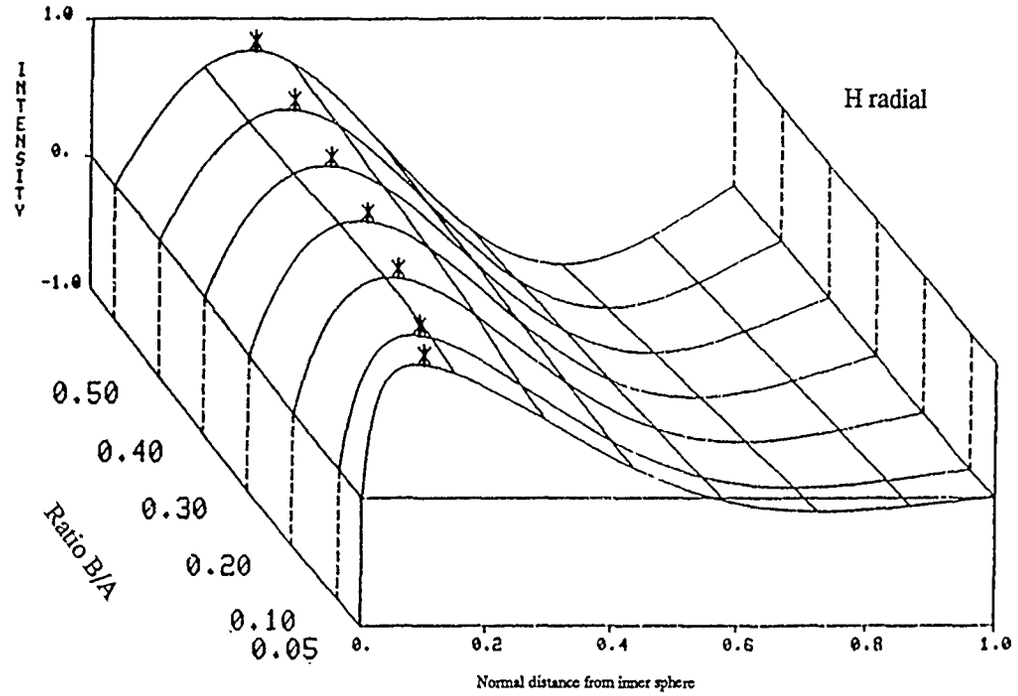

Figure 45. Distribution of the normalized radial magnetic field component in the concentric spherical cavity as a function of the inner to outer conductor radii, $R = b/a$, for the TE12 mode. Asterisk indicates peak value of field with d.

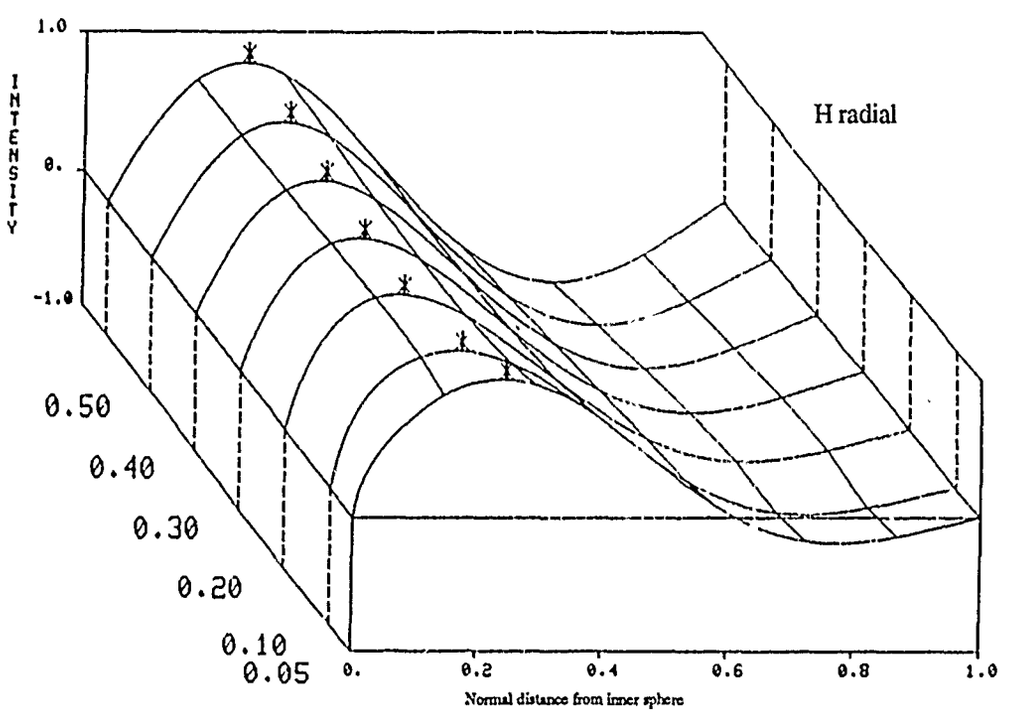

Figure 46. Distribution of the normalized radial magnetic field component in the concentric spherical cavity as a function of the inner to outer conductor radii, $R = b/a$, for the TE22 mode. Asterisk indicates peak value of field with d.

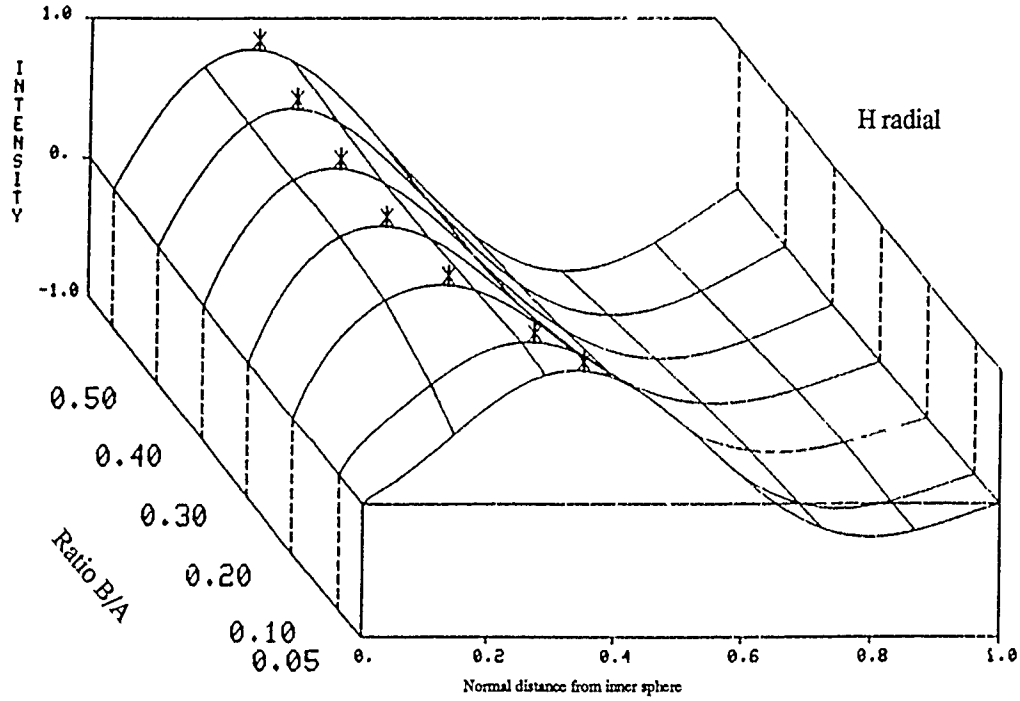

Figure 47. Distribution of the normalized radial magnetic field component in the concentric spherical cavity as a function of the inner to outer conductor radii, $R = b/a$, for the TE32 mode. Asterisk indicates peak value of field with d.

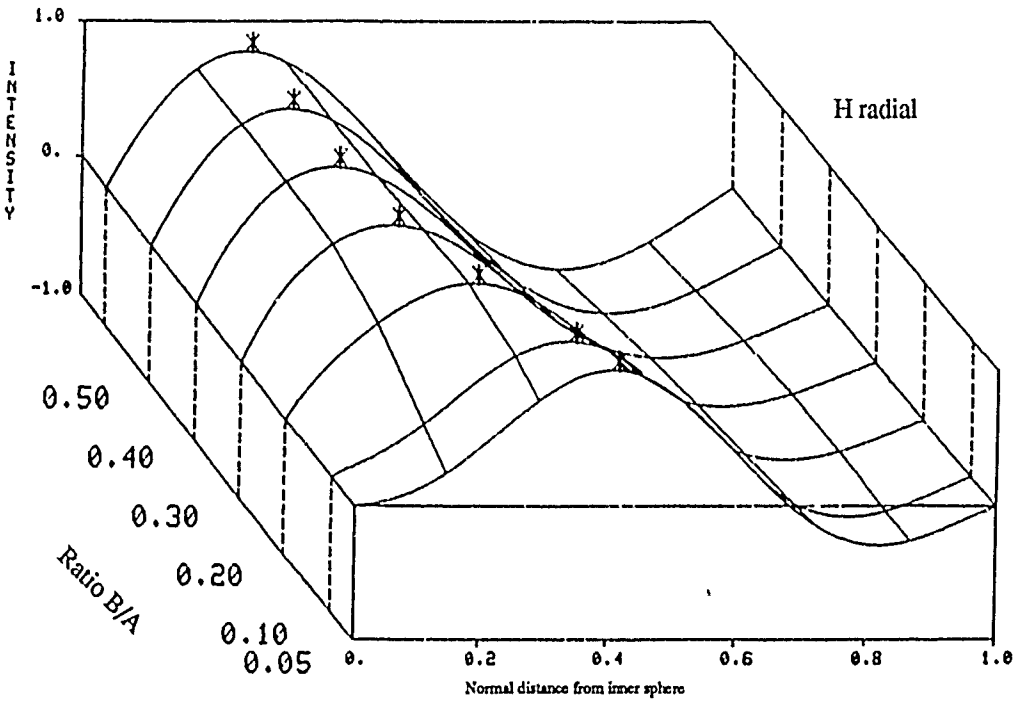

Figure 48. Distribution of the normalized radial magnetic field component in the concentric spherical cavity as a function of the inner to outer conductor radii, $R = b/a$, for the TE42 mode. Asterisk indicates peak value of field with d.

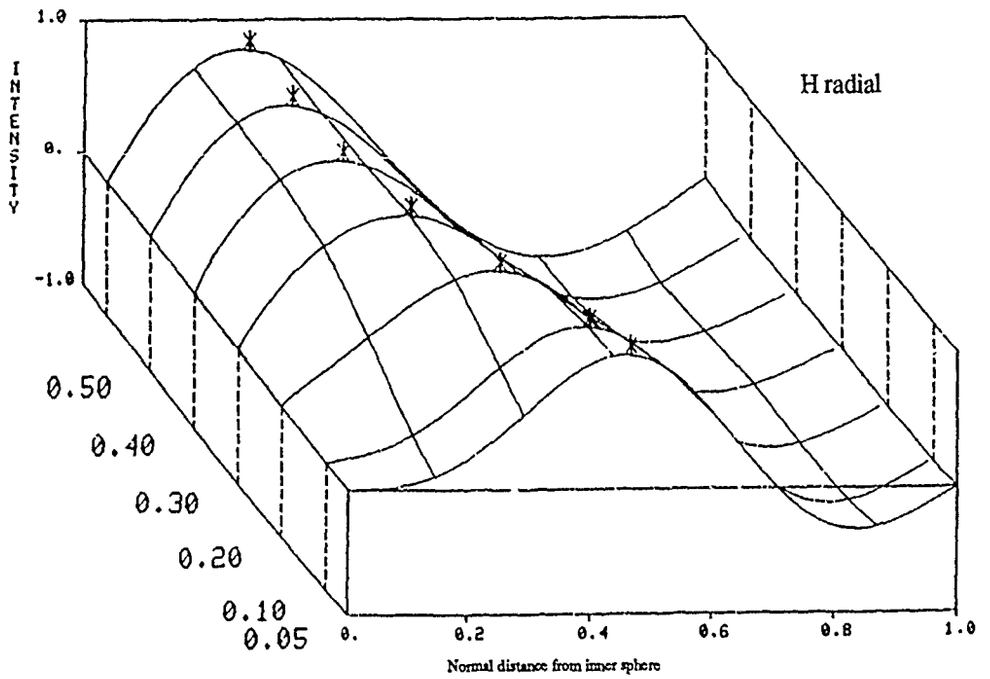

Figure 49. Distribution of the normalized radial magnetic field component in the concentric spherical cavity as a function of the inner to outer conductor radii, $R = b/a$, for the TE52 mode. Asterisk indicates peak value of field with d.

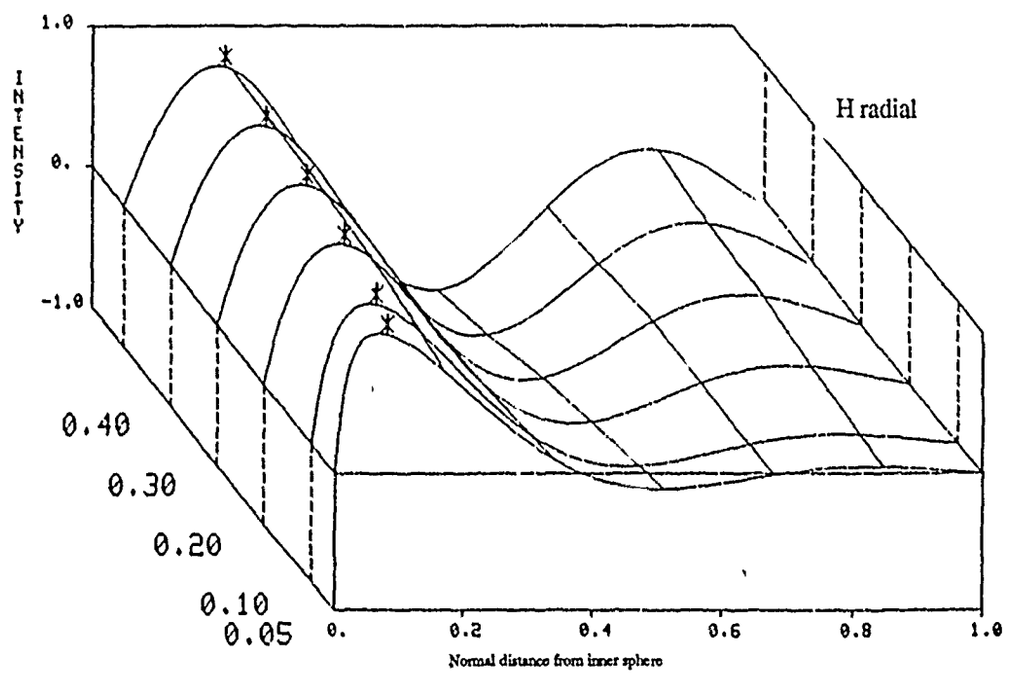

Figure 50. Distribution of the normalized radial magnetic field component in the concentric spherical cavity as a function of the inner to outer conductor radii, $R = b/a$, for the TE13 mode. Asterisk indicates peak value of field with d.

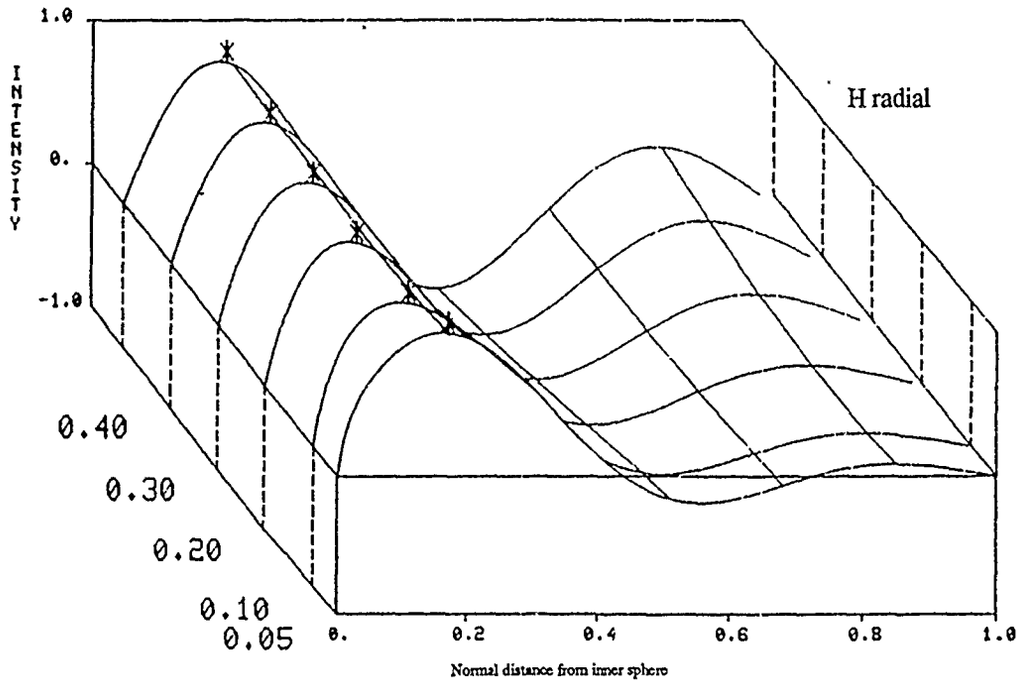

Figure 51. Distribution of the normalized radial magnetic field component in the concentric spherical cavity as a function of the inner to outer conductor radii, $R = b/a$, for the TE23 mode. Asterisk indicates peak value of field with d.

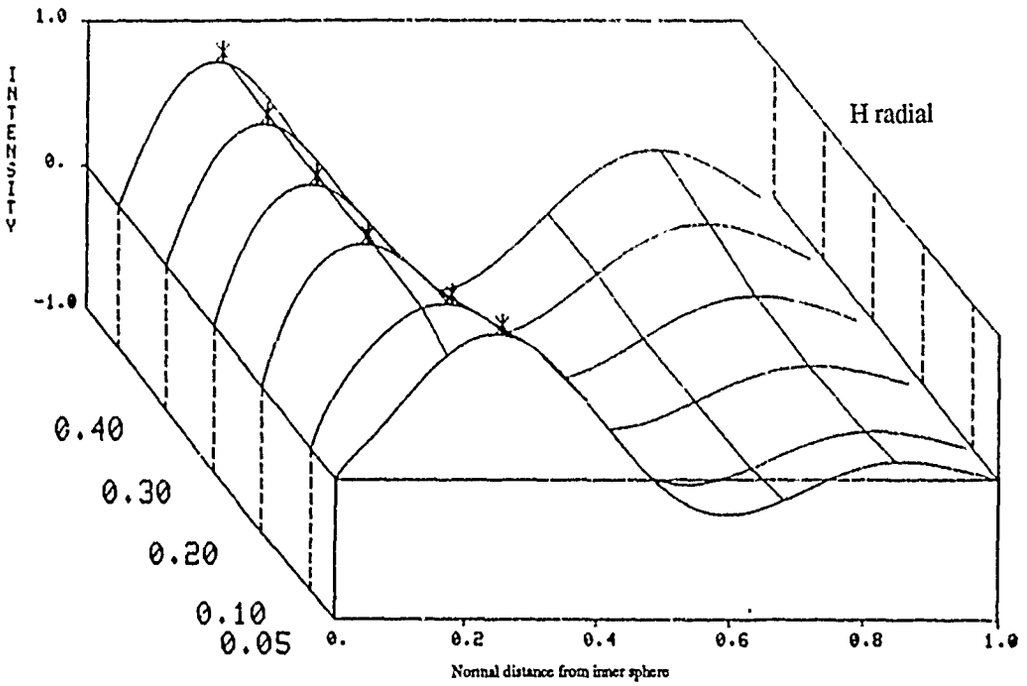

Figure 52. Distribution of the normalized radial magnetic field component in the concentric spherical cavity as a function of the inner to outer conductor radii, $R = b/a$, for the TE33 mode. Asterisk indicates peak value of field with d.

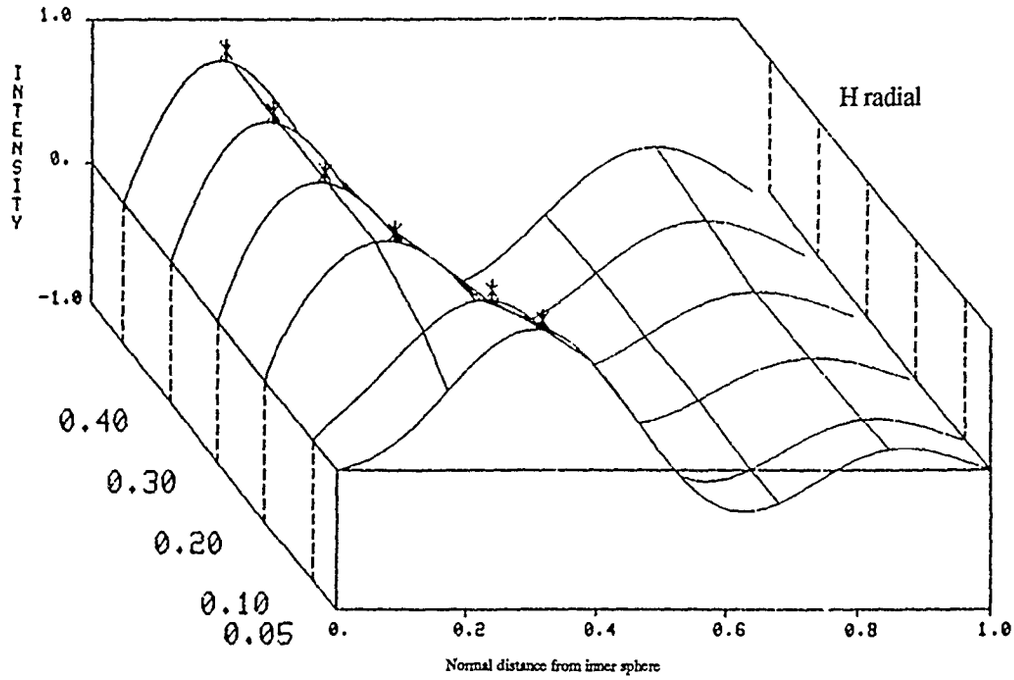

Figure 53. Distribution of the normalized radial magnetic field component in the concentric spherical cavity as a function of the inner to outer conductor radii, $R = b/a$, for the TE43 mode. Asterisk indicates peak value of field with d.

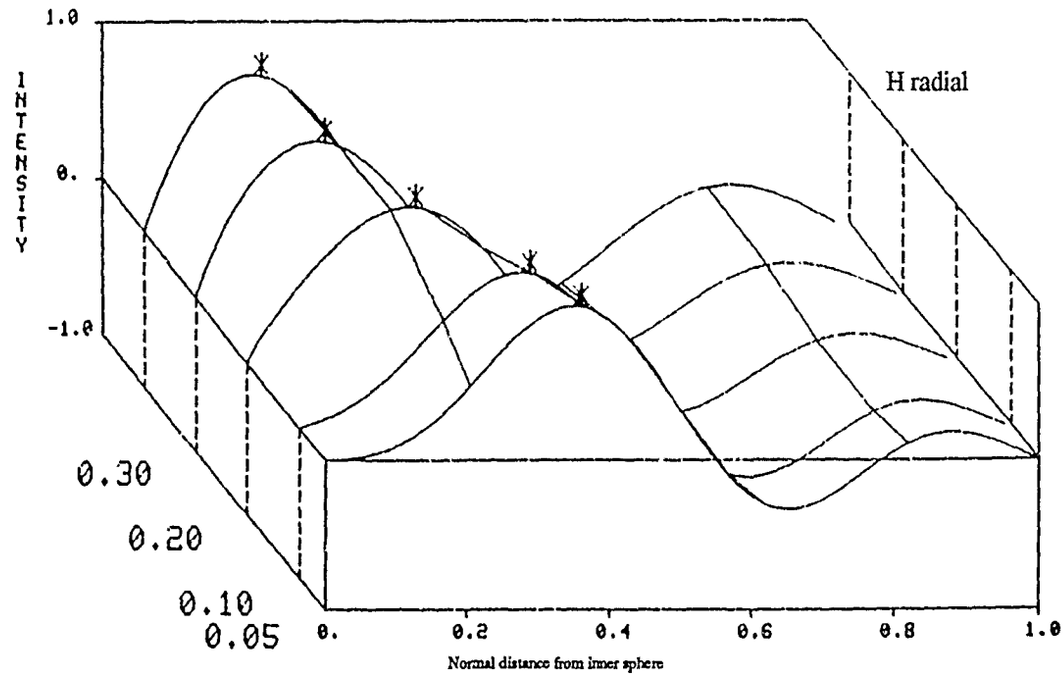

Figure 54. Distribution of the normalized radial magnetic field component in the concentric spherical cavity as a function of the inner to outer conductor radii, $R = b/a$, for the TE53 mode. Asterisk indicates peak value of field with d.

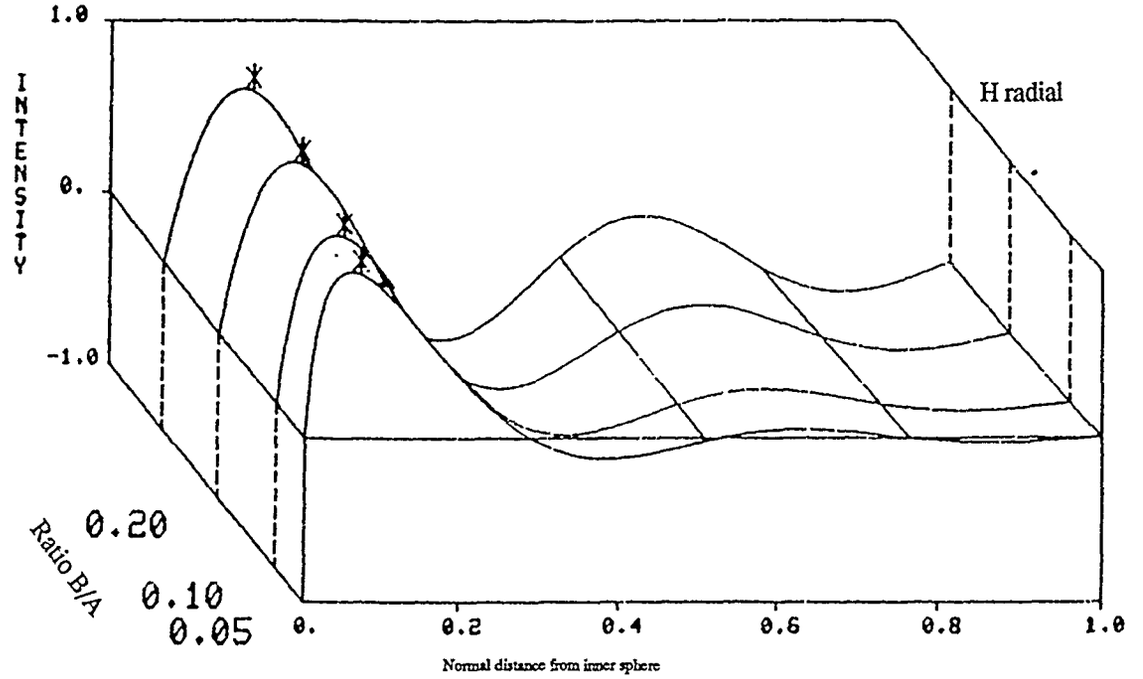

Figure 55. Distribution of the normalized radial magnetic field component in the concentric spherical cavity as a function of the inner to outer conductor radii, $R = b/a$, for the TE14 mode. Asterisk indicates peak value of field with d.

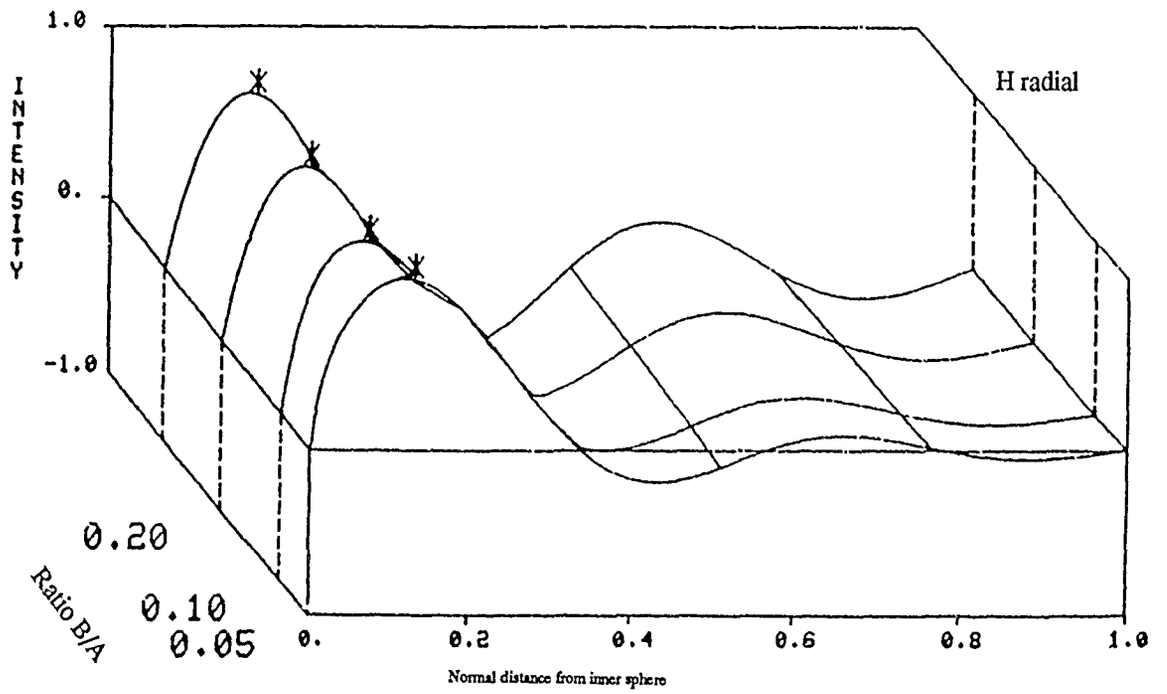

Figure 56. Distribution of the normalized radial magnetic field component in the concentric spherical cavity as a function of the inner to outer conductor radii, $R = b/a$, for the TE24 mode. Asterisk indicates peak value of field with d.

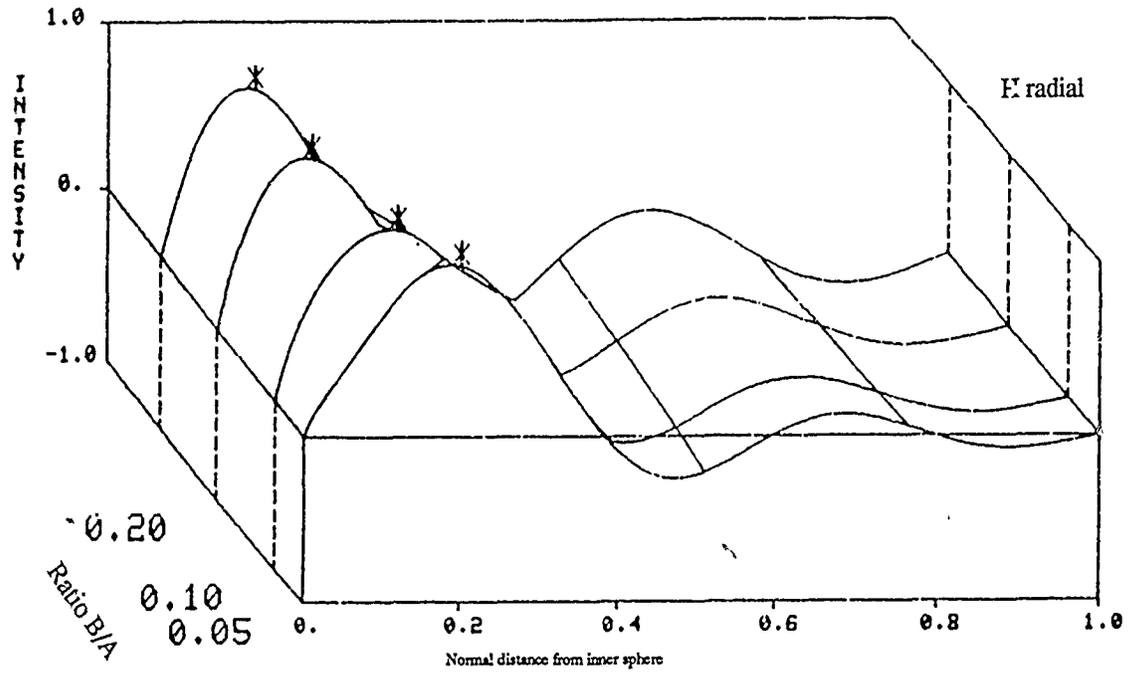

Figure 57. Distribution of the normalized radial magnetic field compone.t in the concentric spherical cavity as a function of the inner to outer conductor radii, $R = b/a$, for the TE34 mode. Asterisk indicates peak value of field with d.

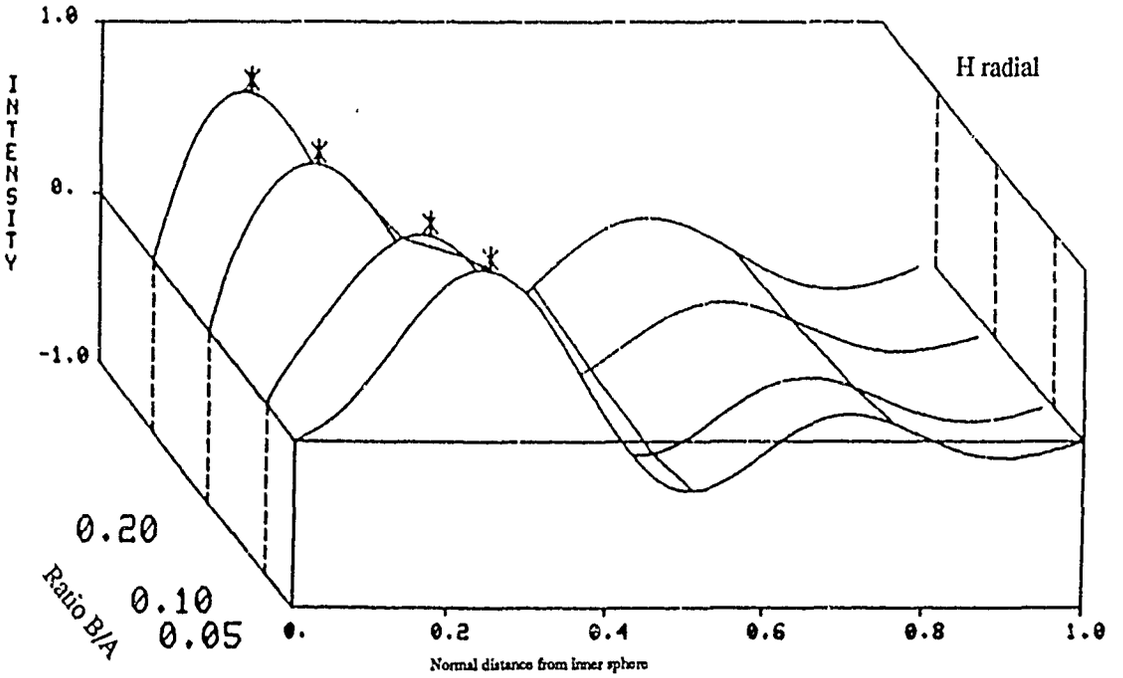

Figure 58. Distribution of the normalized radial magnetic field component in the concentric spherical cavity as a function of the inner to outer conductor radii, $R = b/a$, for the TE44 mode. Asterisk indicates peak value of field with d.

4. Radial Distribution for TM Field Components

4.1 Transverse Magnetic Field Component for TMnp Modes

4.1.1 The p = 1 H-Transverse TMnp Eigenfields for n = 1 to 7

The TM11 is the dominant mode of the concentric cavity system. Figure 59 displays the transverse magnetic field component for the TM11 mode. For $b/a > 0.25$, it resembles the H-transverse of the TE11, in that it is maximum on the inner conducting wall ($d = 0$), and decreases monotonically to the outer conducting wall ($d = 1$). There is no slight upturn near the outer wall as in the TE case. If we were to decrease b/a below 0.2, however, another local maximum emerges, not far from the outer conductor. This local maximum is also the absolute maximum of H-transverse, for the smaller values of b/a for which it was computed here (i.e., $0.05 < b/a < 0.15$).

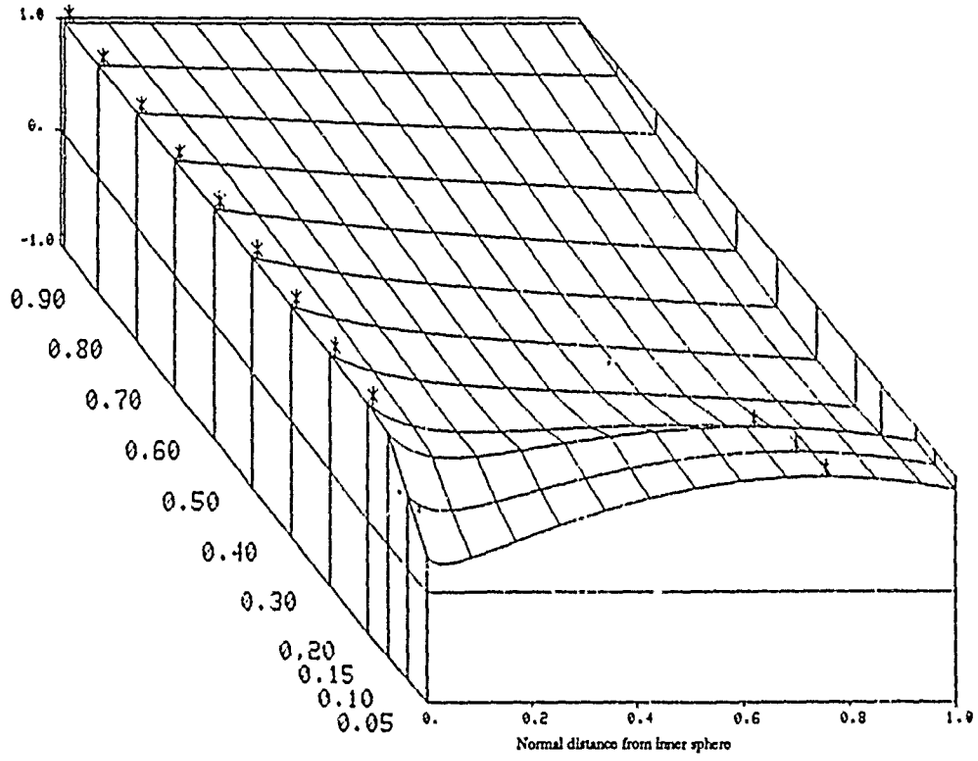

H transverse

Figure 59. Distribution of the normalized transverse magnetic field component in the concentric spherical cavity as a function of the inner to outer conductor radii, $R = b/a$, for the TM11 mode. Asterisk indicates peak value of field with d.

Increasing n from 1 has similar effects to those seen earlier for the TE_{n1} modes. The local maximum occurs at increasingly larger values of d and over an increasingly larger range of b/a (fig. 60 to 65). If we extend n to 7, as shown in figure 65, the region of "smaller" b/a for which this local maximum exists extends to beyond 0.6, and is located at roughly $d = 0.9$, which is quite close to the outer wall. Somewhere between $b/a = 0.6$ and $b/a = 0.7$ for H-transverse of the TM71 mode, the absolute maximum shifts backs to the inner conducting wall. It is noteworthy that these shifts in absolute maximum from one local peak to another occur in such a way that the location of the absolute maximum in d is not a continuous function of b/a. This has been true for almost all the prior eigenfield plots we studied. More will be said on this point in section 5.

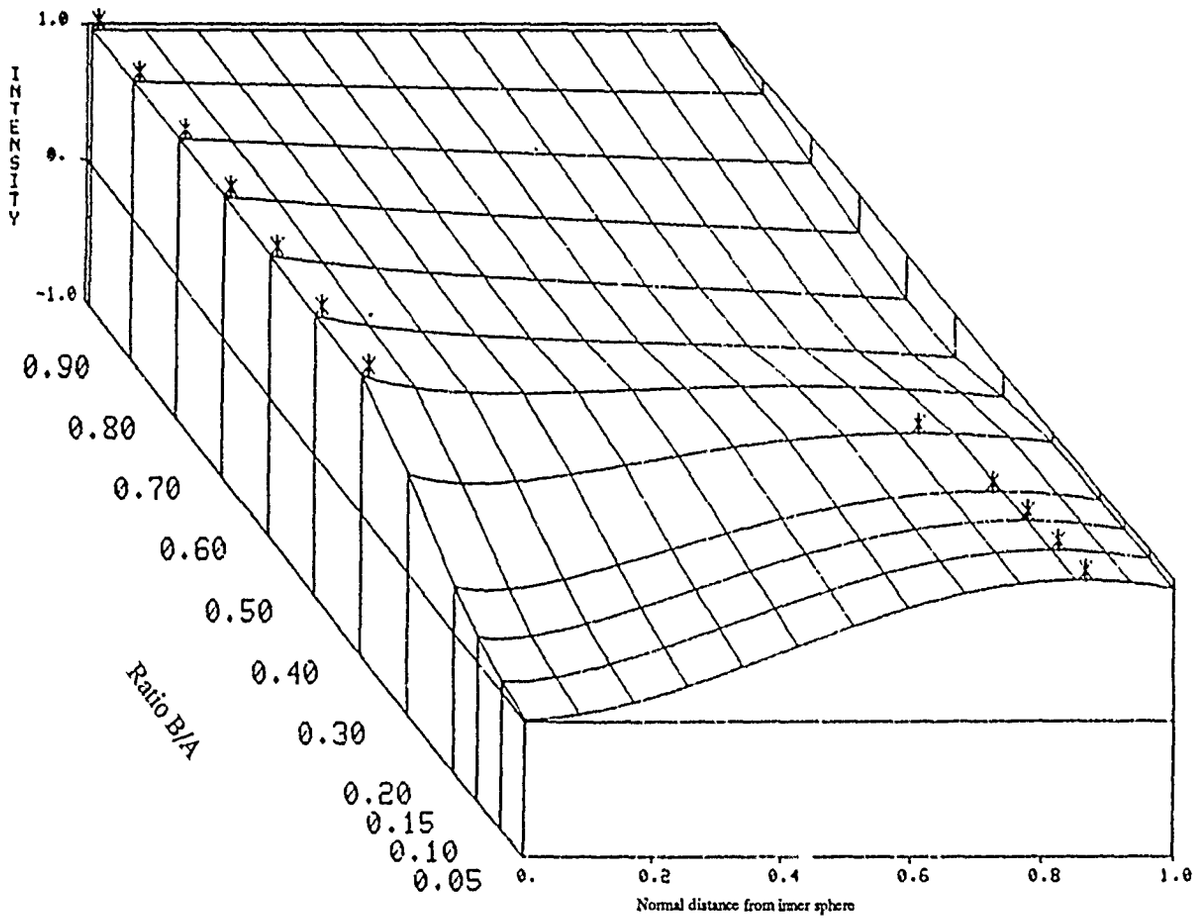

H transverse

Figure 60. Distribution of the normalized transverse magnetic field component in the concentric spherical cavity as a function of the inner to outer conductor radii, $R = b/a$, for the TM21 mode. Asterisk indicates peak value of field with d.

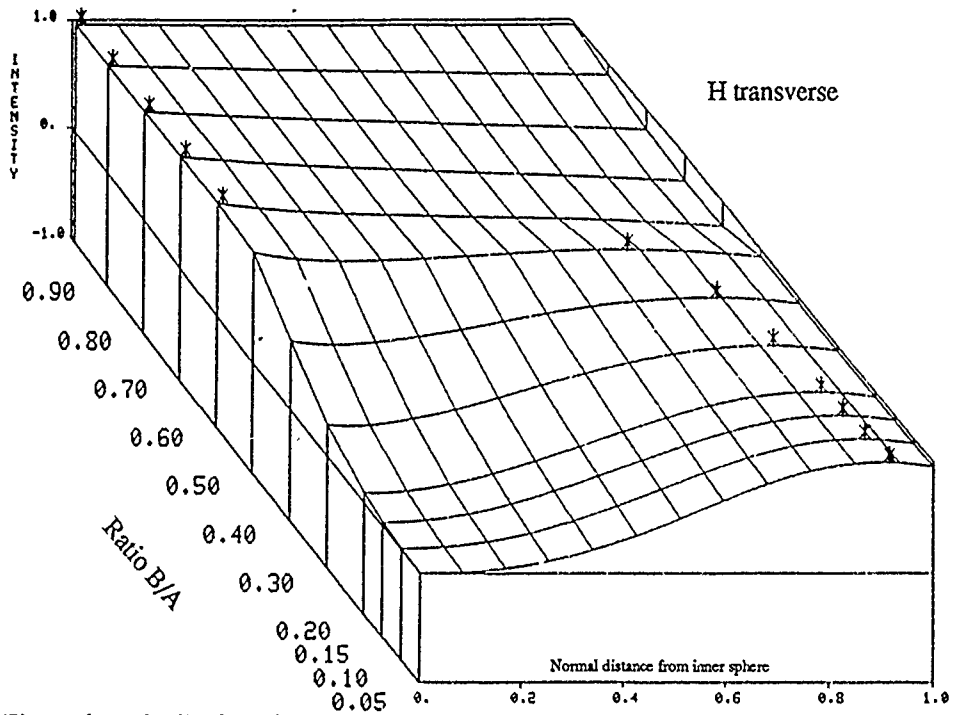

Figure 61. Distribution of the normalized transverse magnetic field component in the concentric spherical cavity as a function of the inner to outer conductor radii, $R = b/a$, for the TM31 mode. Asterisk indicates peak value of field with d.

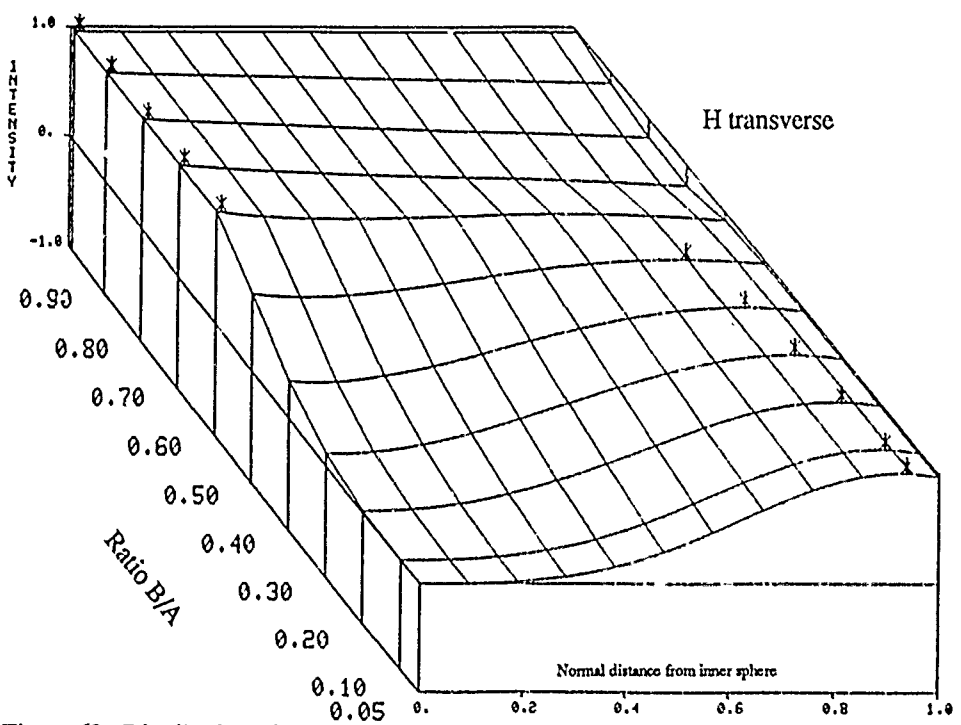

Figure 62. Distribution of the normalized transverse magnetic field component in the concentric spherical cavity as a function of the inner to outer conductor radii, $R = b/a$, for the TM41 mode. Asterisk indicates peak value of field with d.

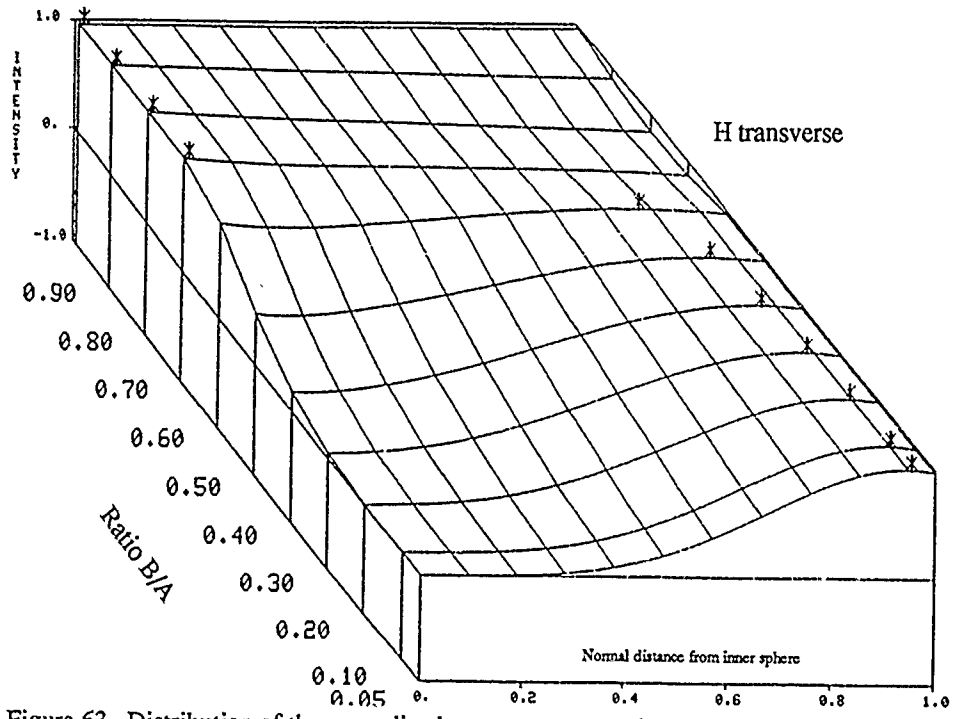

Figure 63. Distribution of the normalized transverse magnetic field component in the concentric spherical cavity as a function of the inner to outer conductor radii, $R = b/a$, for the TM51 mode. Asterisk indicates peak value of field with d.

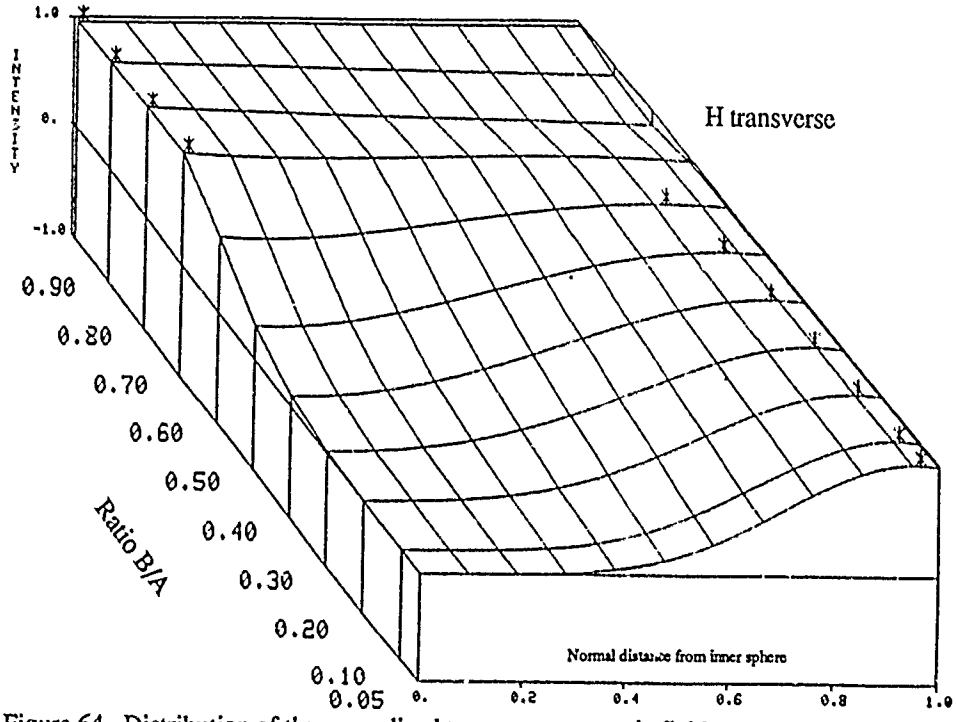

Figure 64. Distribution of the normalized transverse magnetic field component in the concentric spherical cavity as a function of the inner to outer conductor radii, $R = b/a$, for the TM61 mode. Asterisk indicates peak value of field with d.

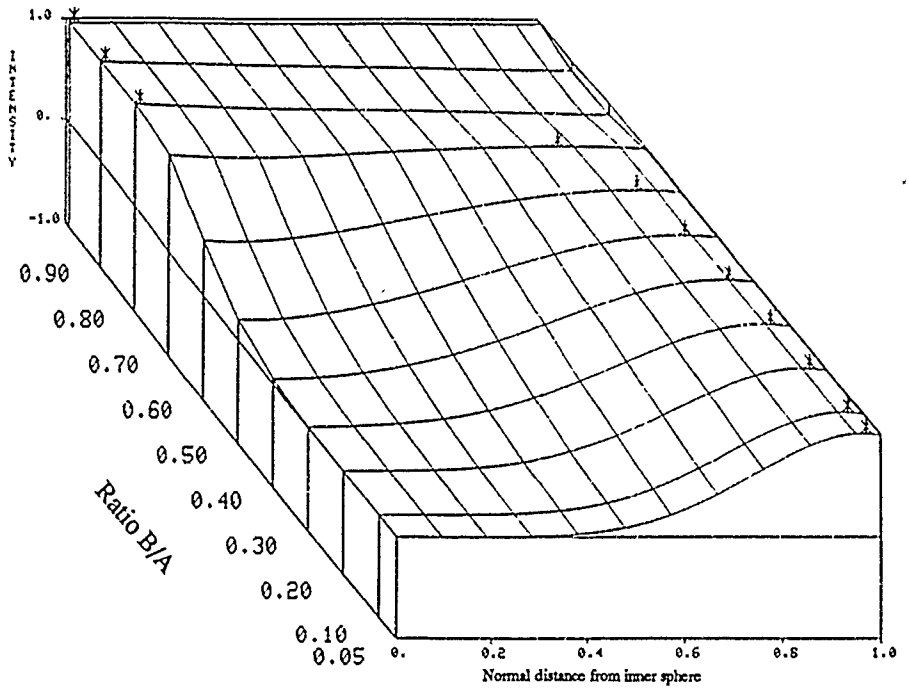

H transverse

Figure 65. Distribution of the normalized transverse magnetic field component in the concentric spherical cavity as a function of the inner to outer conductor radii, $R = b/a$, for the TM71 mode. Asterisk indicates peak value of field with d.

4.1.2 *The p = 2 H-Transverse TMnp Eigenfields for n = 1 to 5*

When p is increased to 2, we obtain, as for the TE modes, an increase in the oscillatory nature of the fields. This is made manifest in the TM12 mode, for example, by the addition of another peak, very close to the outer conducting wall. Thus, for the larger values of b/a, where in the TM11 mode there was a monotonic decrease in the fields from inner to outer conducting wall, there is a small peak at about $d = 0.9$ for the TM12 mode. For smaller values of b/a, where before there were peak values at the inner conductor and at one other local maximum, there are now relative peak values at the inner conductor and at two other local maxima/ minima. The additional peak value, indicated as a local minimum in figure 66, occurs closer to the inner wall (at about $d = 0.3$) than the corresponding peak for the TM11 mode. And this minimum is the location of the absolute maximum of the absolute value of the field component for small b/a, up to about 0.05, before this maximum switches to the inner conductor. When b/a is greater than roughly 0.2, the newly formed minimum disappears entirely.

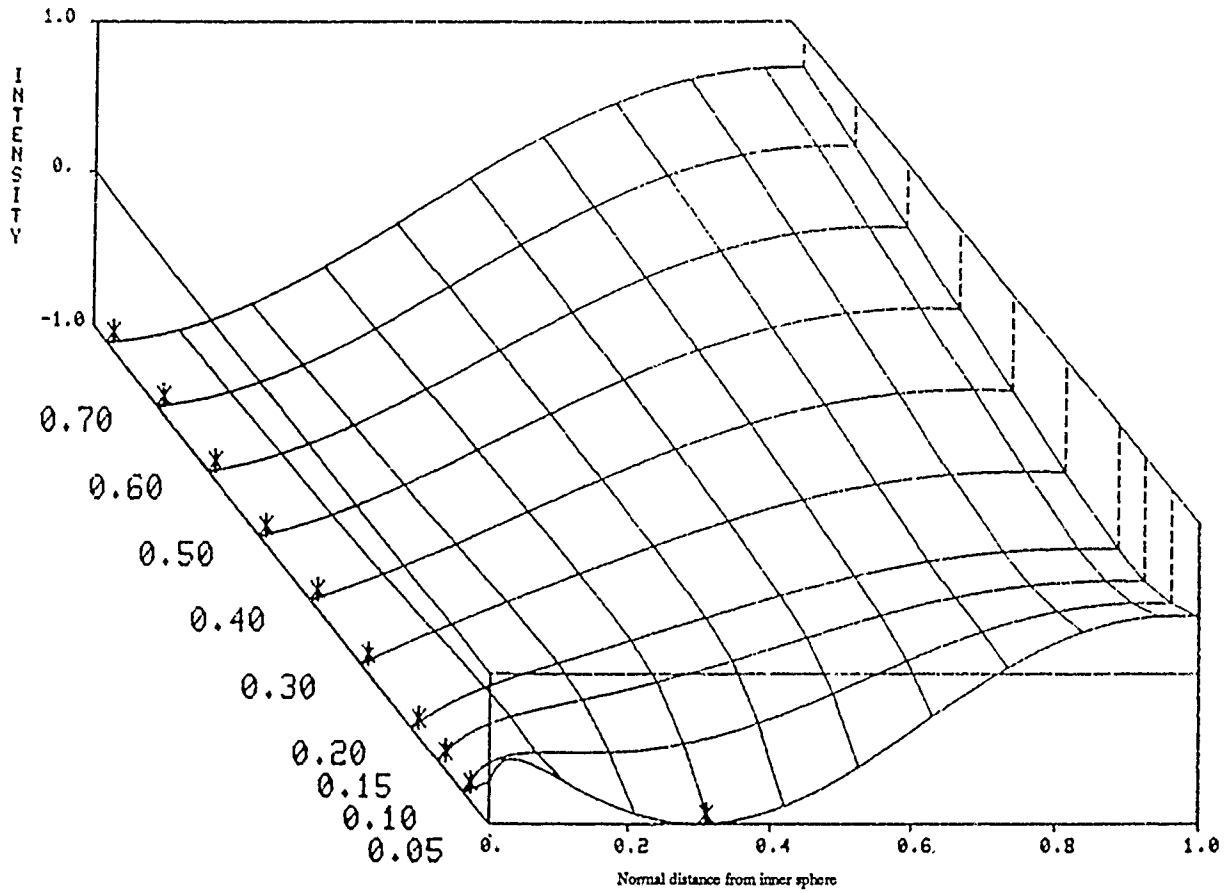

Figure 66. Distribution of the normalized transverse magnetic field component in the concentric spherical cavity as a function of the inner to outer conductor radii, $R = b/a$, for the TM12 mode. Asterisk indicates peak value of field with d.

Increasing n has effects on this TM component which are similar to what was observed in the TE modes. The local peaks shift to slightly higher values in d as n increases. The "new" local minimum extends its range in b/a, until, at $n = 5$, it reaches almost to $b/a = 0.5$ before disappearing. The location of the absolute maximum of the absolute value of the component also remains on the latter mentioned minimum over a greater range in b/a before reverting back to the inner conductor. Figures 67 through 70 illustrate these effects.

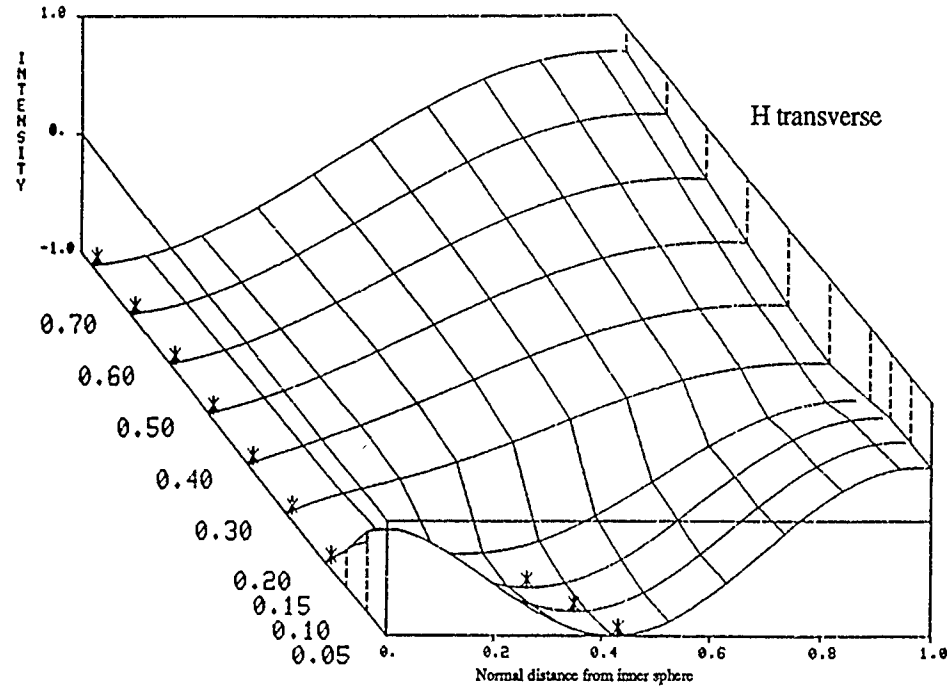

Figure 67. Distribution of the normalized transverse magnetic field component in the concentric spherical cavity as a function of the inner to outer conductor radii, $R = b/a$, for the TM22 mode. Asterisk indicates peak value of field with d.

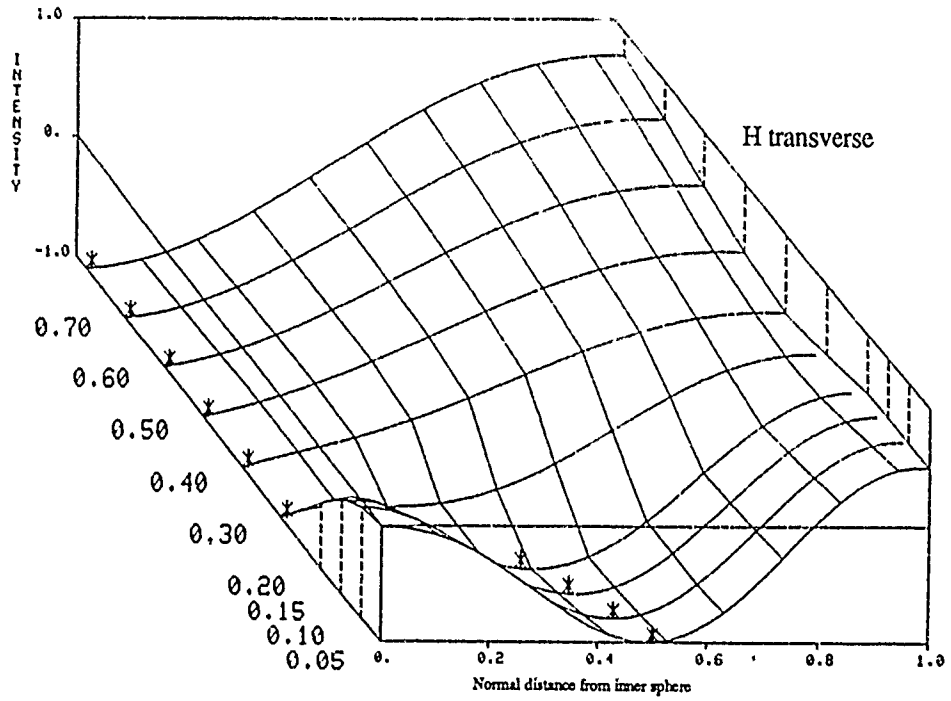

Figure 68. Distribution of the normalized transverse magnetic field component in the concentric spherical cavity as a function of the inner to outer conductor radii, $R = b/a$, for the TM32 mode. Asterisk indicates peak value of field with d.

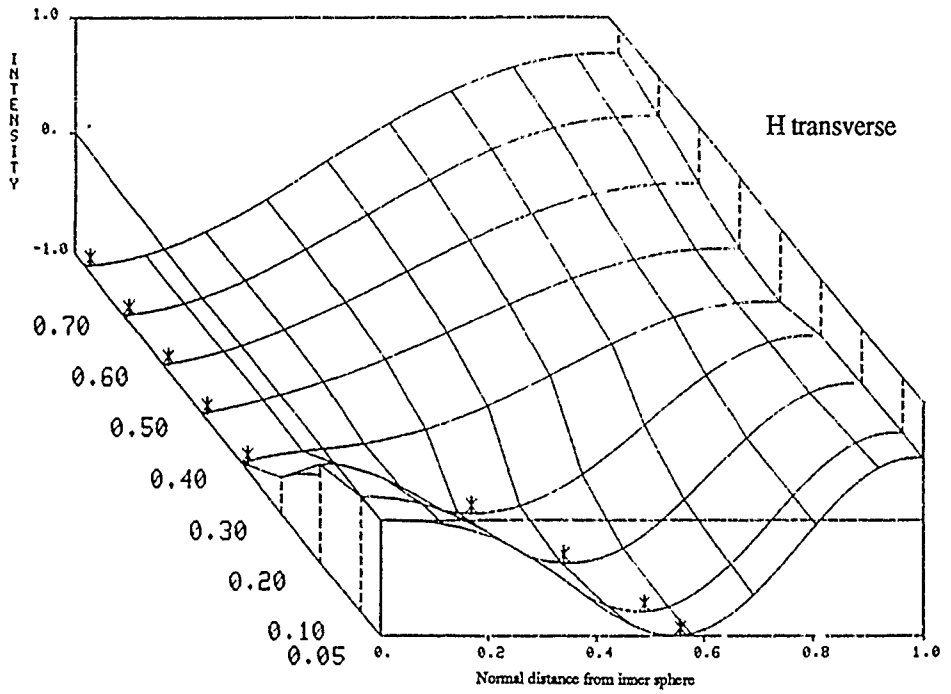

Figure 69. Distribution of the normalized transverse magnetic field component in the concentric spherical cavity as a function of the inner to outer conductor radii, $R = b/a$, for the TM42 mode. Asterisk indicates peak value of field with d.

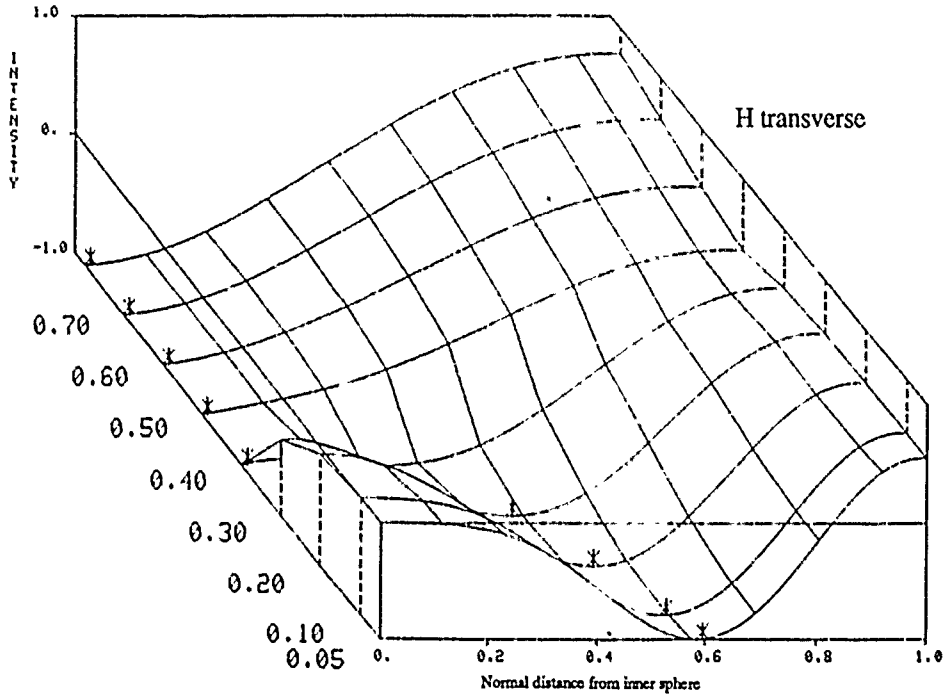

Figure 70. Distribution of the normalized transverse magnetic field component in the concentric spherical cavity as a function of the inner to outer conductor radii, $R = b/a$, for the TM52 mode. Asterisk indicates peak value of field with d.

4.1.3 *The p = 3 H-Transverse TMnp Eigenfields for n = 1 to 5*

We next turn our attention to the TM H-transverse component for $p = 3$, as shown in figures 71 through 75. By now we are expecting to find increased oscillation when we increase p. However, a quick look at the figures gives the impression that the number of local maxima/minima has not increased overall, and that the local maximum which was close to the outer wall when p equalled 2 has been replaced by one around $d = 0.5$ or 0.6, close to the center of the cavity. A more careful examination, though, reveals that there still exists a very small turn, or peak, close to the outer wall, at about $d = 0.95$ or more. Thus the increase in oscillation is still maintained with increased p, although not as pronounced as it was in the TE modes.

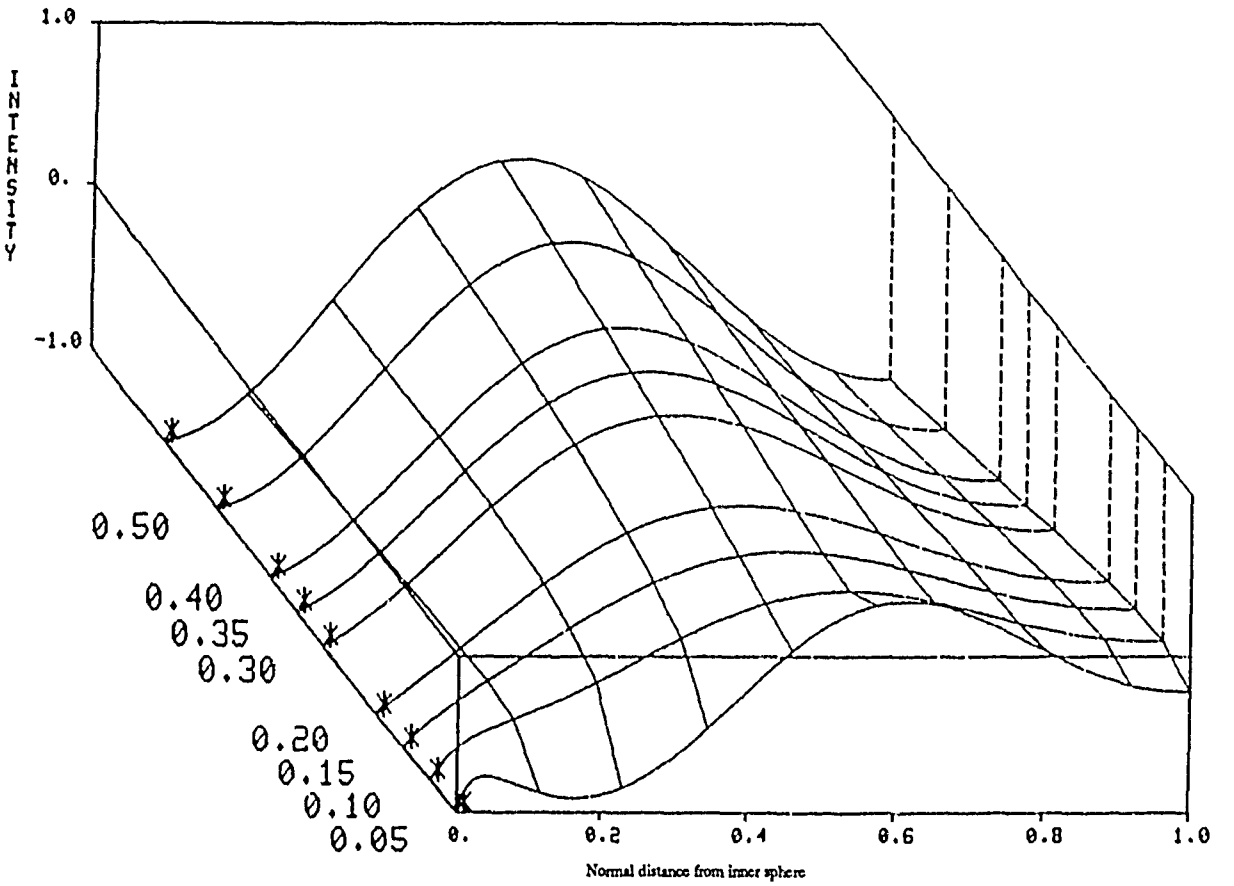

H transverse

Figure 71. Distribution of the normalized transverse magnetic field component in the concentric spherical cavity as a function of the inner to outer conductor radii, $R = b/a$, for the TM13 mode. Asterisk indicates peak value of field with d.

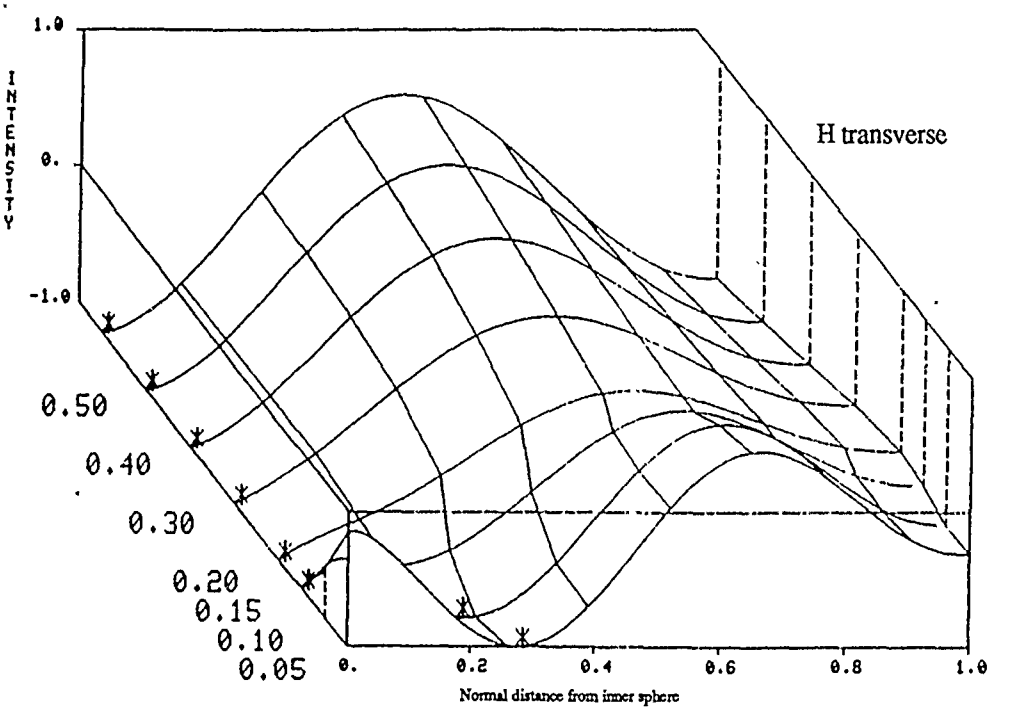

Figure 72. Distribution of the normalized transverse magnetic field component in the concentric spherical cavity as a function of the inner to outer conductor radii, $R = b/a$, for the TM23 mode. Asterisk indicates peak value of field with d.

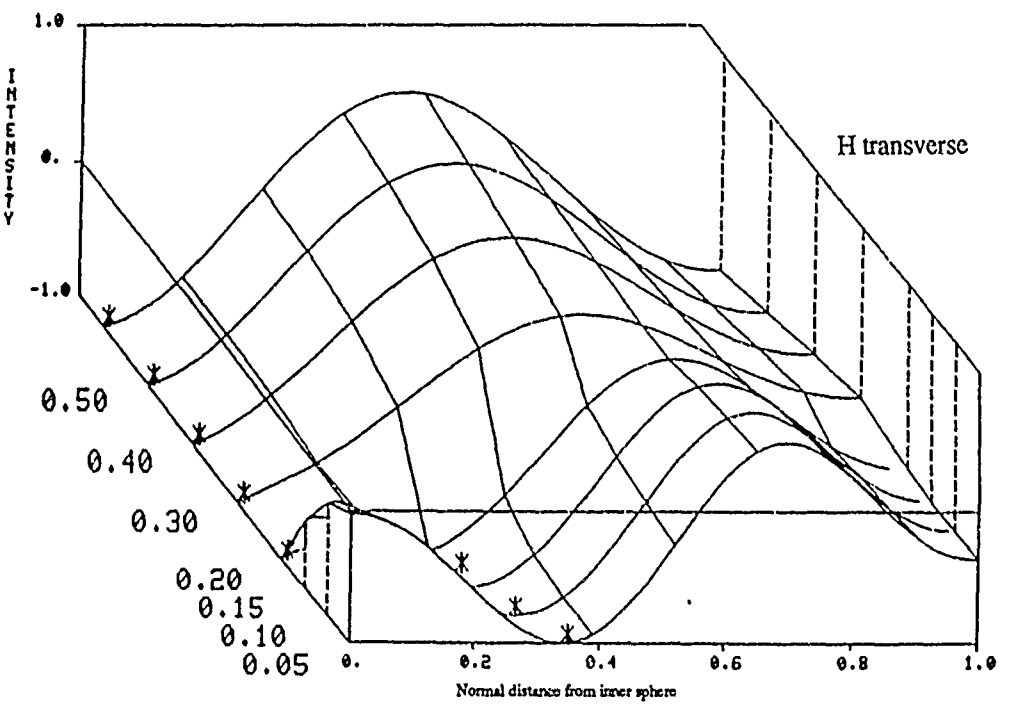

Figure 73. Distribution of the normalized transverse magnetic field component in the concentric spherical cavity as a function of the inner to outer conductor radii, $R = b/a$, for the TM33 mode. Asterisk indicates peak value of field with d.

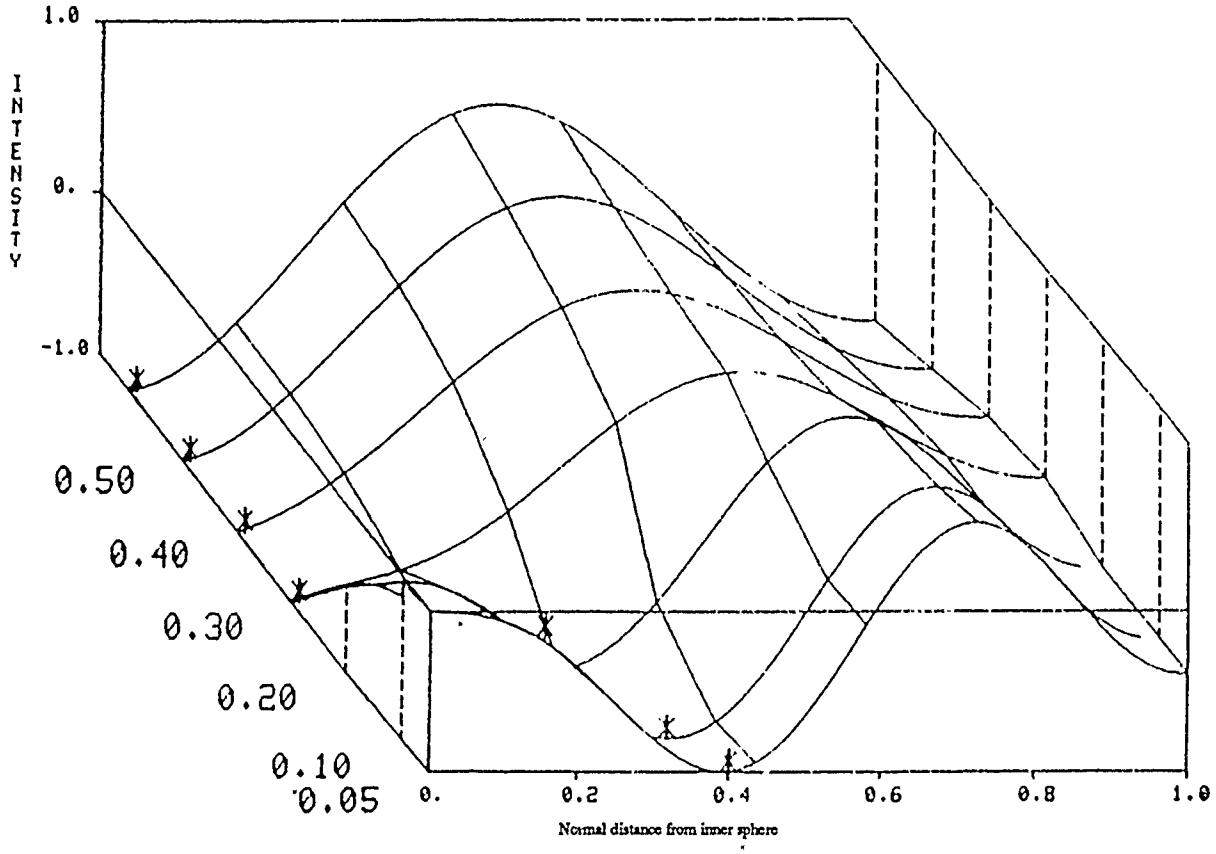

H transverse

Figure 74. Distribution of the normalized transverse magnetic field component in the concentric spherical cavity as a function of the inner to outer conductor radii, $R = b/a$, for the TM43 mode. Asterisk indicates peak value of field with d.

When n is equal to unity, the absolute maximum of the absolute value of the field strength is on the inner conductor for all values of b/a which were solved for $0.05 < b/a < 0.6$. This is in contrast with the TM11 and TM12 cases, whose absolute maxima were located differently for smaller b/a. As in the cases where $p = 1$ and 2, there is a local peak value (at around $d = 0.25$ for $p = 3$) which exists only for smaller values of b/a. When n is increased to 2, the maximum value indeed shifts to this local peak for the smaller values of b/a. As for $p = 1$ and 2, increasing n increases the range in b/a over which the absolute maximum is on this local peak. And increasing n also has the effect of shifting all the interior local peaks to slightly larger values in d.

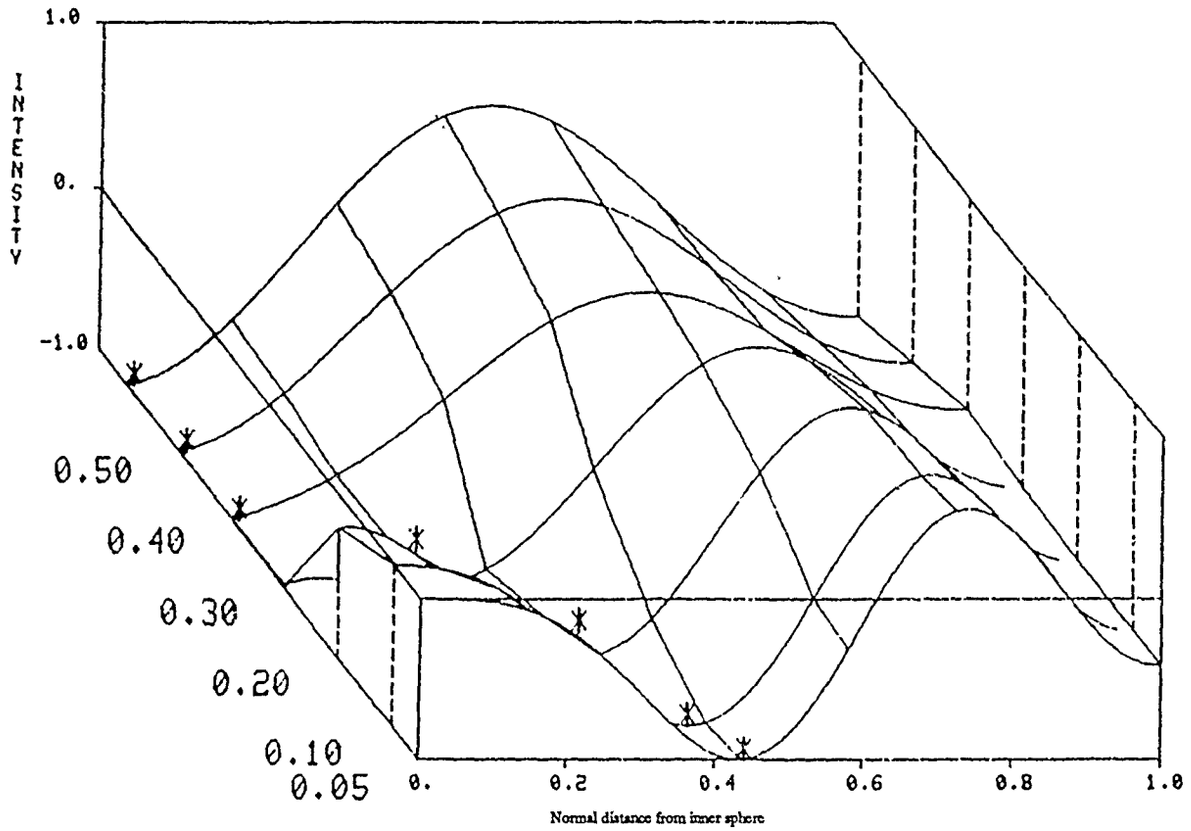

Figure 75. Distribution of the normalized transverse magnetic field component in the concentric spherical cavity as a function of the inner to outer conductor radii, $R = b/a$, for the TM53 mode. Asterisk indicates peak value of field with d.

4.1.4 The p = 4 H-Transverse TMnp Eigenfields for n = 1 to 5

Increasing p to 4 once again adds oscillation in a predictable manner. There exists once again a subtle turn or peak in the curve at $d = 0.95$ or more. There is a local peak added at about $d = 0.7$, another still exists at about 0.4, and then there is the one at about $d = 0.25$ which exists for smaller values of b/a only. The absolute maximum value of the absolute value of the field is on the inner conductor for all b/a calculated when $n = 1$. When n is increased to 2, this absolute maximum is on the next closest peak to the inner wall for smaller values of b/a. As n is increased, the range in b/a for which the absolute maximum exists on this local peak increases, and the local peaks in general shift to locations of slightly larger values of d. See figures 76 through 80.

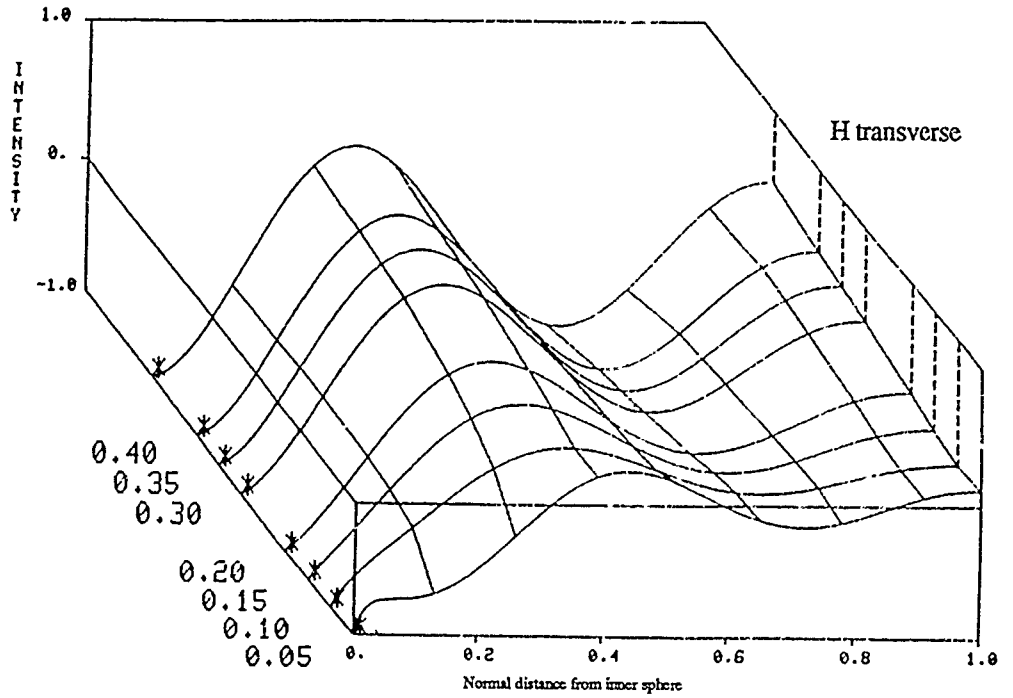

Figure 76. Distribution of the normalized transverse magnetic field component in the concentric spherical cavity as a function of the inner to outer conductor radii, $R = b/a$, for the TM14 mode. Asterisk indicates peak value of field with d.

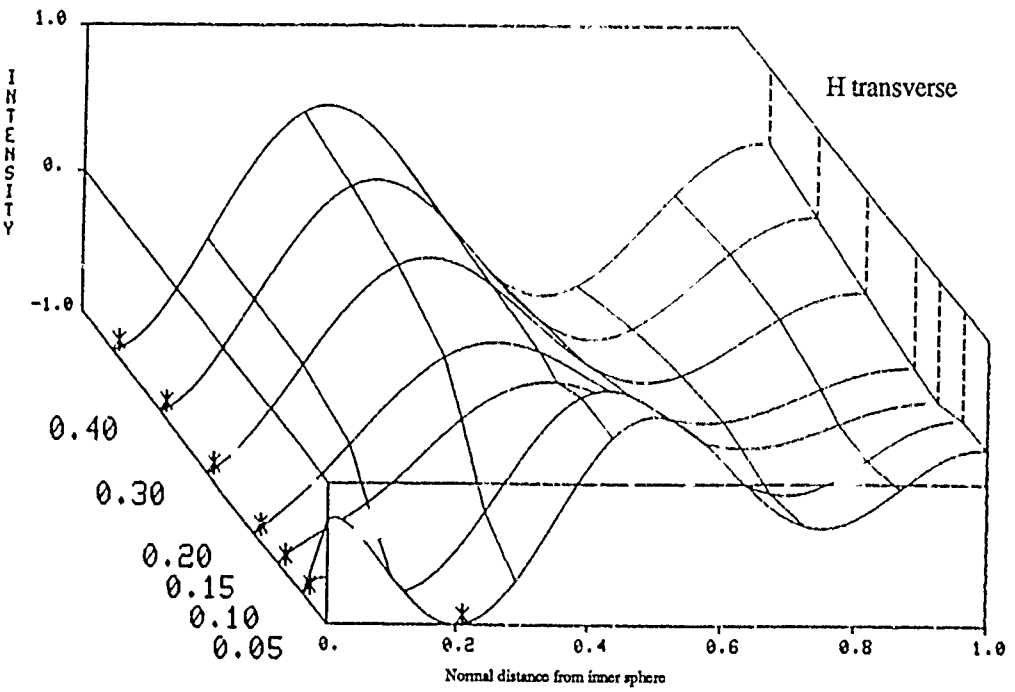

Figure 77. Distribution of the normalized transverse magnetic field component in the concentric spherical cavity as a function of the inner to outer conductor radii, $R = b/a$, or the TM24 mode. Asterisk indicates peak value of field with d.

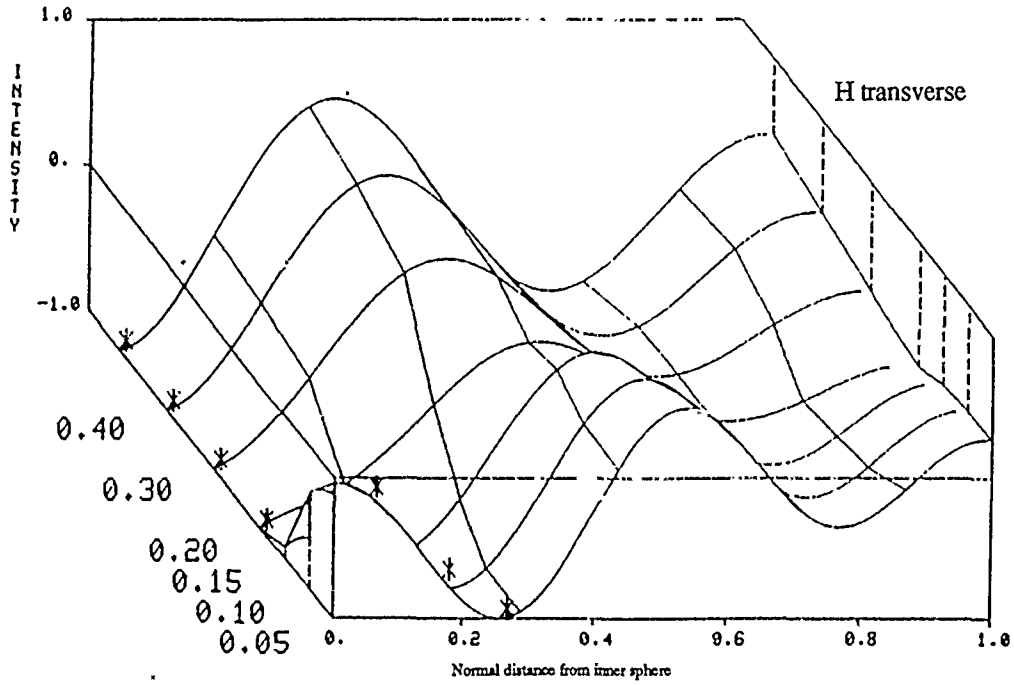

Figure 78. Distribution of the normalized transverse magnetic field component in the concentric spherical cavity as a function of the inner to outer conductor radii, $R = b/a$, for the TM34 mode. Asterisk indicates peak value of field with d.

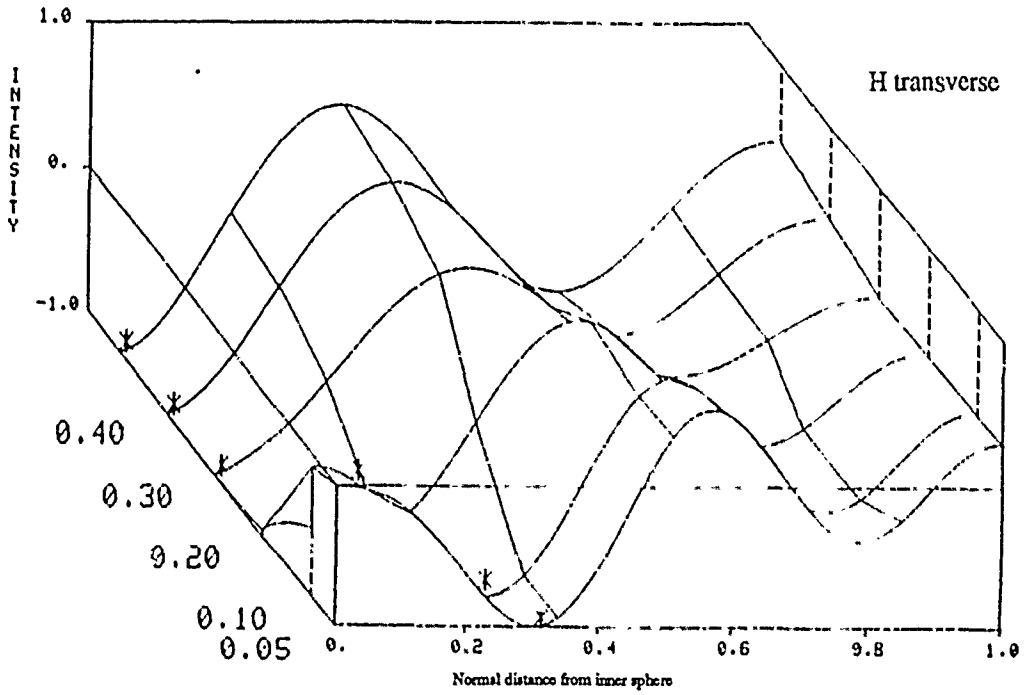

Figure 79. Distribution of the normalized transverse magnetic field component in the concentric spherical cavity as a function of the inner to outer conductor radii, $R = b/a$, for the TM44 mode. Asterisk indicates peak value of field with d.

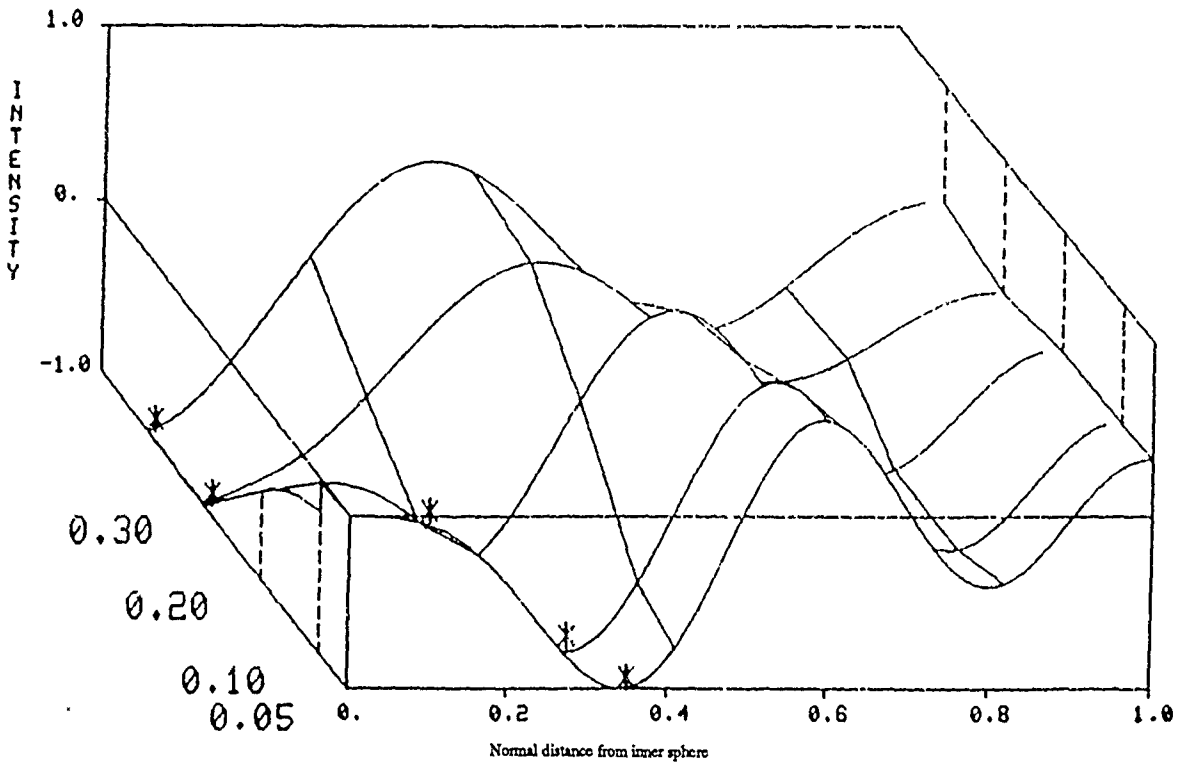

H transverse

Figure 80. Distribution of the normalized transverse magnetic field component in the concentric spherical cavity as a function of the inner to outer conductor radii, $R = b/a$, for the TM54 mode. Asterisk indicates peak value of field with d.

4.2 Transverse Electric Field Component for TMnp Modes

4.2.1 The p = 1 E-Transverse TMnp Eigenfields for n = 1 to 7

The transverse component of the electric field for the TM11 (dominant) mode must go to zero on the two conducting walls, and has a single peak value in between. It therefore resembles a "tunnel" when plotted in our three-dimensional format, much as it did in the TE11 case. However, consistent with the more complicated algebraic expressions utilized in the TM case, the "tunnel" is somewhat distorted, almost resembling the H-radial dependence of the TE11 mode, with the maximum value close to the inner conductor for smaller b/a, and close to the center of the cavity for large b/a. Figure 81 illustrates these characteristics. Increasing n, as illustrated in figures 82 through 87, has the effect, as expected, of shifting the peak values to larger values of d, especially for smaller b/a.

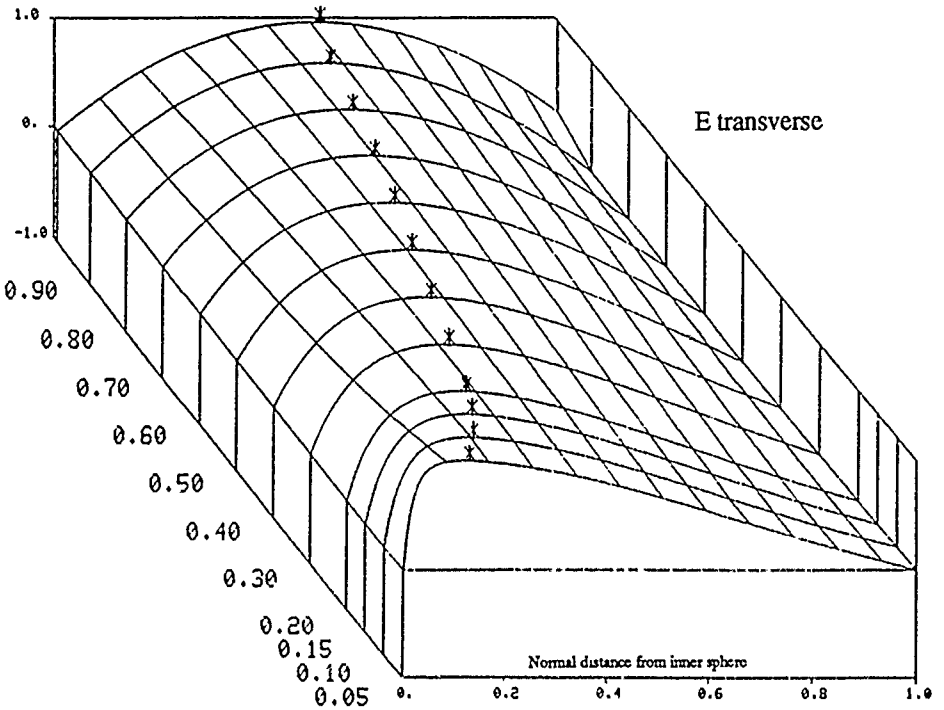

Figure 81. Distribution of the normalized transverse electric field component in the concentric spherical cavity as a function of the inner to outer conductor radii, $R = b/a$, for the TM11 mode. Asterisk indicates peak value of field with d.

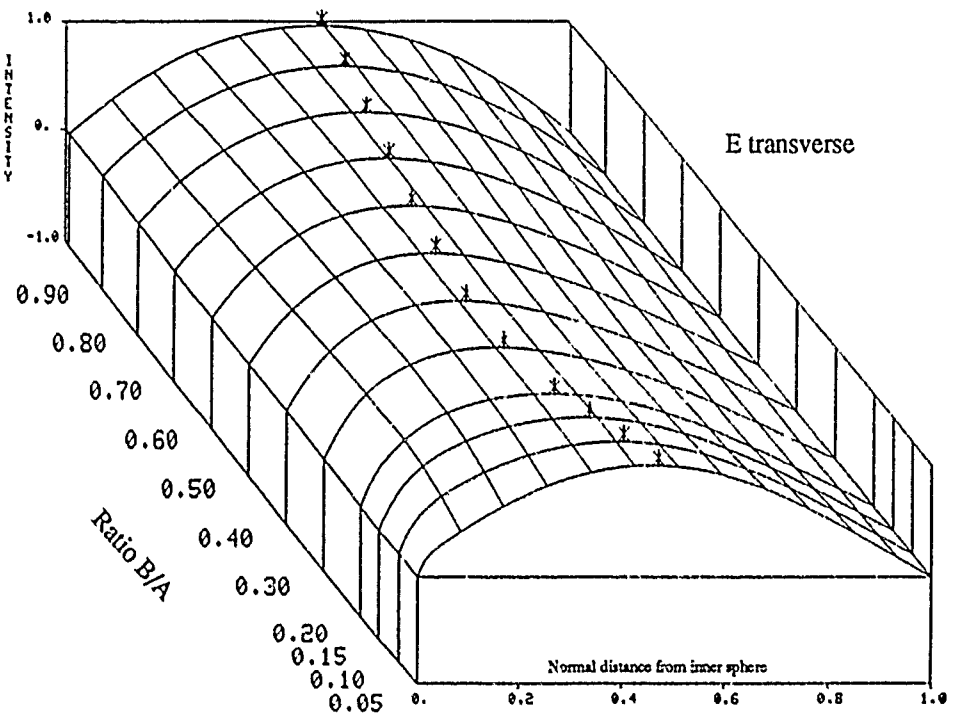

Figure 82. Distribution of the normalized transverse electric field component in the concentric spherical cavity as a function of the inner to outer conductor radii, $R = b/a$, for the TM21 mode. Asterisk indicates peak value of field with d.

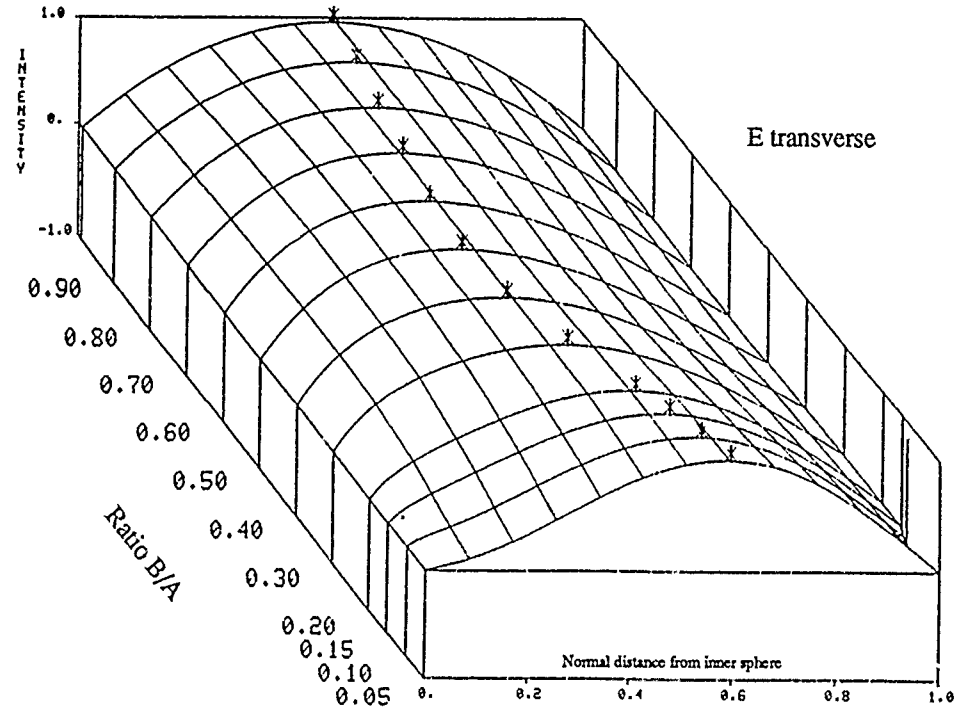

Figure 83. Distribution of the normalized transverse electric field component in the concentric spherical cavity as a function of the inner to outer conductor radii, $R = b/a$, for the TM31 mode. Asterisk indicates peak value of field with d.

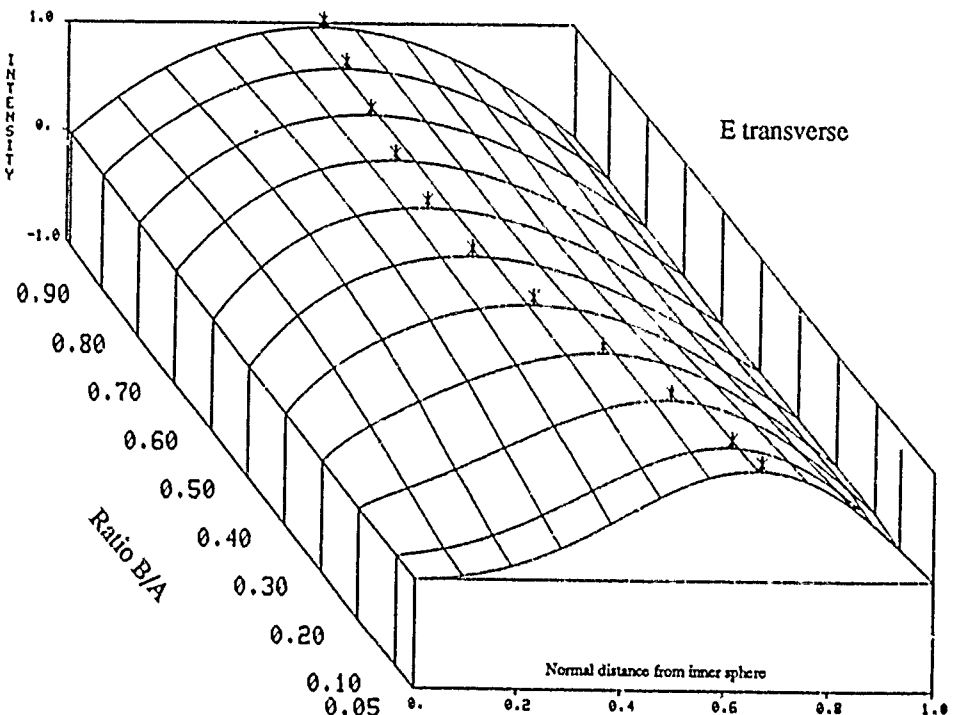

Figure 84. Distribution of the normalized transverse electric field component in the concentric spherical cavity as a function of the inner to outer conductor radii, $R = b/a$, for the TM41 mode. Asterisk indicates peak value of field with d.

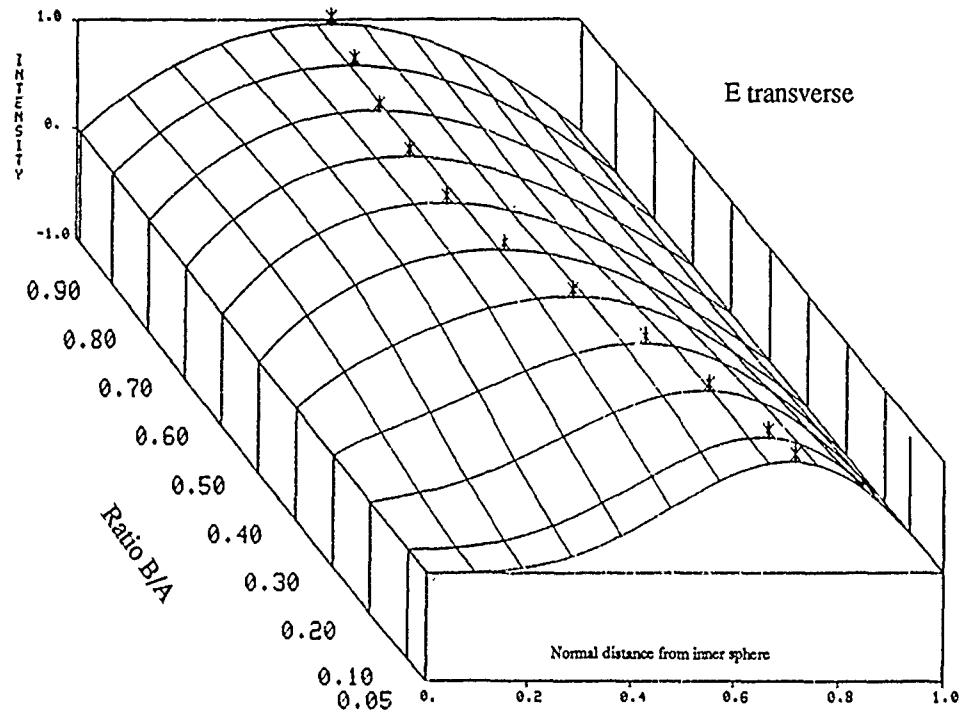

Figure 85. Distribution of the normalized transverse electric field component in the concentric spherical cavity as a function of the inner to outer conductor radii, $R = b/a$, for the TM51 mode. Asterisk indicates peak value of field with d.

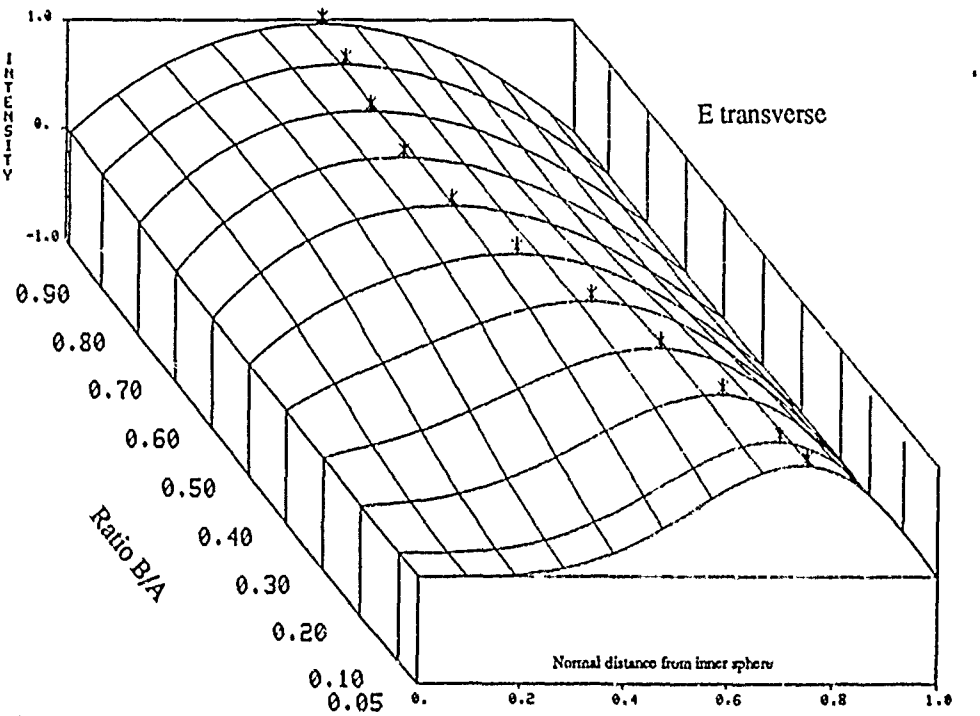

Figure 86. Distribution of the normalized transverse electric field component in the concentric spherical cavity as a function of the inner to outer conductor radii, $R = b/a$, for the TM61 mode. Asterisk indicates peak value of field with d.

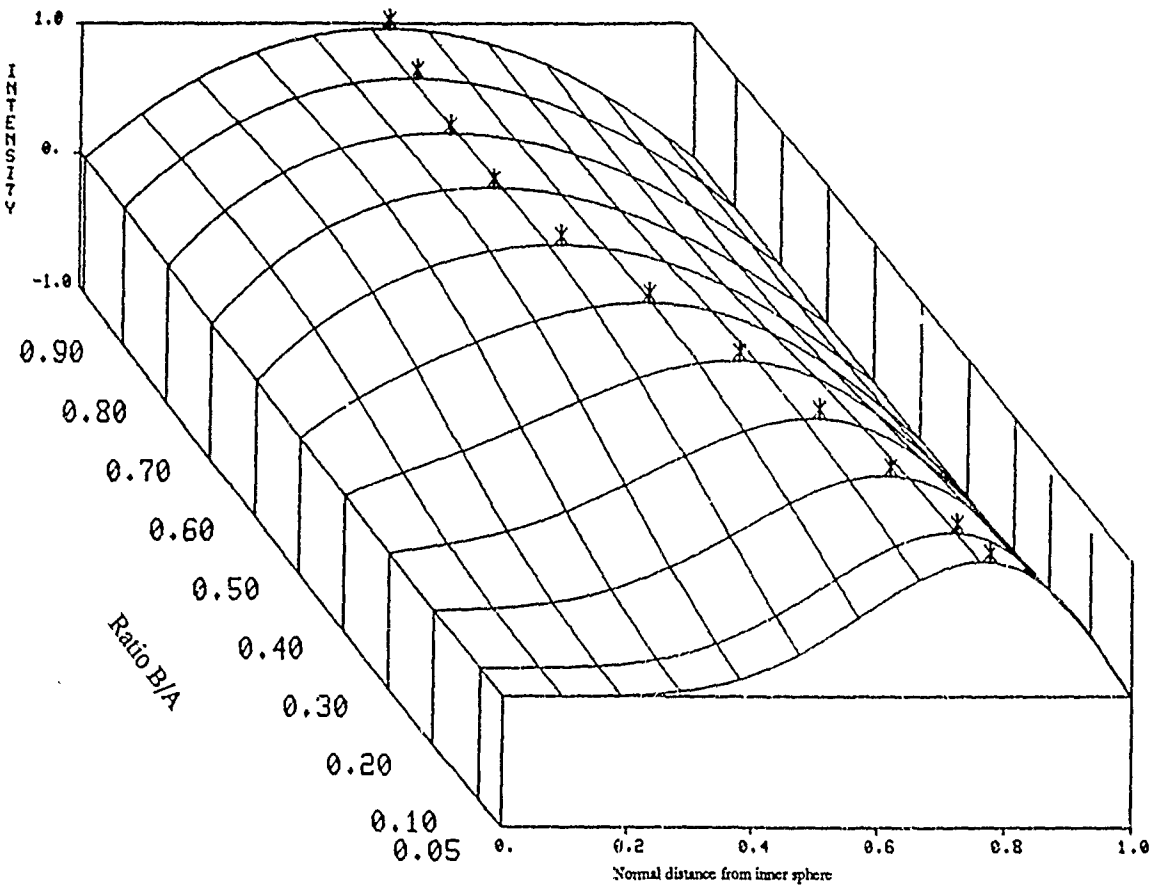

E transverse

Figure 87. Distribution of the normalized transverse electric field component in the concentric spherical cavity as a function of the inner to outer conductor radii, $R = b/a$, for the TM71 mode. Asterisk indicates peak value of field with d.

4.2.2 The p = 2 E-Transverse TMnp Eigenfields for n = 1 to 5

We have just observed that with increased p, the H-transverse component becomes more oscillatory, but not as pronounced as for the TE modes. Comparing figure 88 for the TM12 E-transverse component with figure 7 for the TE12 E-transverse component, we see that the same can be said for the transverse electric fields. A second peak, which is indicated as a local minimum, is added to the surface of the TM mode, fairly close to the inner wall. But, unlike its TE counterpart, this added peak exists for only part of the range of b/a, beginning with the lowest value of b/a calculated (0.05), and reaching somewhere between $b/a = 0.2$ and $b/a = 0.3$ before disappearing. The absolute maximum of the absolute value of the field compo-

nent is on this additional local peak, for *b/a* less than some value between 0.1 and 0.15, at which point this absolute maximum switches to the other local peak for the greater values of *b/a*. Of course, the fields on the two conducting boundaries must still go to zero.

When *n* is increased to 2 and 3, as shown in figures 89 and 90, the range in *b/a* over which the "added" local minimum occurs is increased, as is the range in *b/a* over which this local minimum contains the absolute maximum of the absolute value of the field component. Increasing *n* further to 4 and 5 further increases the range over which the "added" minimum exists. However, the field strength starts diminishing on this minimum, so that it no longer contains the absolute maximum, which now exists on the other local peak for the entire range of *b/a* considered (fig. 91 and 92).

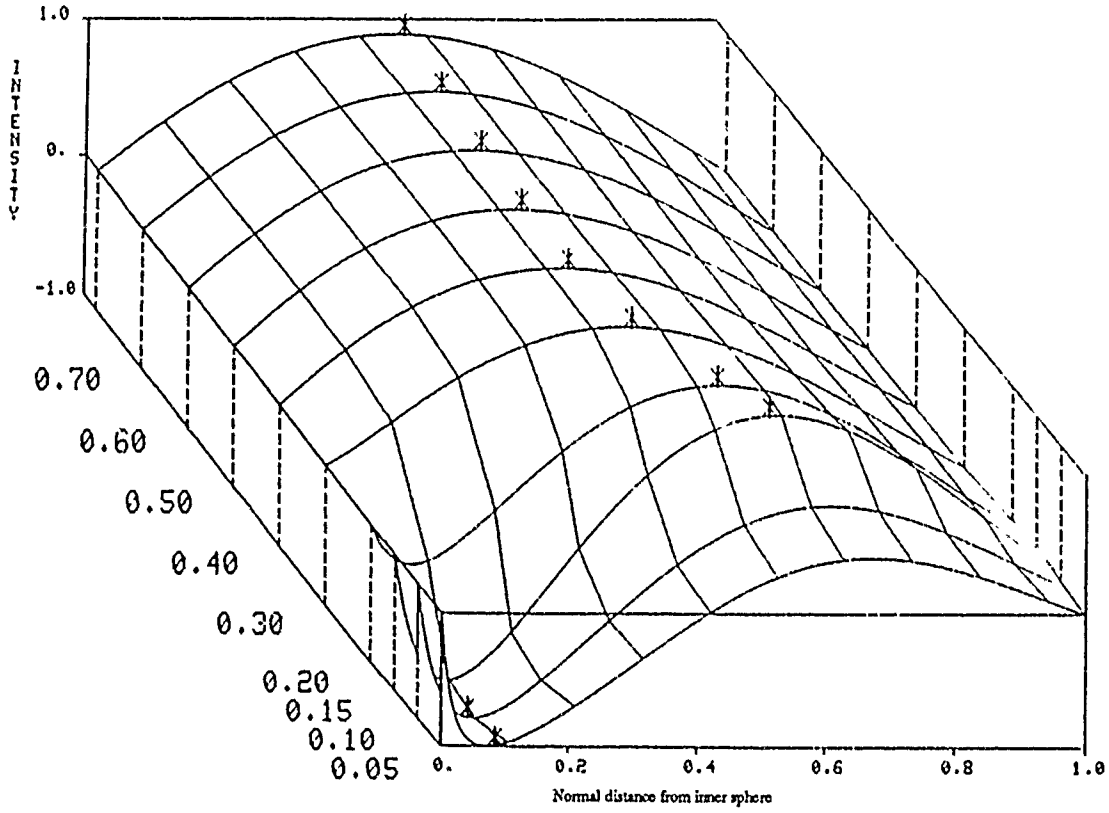

E transverse

Figure 88. Distribution of the normalized transverse electric field component in the concentric spherical cavity as a function of the inner to outer conductor radii, $R = b/a$, for the TM12 mode. Asterisk indicates peak value of field with *d*.

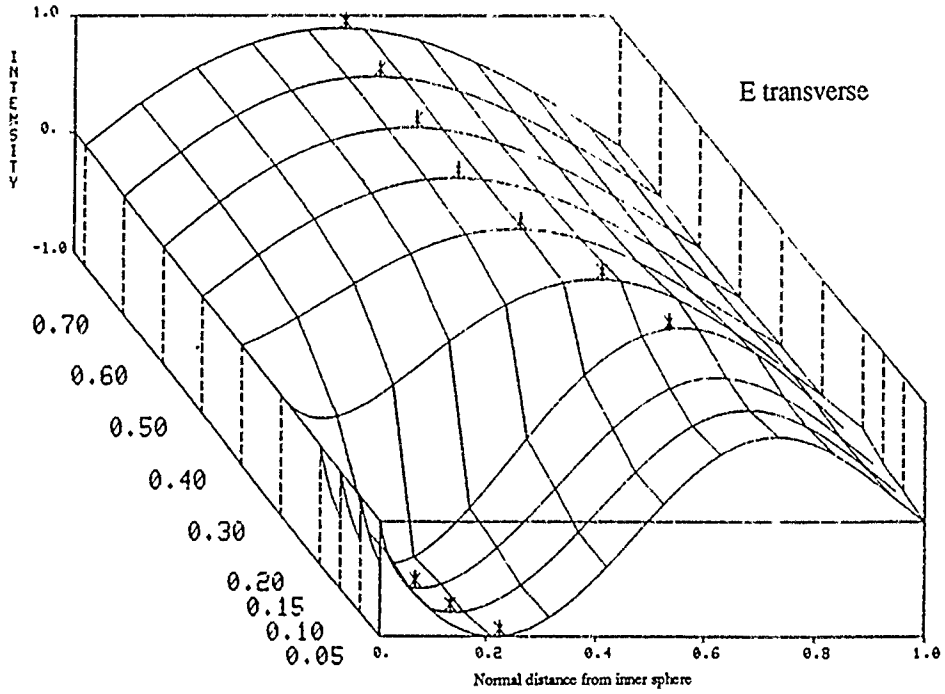

Figure 89. Distribution of the normalized transverse electric field component in the concentric spherical cavity as a function of the inner to outer conductor radii, $R = b/a$, for the TM22 mode. Asterisk indicates peak value of field with d.

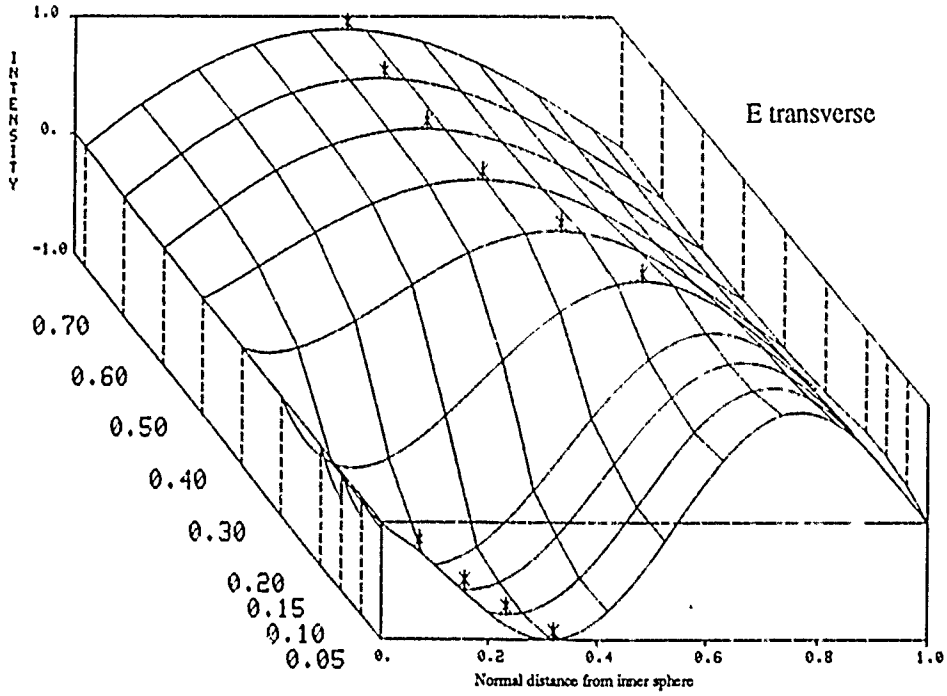

Figure 90. Distribution of the normalized transverse electric field component in the concentric spherical cavity as a function of the inner to outer conductor radii, $R = b/a$, for the TM32 mode. Asterisk indicates peak value of field with d.

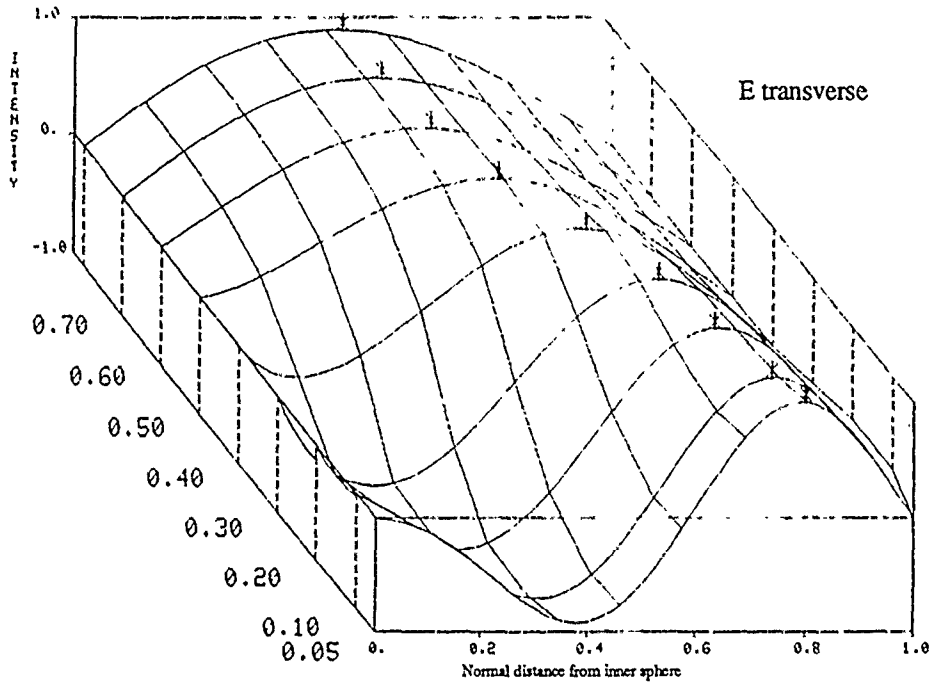

Figure 91. Distribution of the normalized transverse electric field component in the concentric spherical cavity as a function of the inner to outer conductor radii, $R = b/a$, for the TM42 mode. Asterisk indicates peak value of field with d.

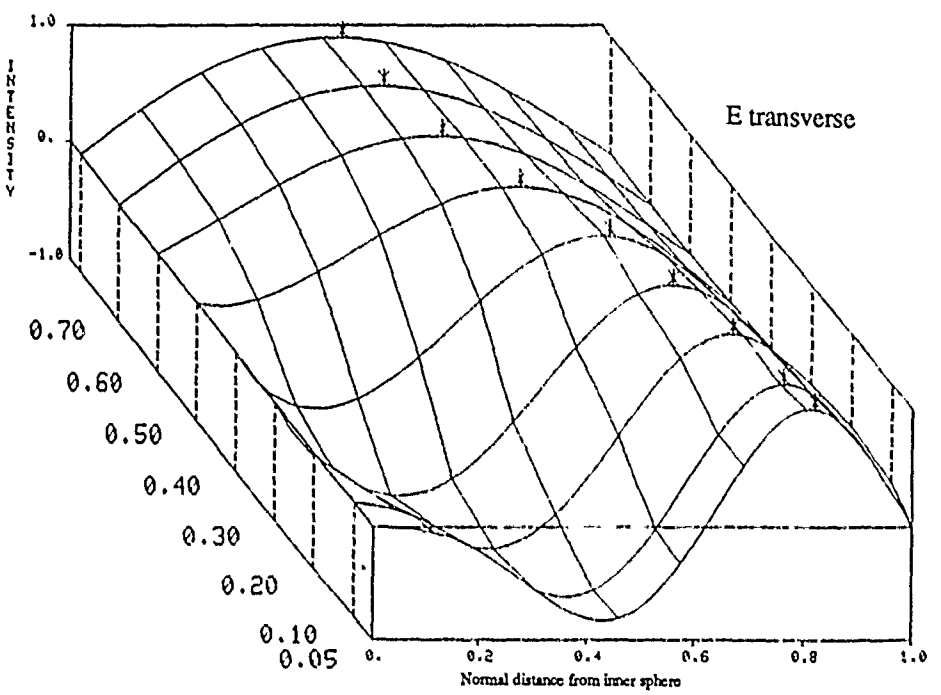

Figure 92. Distribution of the normalized transverse electric field component in the concentric spherical cavity as a function of the inner to outer conductor radii, $R = b/a$, for the TM32 mode. Asterisk indicates peak value of field with d.

4.2.3 *The p = 3 E-Transverse TMnp Eigenfields for n = 1 to 5*

We next investigate the case where p is increased to 3, and find that there is a more substantial increase of oscillation. The two local peaks that were present when p equalled 2 are now located closer to the inner conductor (at approximately $d = 0.06$ and $d = 0.23$ for the TM13 mode) (fig. 93). A new peak occurs at about $d = 0.75$, and is indicated as a local minimum in the surface plot. As n is increased from unity to five, these peaks occur at slightly higher values of d, shifting more for smaller values in b/a, as expected from our studies into the previous modes, and as seen in figures 94 through 97.

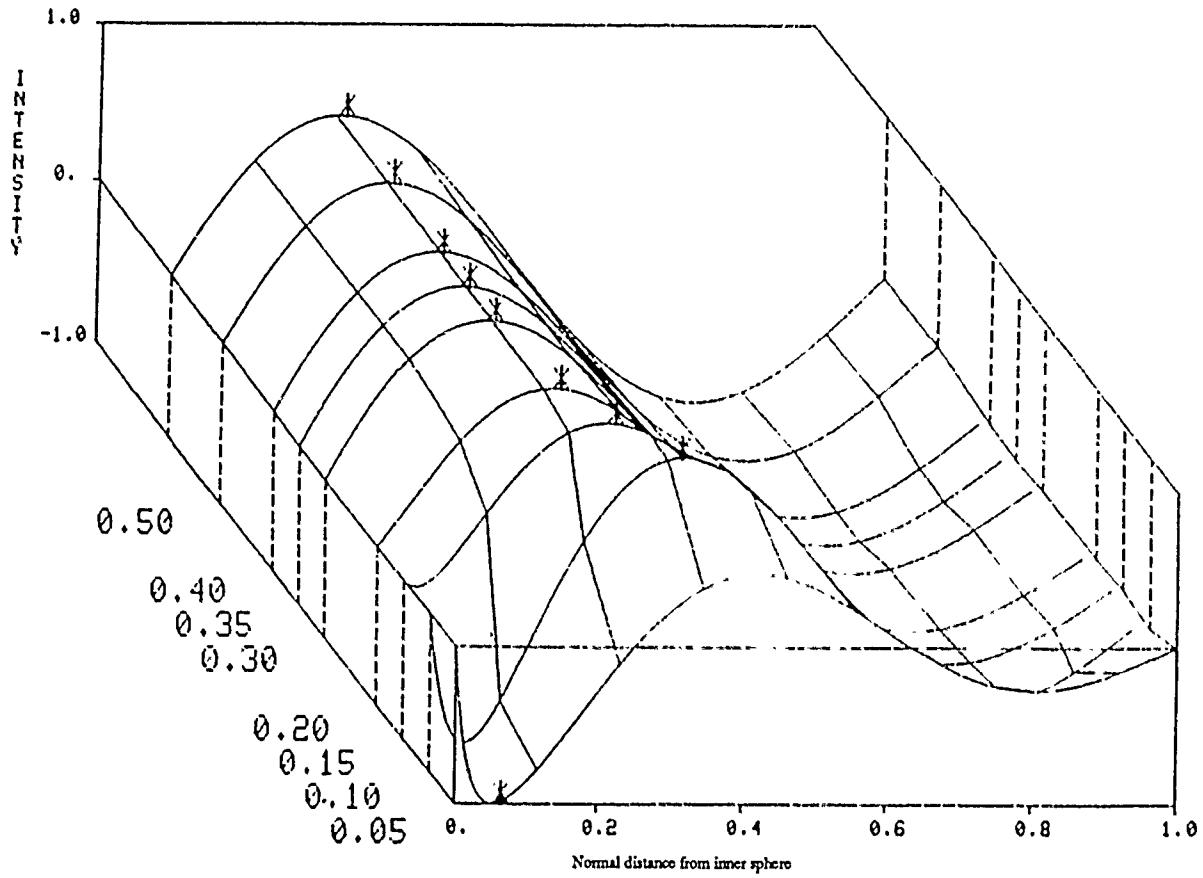

E transverse

Figure 93. Distribution of the normalized transverse electric field component in the concentric spherical cavity as a function of the inner to outer conductor radii, $R = b/a$, for the TM13 mode. Asterisk indicates peak value of field with d.

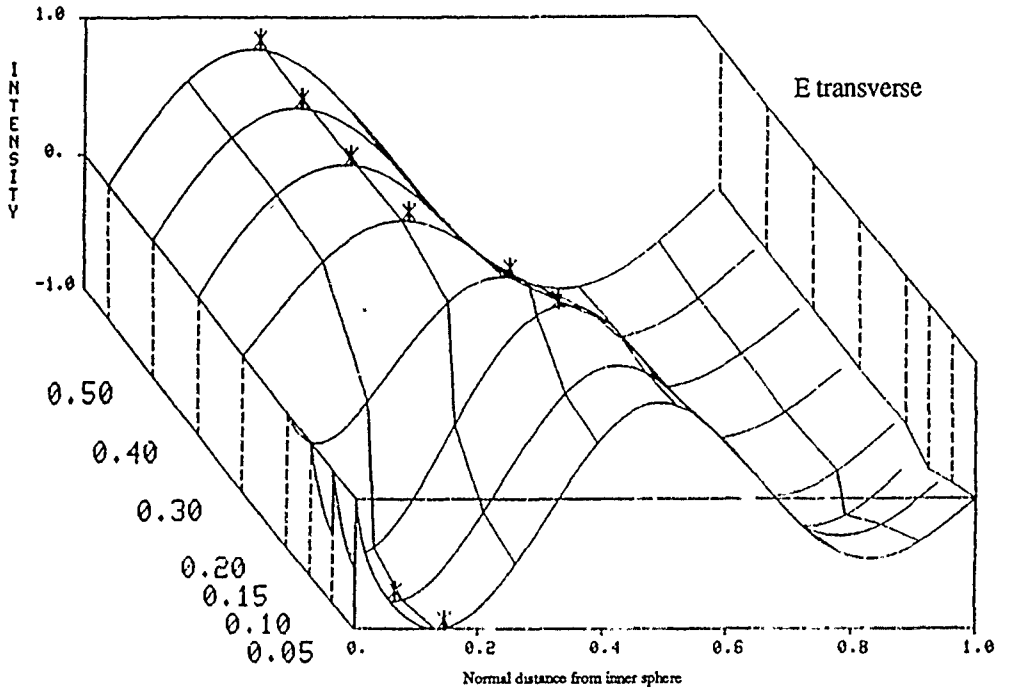

Figure 94. Distribution of the normalized transverse electric field component in the concentric spherical cavity as a function of the inner to outer conductor radii, $R = b/a$, for the TM23 mode. Asterisk indicates peak value of field with d.

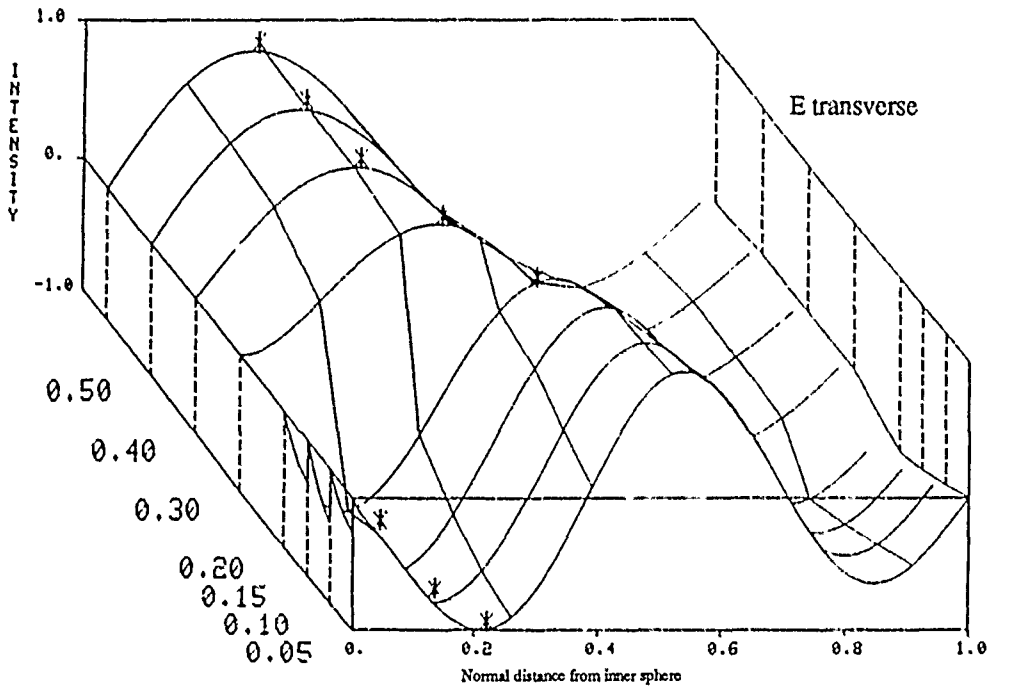

Figure 95. Distribution of the normalized transverse electric field component in the concentric spherical cavity as a function of the inner to outer conductor radii, $R = b/a$, for the TM33 mode. Asterisk indicates peak value of field with d.

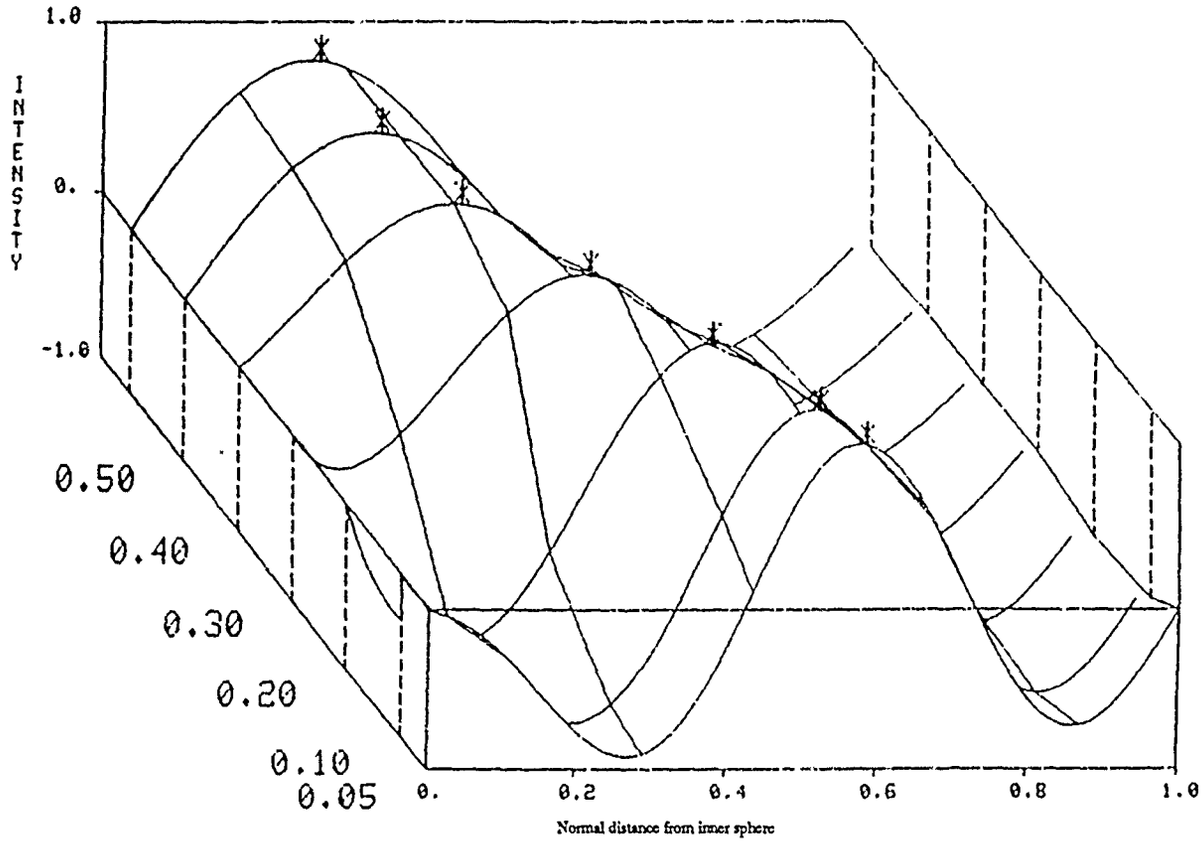

E transverse

Figure 96. Distribution of the normalized transverse electric field component in the concentric spherical cavity as a function of the inner to outer conductor radii, $R = b/a$, for the TM43 mode. Asterisk indicates peak value of field with d.

We next draw attention to the location (in d) of the absolute maximum value of the absolute value of the field component. Beginning with the TM13 mode, it occurs on the nearest local minimum to the inner metallic boundary for small b/a. Somewhere between 0.05 and 0.1, it switches to the next closest peak for the larger values of b/a. Increasing n to 2 and 3 has the effect not only of extending the range over which the absolute value resides on the closest minimum, but it also extends the range in b/a over which this minimum exists. When n is increased to 4 and 5, the range over which the inner local minimum exists is increased, but the field strength there becomes diminished, causing the absolute maximum to occur on the second closest local peak to the inner wall for all values of b/a computed. All of this is consistent with what has gone before.

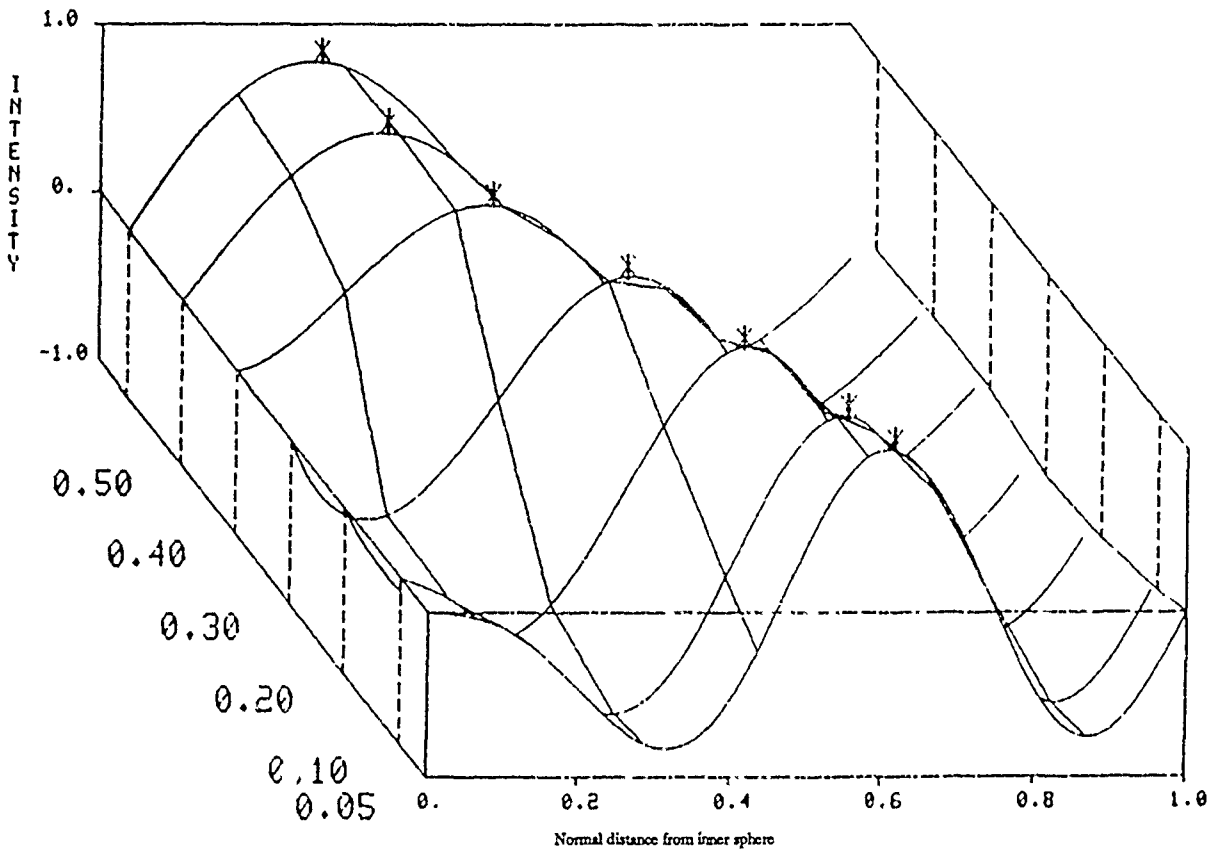

E transverse

Figure 97. Distribution of the normalized transverse electric field component in the concentric spherical cavity as a function of the inner to outer conductor radii, $R = b/a$, for the TM53 mode. Asterisk indicates peak value of field with d.

4.2.4 The p = 4 E-Transverse TMnp Eigenfields for n = 1 to 5

When n is increased to 4, one more local maximum near to $d = 0.8$ is added to the surface plots. For the TM14 mode, as shown in figure 98, the three already existing local peaks which were present when p was 3 have shifted down to approximately $d = 0.04$, 0.15, and 0.5, respectively. Increasing n has the effect of shifting the local peaks to higher d, especially for smaller b/a, as before. A discussion of the location of the absolute maximum value of the absolute value of the field component is very much the same as for the $p = 3$ case, and we shall therefore refer to figure 99 through 102 without further discussion.

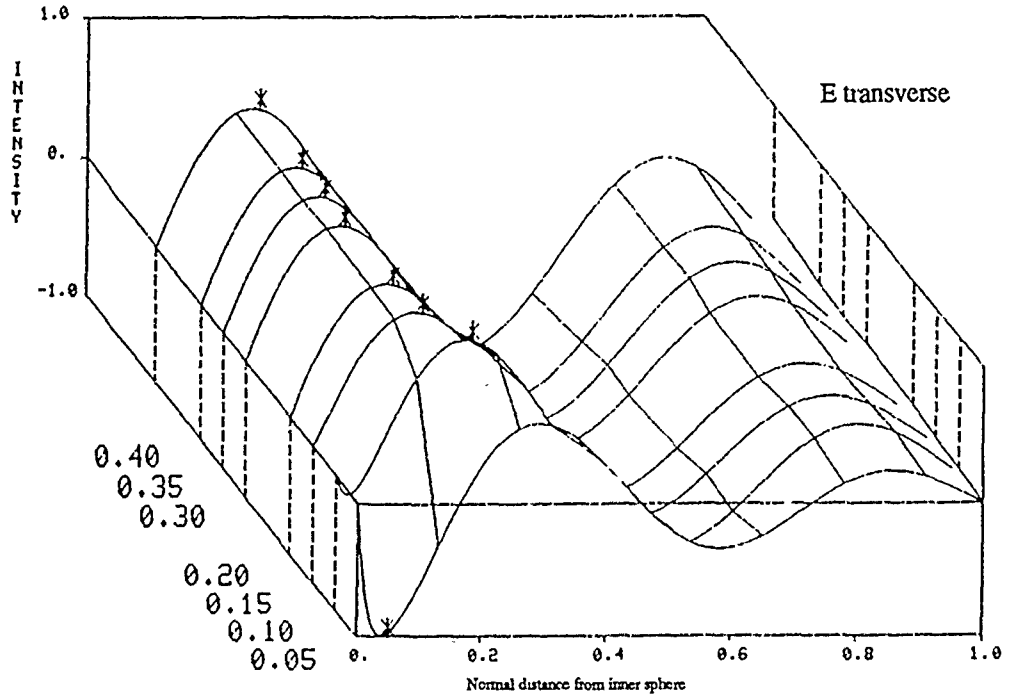

Figure 98. Distribution of the normalized transverse electric field component in the concentric spherical cavity as a function of the inner to outer conductor radii, $R = b/a$, for the TM14 mode. Asterisk indicates peak value of field with d.

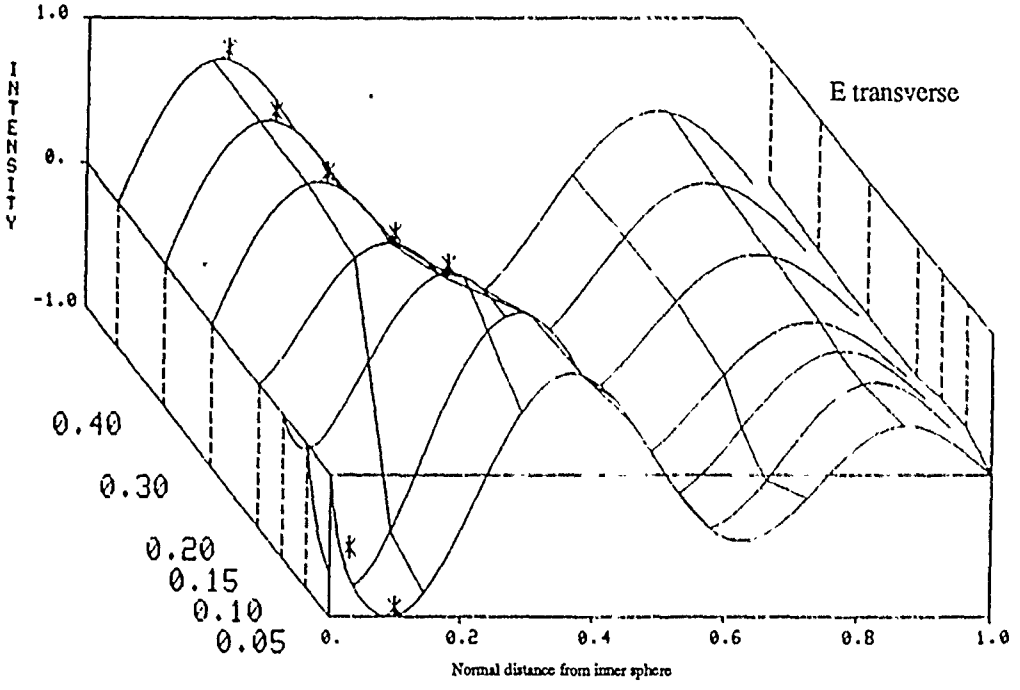

Figure 99. Distribution of the normalized transverse electric field component in the concentric spherical cavity as a function of the inner to outer conductor radii, $R = b/a$, for the TM24 mode. Asterisk indicates peak value of field with d.

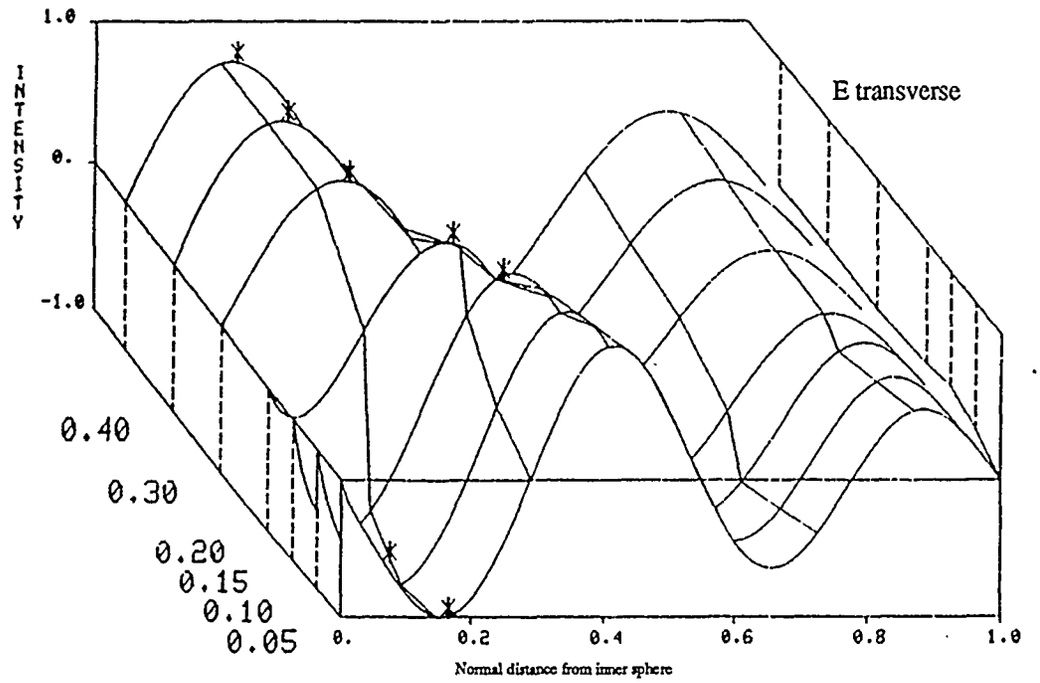

Figure 100. Distribution of the normalized transverse electric field component in the concentric spherical cavity as a function of the inner to outer conductor radii, $R = b/a$, for the TM34 mode. Asterisk indicates peak value of field with d.

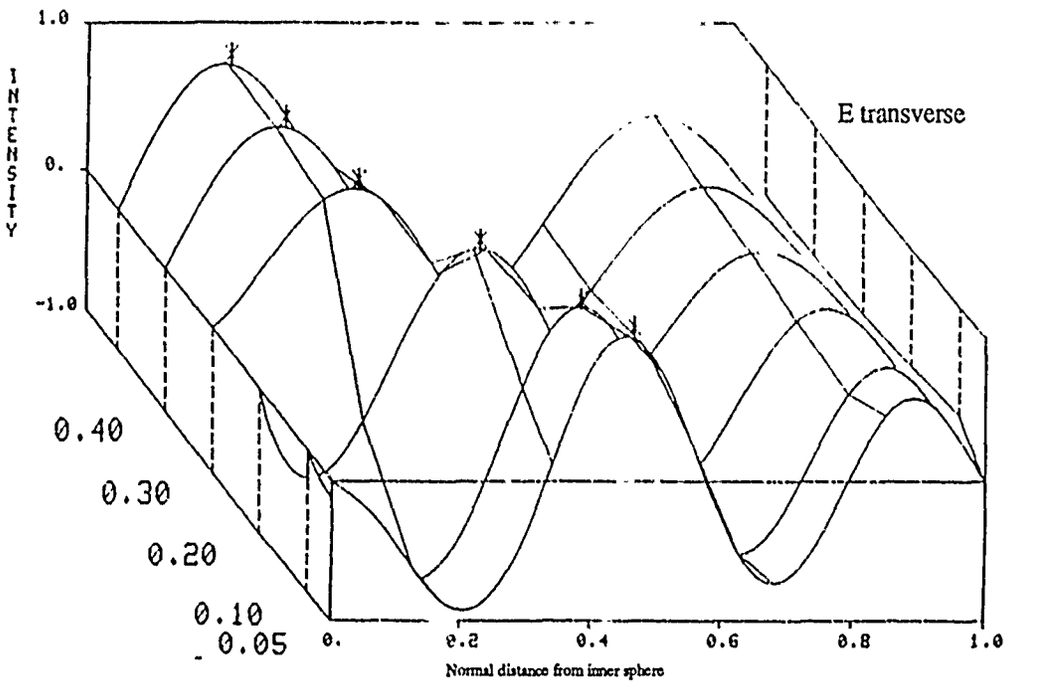

Figure 101. Distribution of the normalized transverse electric field component in the concentric spherical cavity as a function of the inner to outer conductor radii, $R = b/a$, for the TM44 mode. Asterisk indicates peak value of field with d.

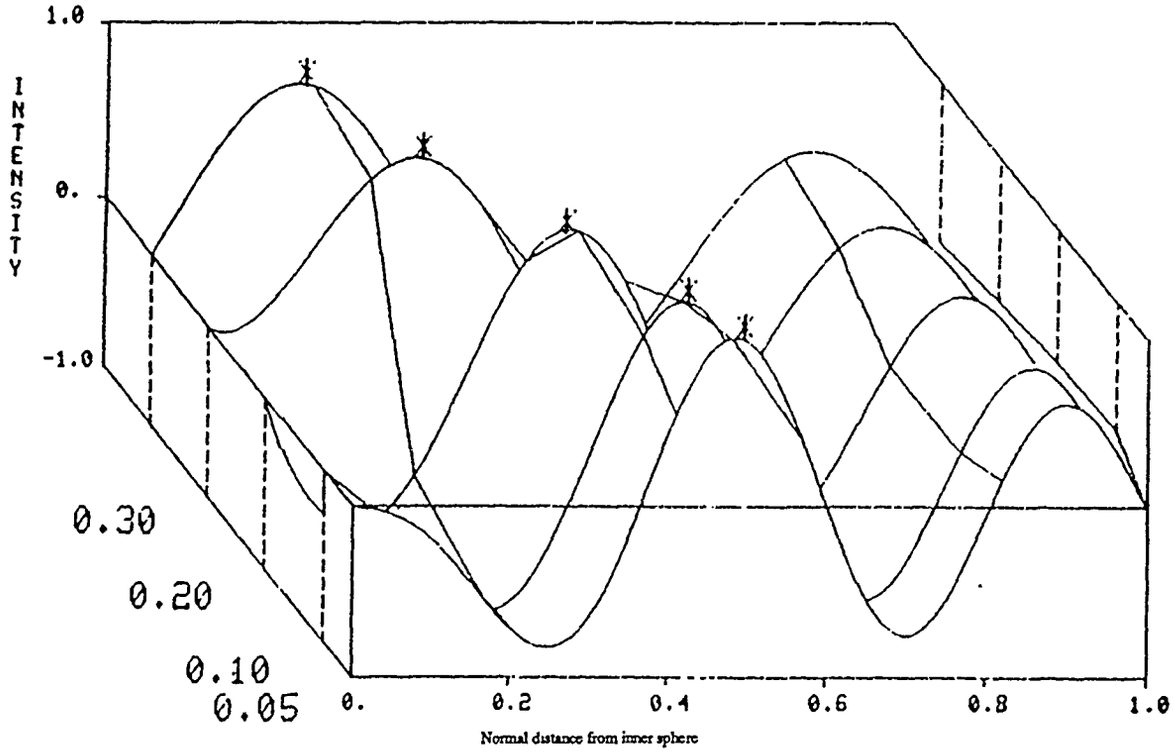

E transverse

Figure 102. Distribution of the normalized transverse electric field component in the concentric spherical cavity as a function of the inner to outer conductor radii, $R = b/a$, for the TM54 mode. Asterisk indicates peak value of field with d.

4.3 Radial Electric Field Component for TMnp Modes

4.3.1 The p = 1 E-Radial TMnp Eigenfields for n = 1 to 7

The final component left to be studied is the radial electric field. We recall from section 2.2 that this component is readily derivable from the transverse magnetic component, essentially through a division by the normalized radius, r/a. The reasoning behind the energy distribution which results is in some respects parallel to the case of the TE radial magnetic field, which was obtained by means of a similar division (sect. 3.3). The radial dependence of the radial electric field for a given TM mode is seen, then, as an enhancement of the dependence of the transverse magnetic field, more for smaller values of b/a than for larger, and more for smaller d than for larger. Thus, while the overall surface plot characteristics are the same as for the transverse magnetic field, the radial electric fields' local maxima/minima will be shifted to smaller values of d. Also, the abso-

lute maximum value of the absolute value of the component will be more apt to peak at a smaller d value than in the case of the H-transverse component.

Beginning with the $p = 1$ case, as shown in figures 103 through 109, we see that when $n = 1$, the absolute maximum exists on the inner conducting wall for all values of b/a computed (0.05, b/a, 0.99), and there is no other local maxima/minima discernable. Increasing n produces the local maximum that exists over part of the range in b/a, as it did for H-transverse. However, this peak is not as close to the outer wall, and the range over which the absolute maximum value of the component rests on it is not as large.

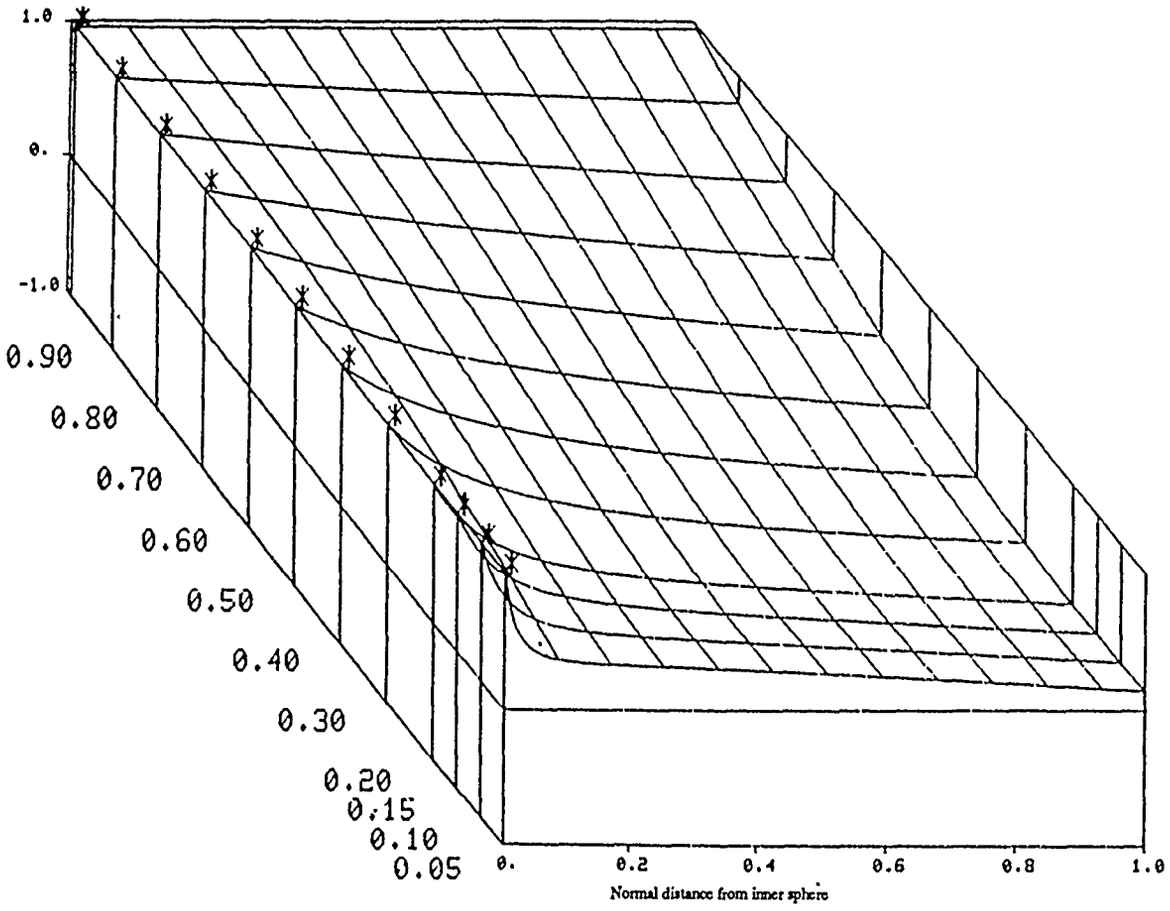

E radial

Figure 103. Distribution of the normalized radial electric field component in the concentric spherical cavity as a function of the inner to outer conductor radii, $R = b/a$, for the TM11 mode. Asterisk indicates peak value of field with d.

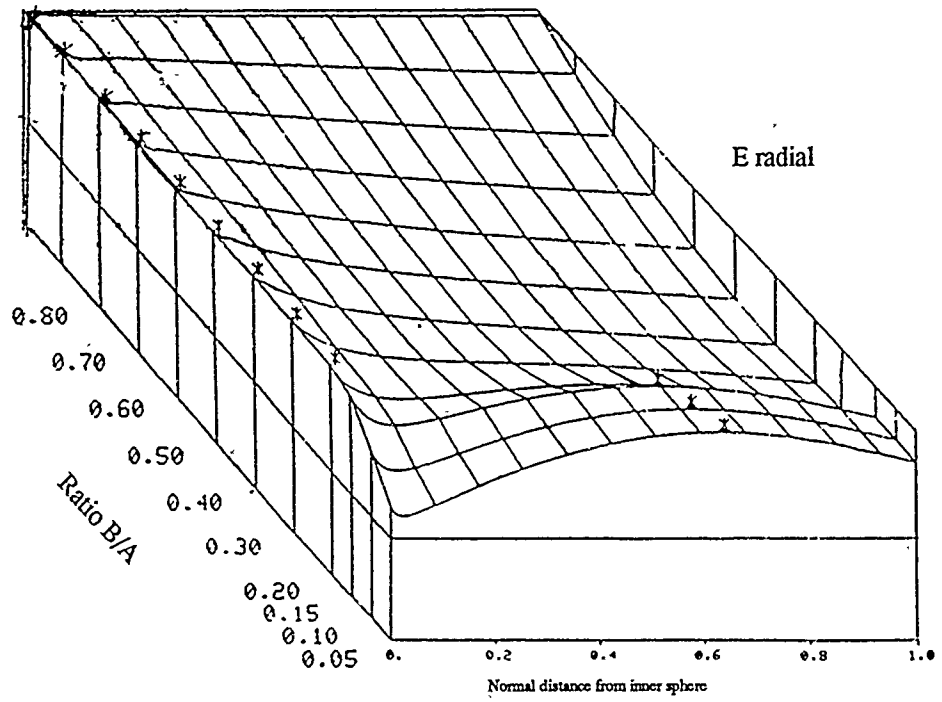

Figure 104. Distribution of the normalized radial electric field component in the concentric spherical cavity as a function of the inner to outer conductor radii, $R = b/a$, for the TM21 mode. Asterisk indicates peak value of field with d.

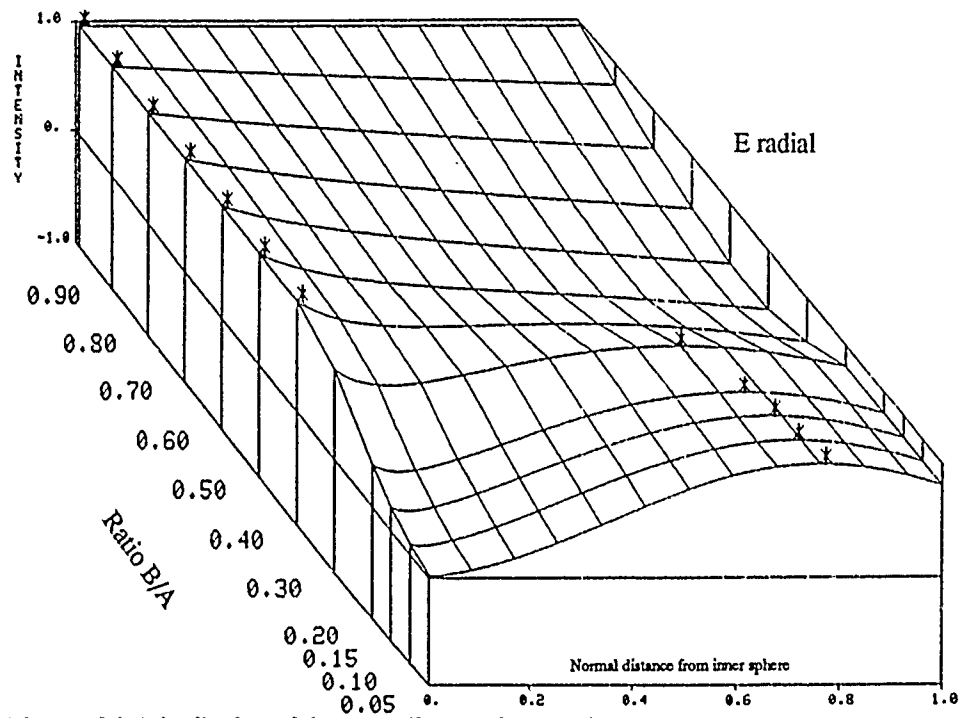

Figure 105. Distribution of the normalized radial electric field component in the concentric spherical cavity as a function of the inner to outer conductor radii, $R = b/a$, for the TM31 mode. Asterisk indicates peak value of field with d.

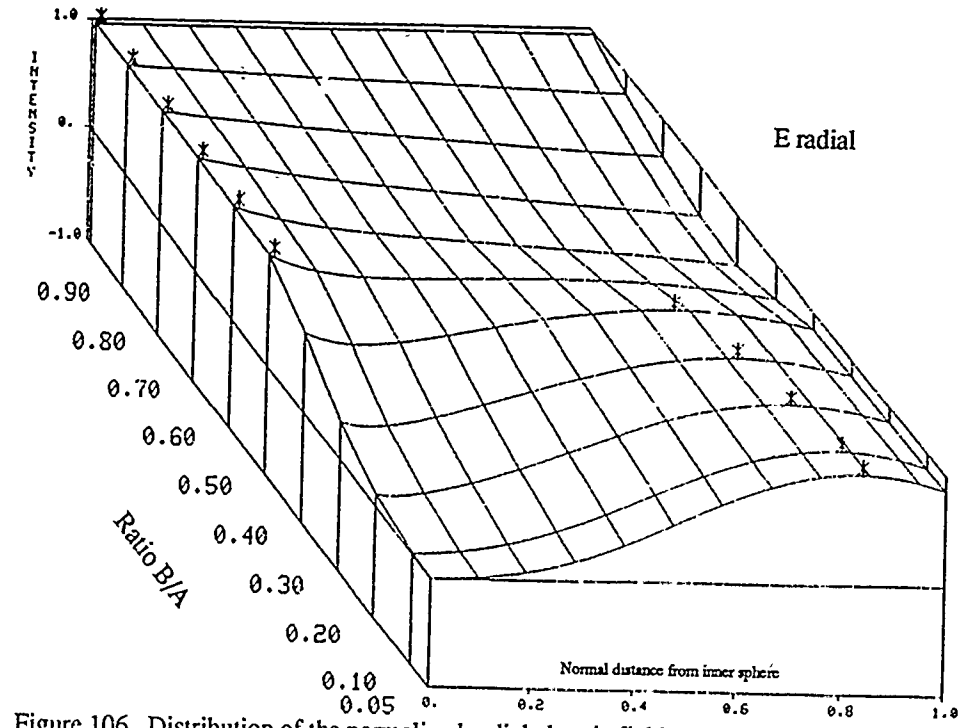

Figure 106. Distribution of the normalized radial electric field component in the concentric spherical cavity as a function of the inner to outer conductor radii, $R = b/a$, for the TM41 mode. Asterisk indicates peak value of field with d.

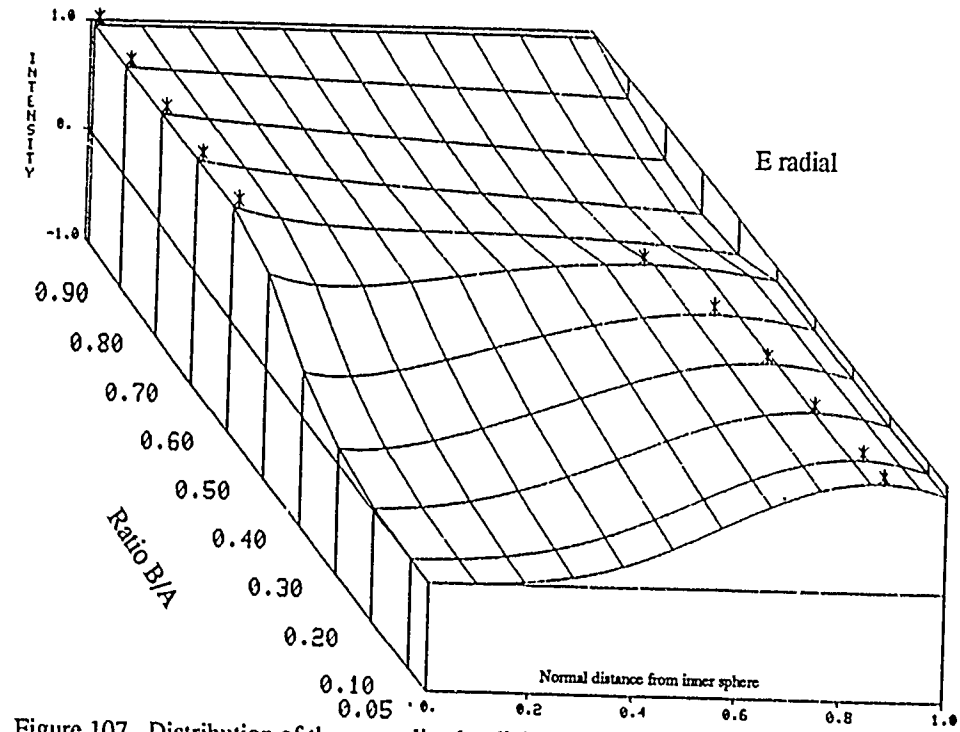

Figure 107. Distribution of the normalized radial electric field component in the concentric spherical cavity as a function of the inner to outer conductor radii, $R = b/a$, for the TM51 mode. Asterisk indicates peak value of field with d.

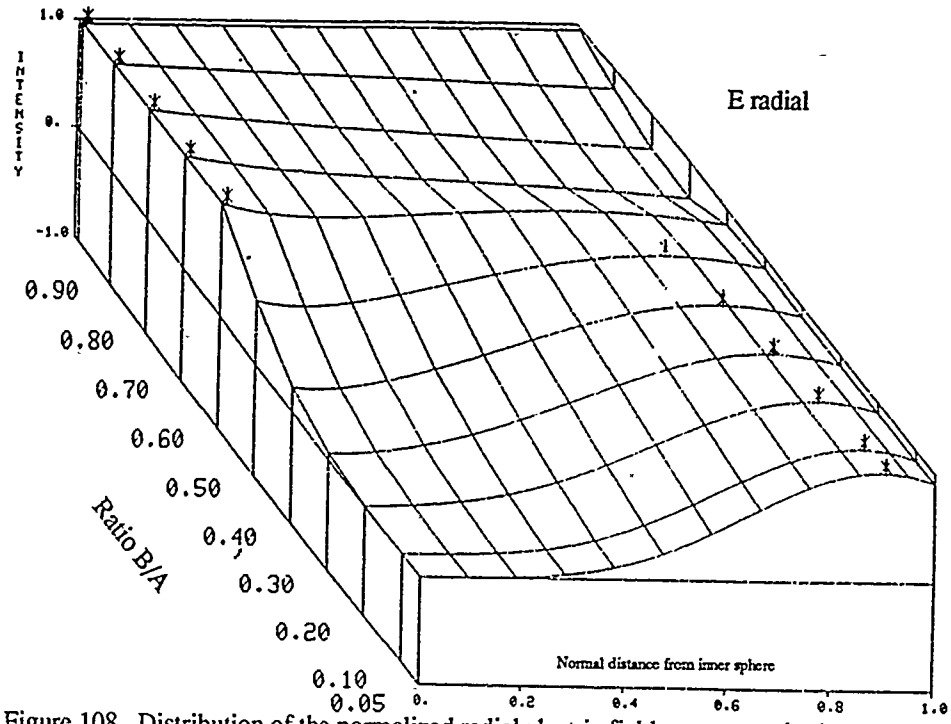

Figure 108. Distribution of the normalized radial electric field component in the concentric spherical cavity as a function of the inner to outer conductor radii, $R = b/a$, for the TM61 mode. Asterisk indicates peak value of field with d.

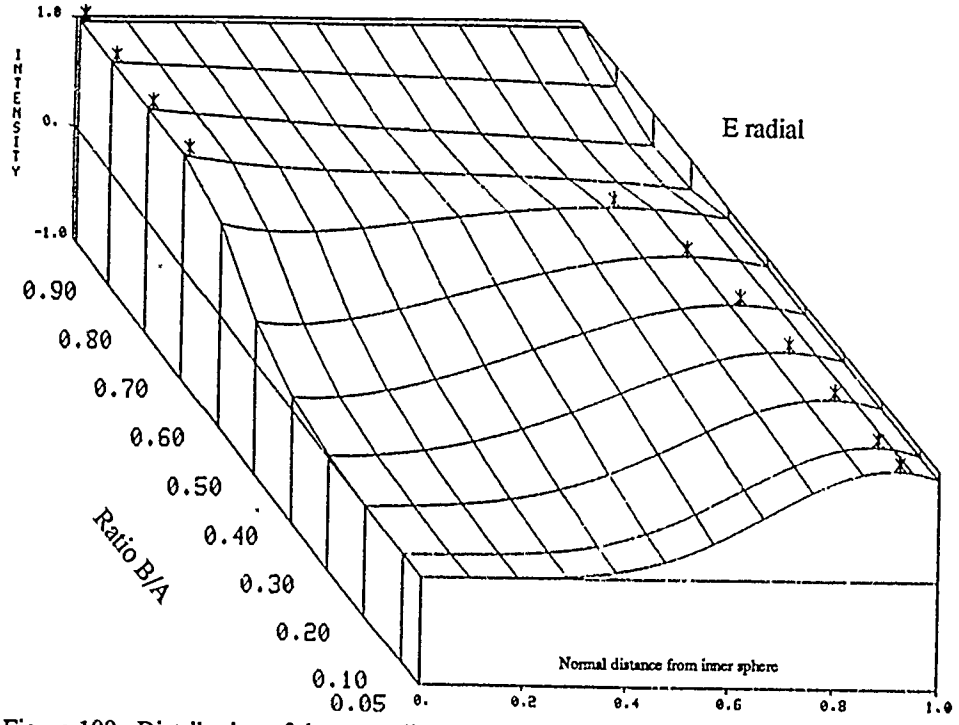

Figure 109. Distribution of the normalized radial electric field component in the concentric spherical cavity as a function of the inner to outer conductor radii, $R = b/a$, for the TM71 mode. Asterisk indicates peak value of field with d.

4.3.2 *The p = 2 E-Radial TMnp Eigenfields for n = 1 to 5*

Increasing p to 2 adds another local peak close to the outer wall, but due to the nature of the r/a division, this peak is a very mild one. The other local peak, which was present when p was unity for part of the range of b/a, has moved substantially closer to the inner wall, wherever that peak existed. The absolute maximum value of the absolute value of the field remains on the inner wall for all calculated values of b/a when $n = 1$ (fig. 110). When n is greater than unity, the location of this absolute maximum divides itself once again between the inner conductor for larger b/a, and on the closest local peak for smaller b/a. The absolute maximum resides on this peak for an even smaller range of b/a than it did when p was unity (fig. 111–114).

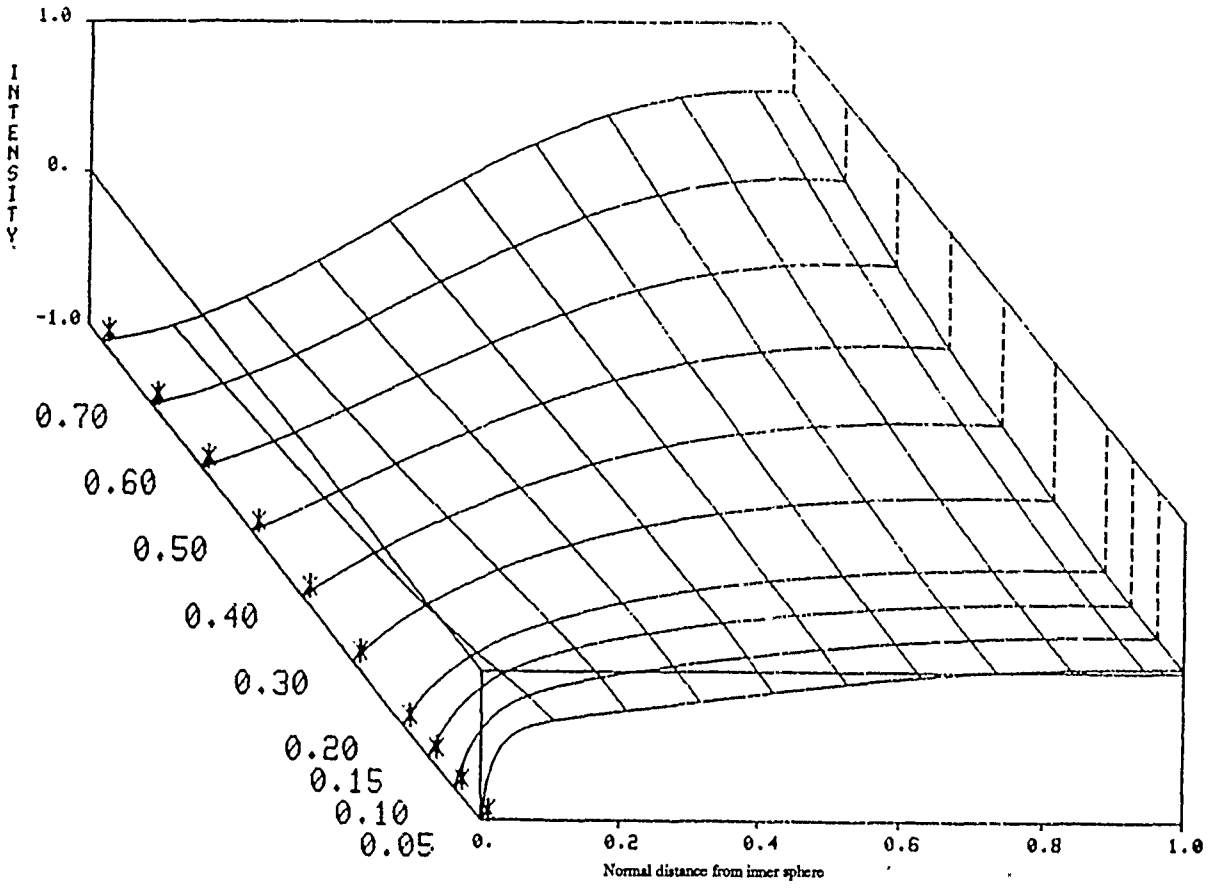

E radial

Figure 110. Distribution of the normalized radial electric field component in the concentric spherical cavity as a function of the inner to outer conductor radii, $R = b/a$, for the TM12 mode. Asterisk indicates peak value of field with d.

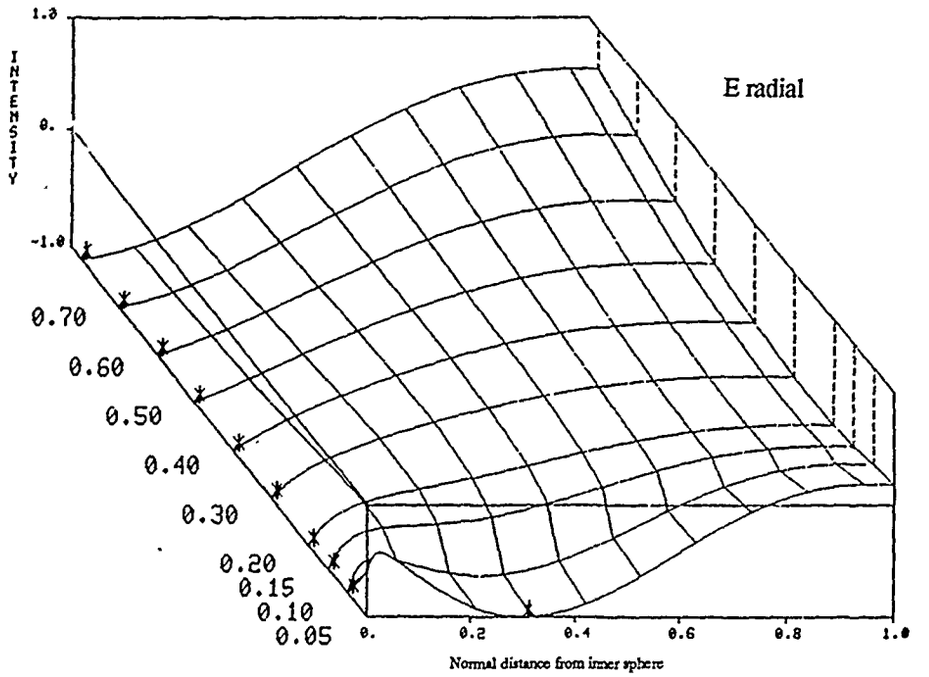

Figure 111. Distribution of the normalized radial electric field component in the concentric spherical cavity as a function of the inner to outer conductor radii, $R = b/a$, for the TM22 mode. Asterisk indicates peak value of field with d.

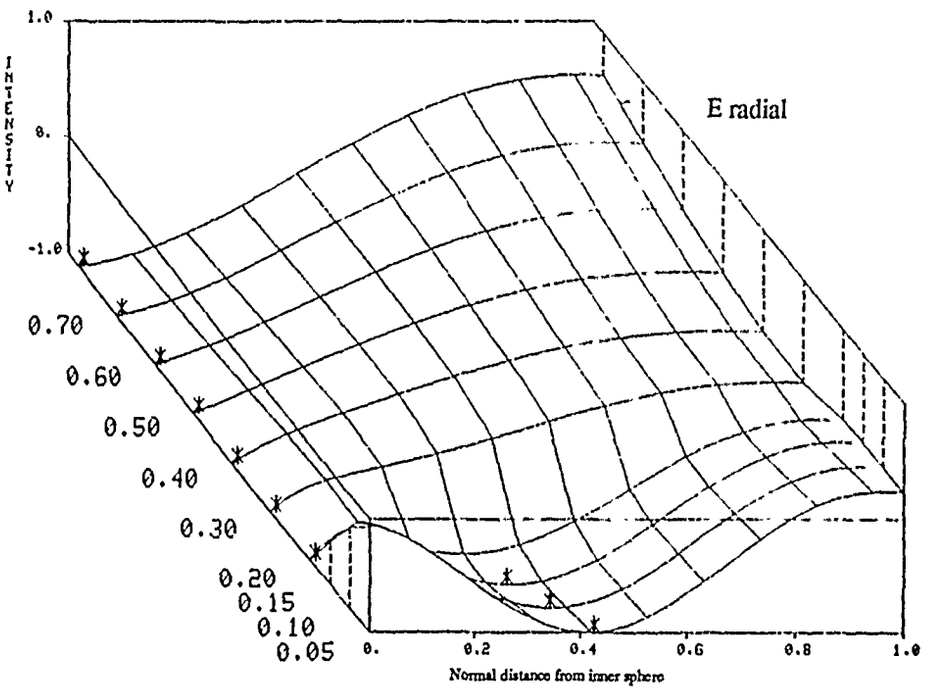

Figure 112. Distribution of the normalized radial electric field component in the concentric spherical cavity as a function of the inner to outer conductor radii, $R = b/a$, for the TM32 mode.Asterisk indicates peak value of field with d.

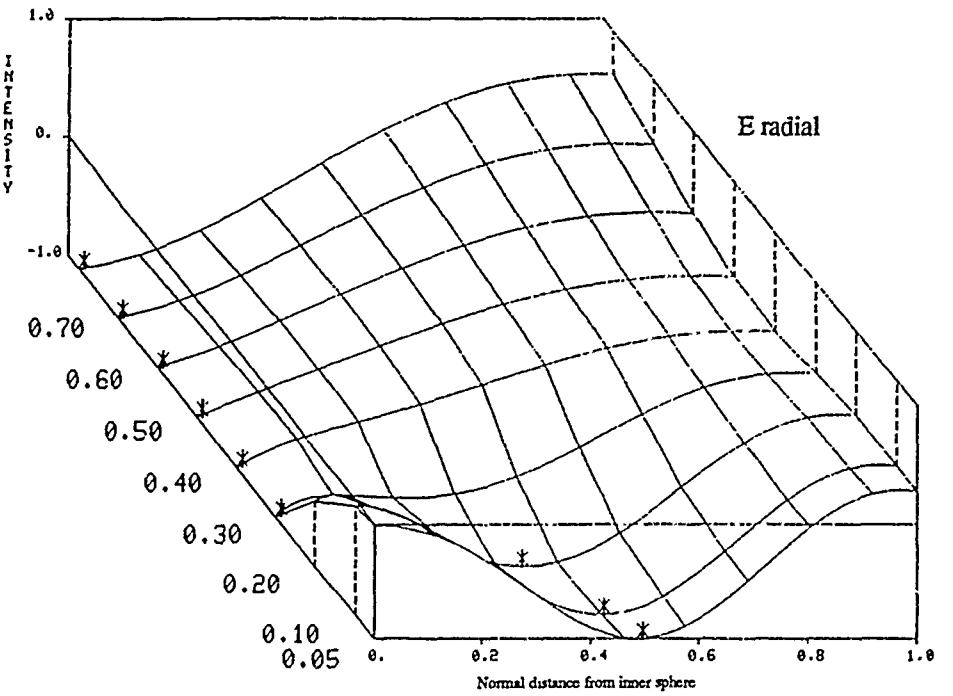

Figure 113. Distribution of the normalized radial electric field component in the concentric spherical cavity as a function of the inner to outer conductor radii, $R = b/a$, for the TM42 mode. Asterisk indicates peak value of field with d.

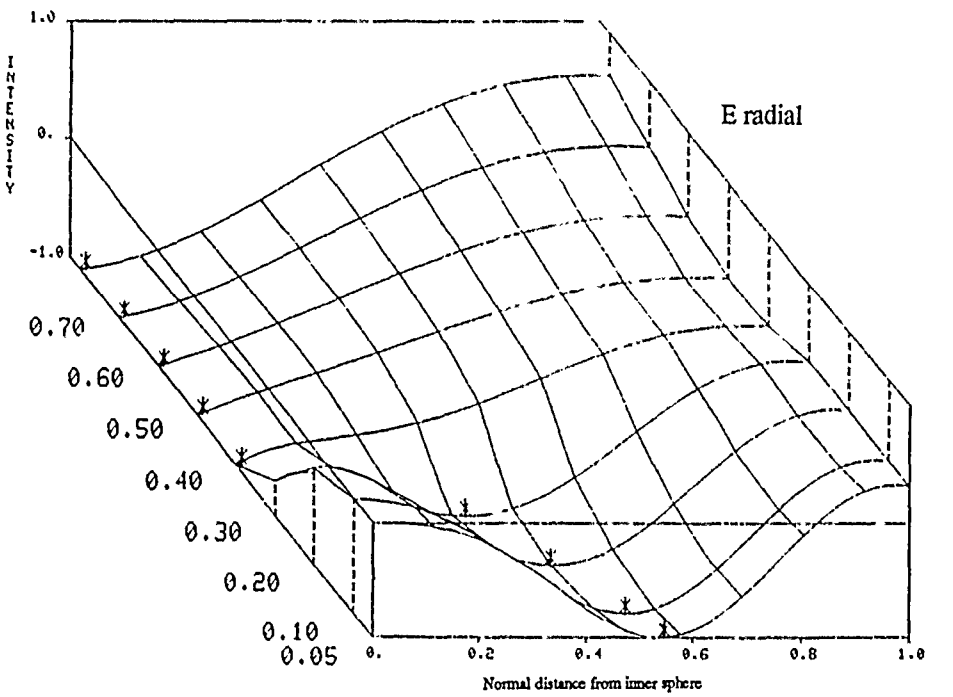

Figure 114. Distribution of the normalized radial electric field component in the concentric spherical cavity as a function of the inner to outer conductor radii, $R = b/a$, for the TM52 mode. Asterisk indicates peak value of field with d.

4.3.3 *The p = 3 E-Radial TMnp Eigenfields for n = 1 to 5*

When p is raised to 3, the two local peaks present in the component when $p = 2$ are moved again substantially closer to the inner conductor. The r/a division is felt as a stronger enhancement nearer the inner wall, so that these peaks are not as mild as for $p = 2$. Another local peak is added close to the outer wall, and this one is very mild. The absolute maximum value of the absolute value of the field remains located on the inner wall for larger values of b/a, and on the closest local peak to the inner wall for smaller b/a. But the range in b/a for which this absolute maximum resides on the local peak is diminished even more for $p = 3$ (fig. 115 through 119).

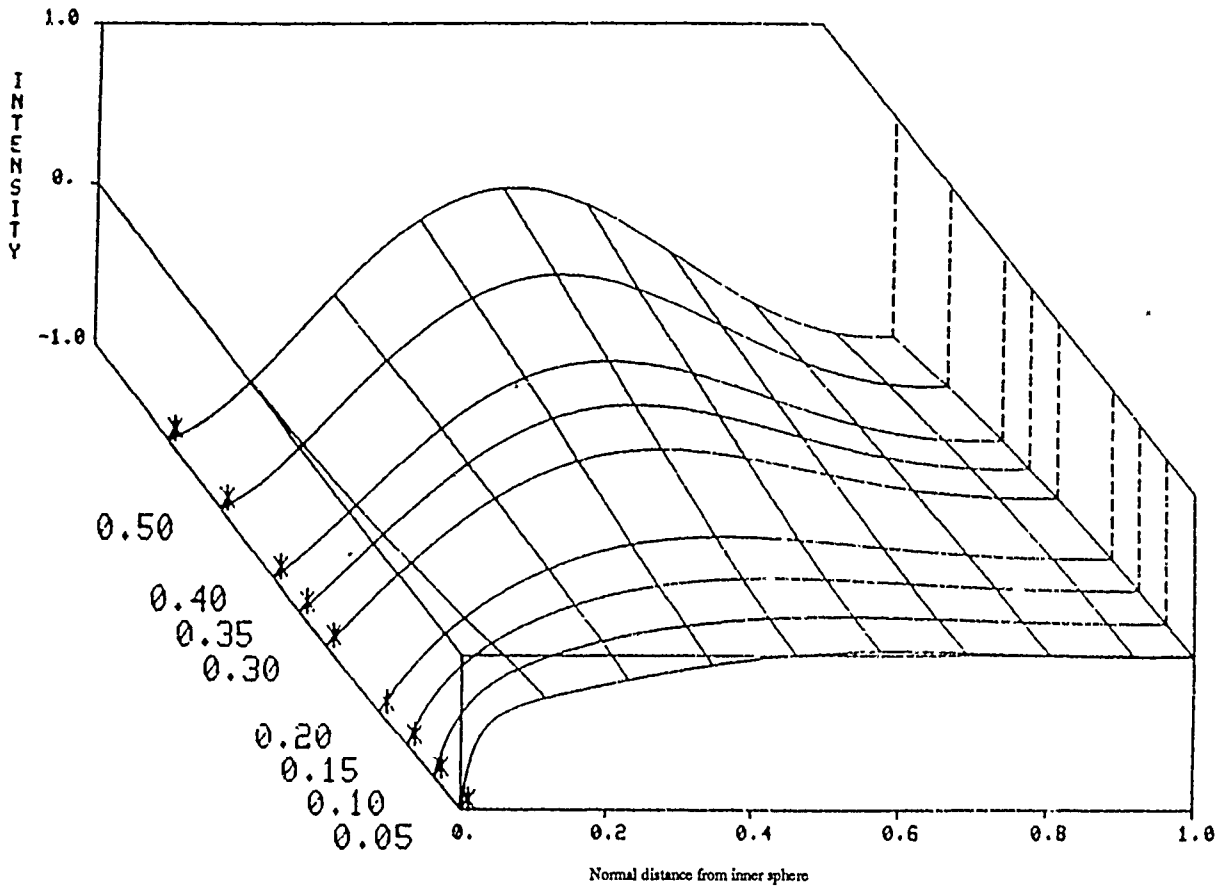

E radial

Figure 115. Distribution of the normalized radial electric field component in the concentric spherical cavity as a function of the inner to outer conductor radii, $R = b/a$, for the TM13 mode. Asterisk indicates peak value of field with d.

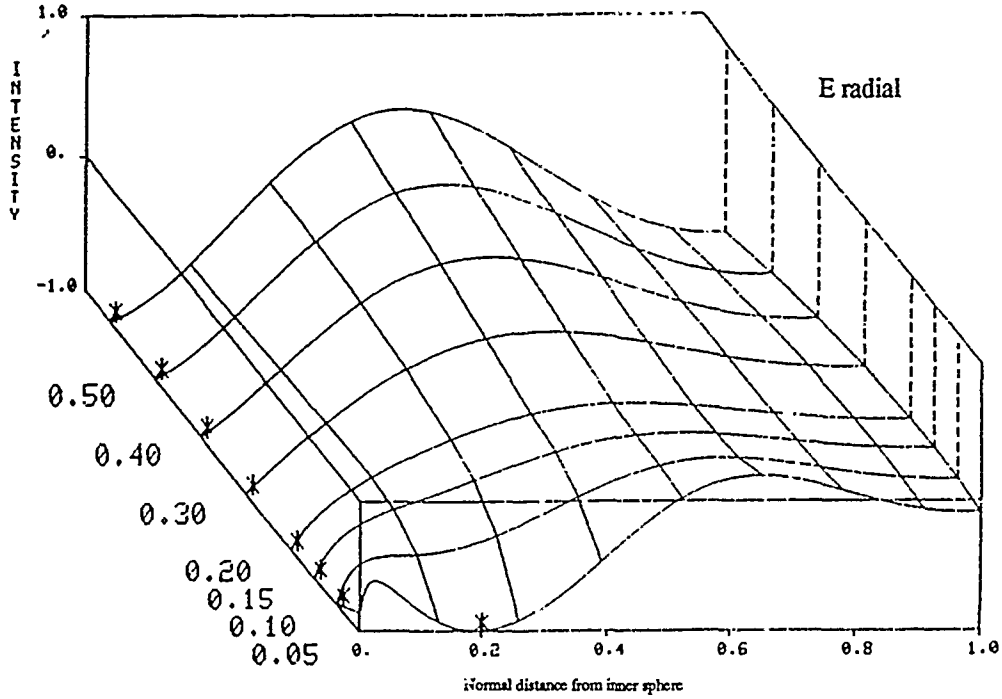

Figure 116. Distribution of the normalized radial electric field component in the concentric spherical cavity as a function of the inner to outer conductor radii, $R = b/a$, for the TM23 mode. Asterisk indicates peak value of field with d.

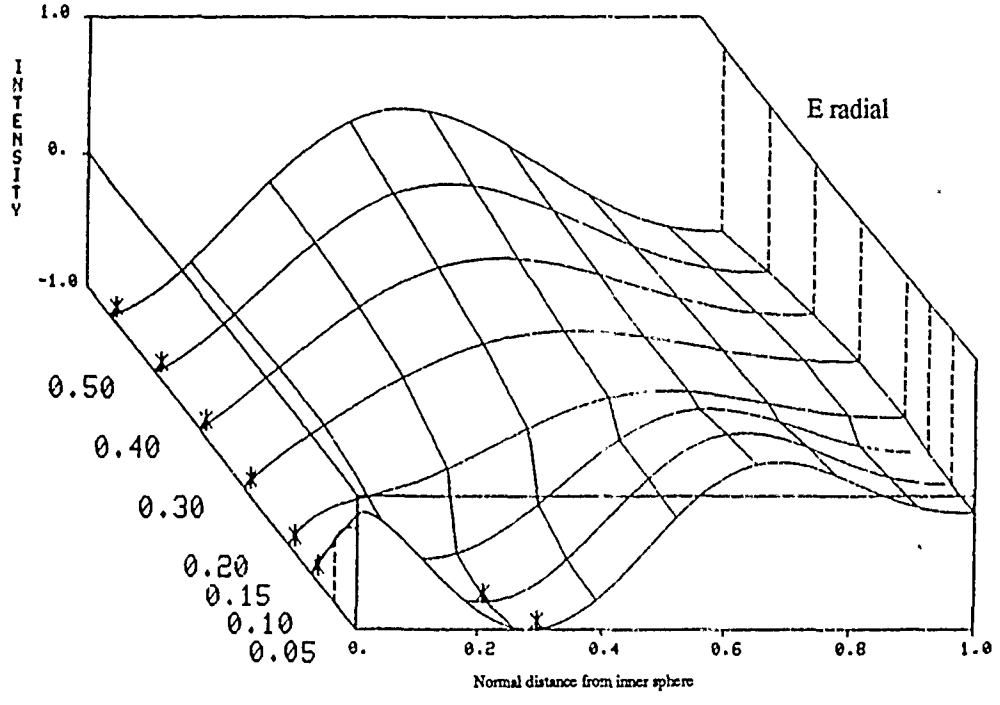

Figure 117. Distribution of the normalized radial electric field component in the concentric spherical cavity as a function of the inner to outer conductor radii, $R = b/a$, for the TM33 mode. Asterisk indicates peak value of field with d.

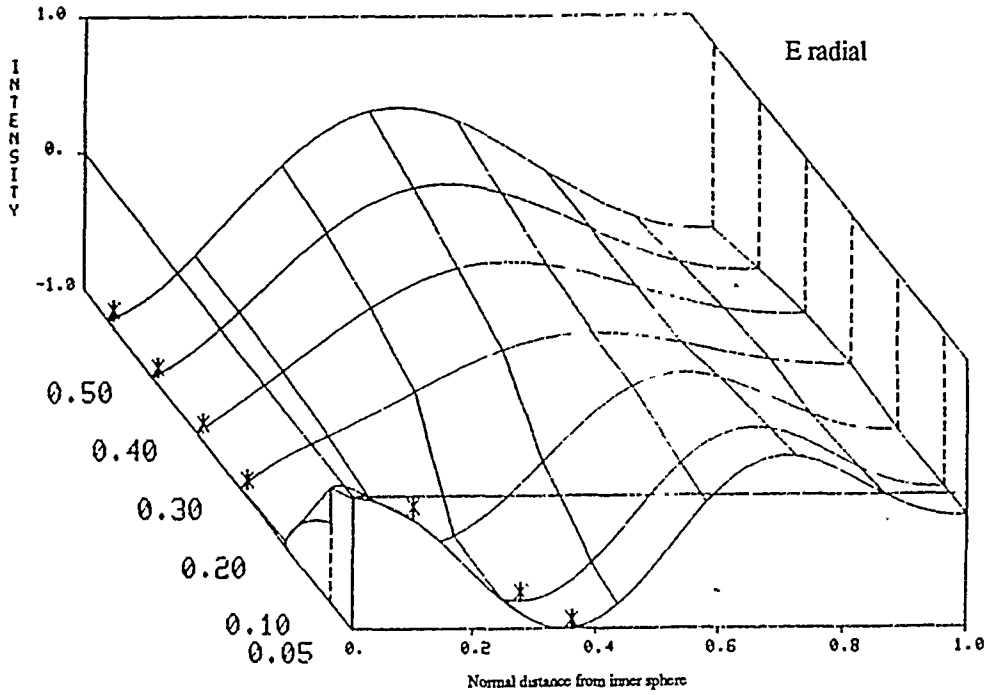

Figure 118. Distribution of the normalized radial electric field component in the concentric spherical cavity as a function of the inner to outer conductor radii, $R = b/a$, for the TM43 mode. Asterisk indicates peak value of field with d.

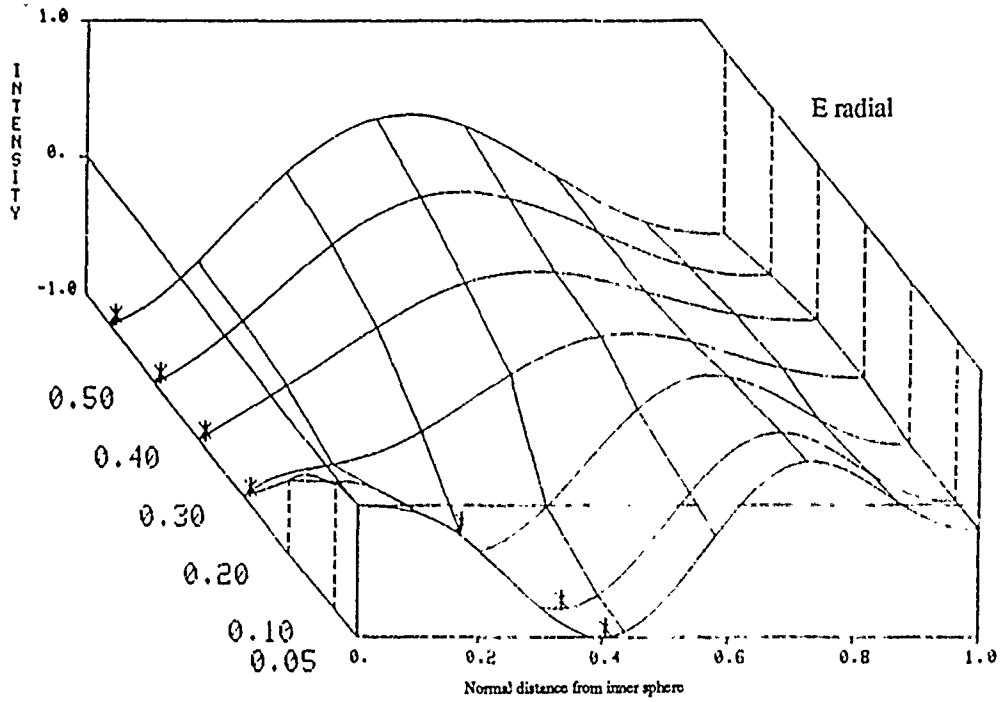

Figure 119. Distribution of the normalized radial electric field component in the concentric spherical cavity as a function of the inner to outer conductor radii, $R = b/a$, for the TM53 mode. Asterisk indicates peak value of field with d.

4.3.4 *The p = 4 E-Radial TMnp Eigenfields for n = 1 to 5*

As expected, increasing p once more to 4 adds still another very mild local peak quite close to the outer wall while moving the others closer to the inner wall. When $n = 1$, the local peak closest to the inner wall has become just an indent that exists only for 0.05, the smallest value of b/a calculated. While this local peak reappears for $n = 2$ and above, the range in b/a over which it exists, as well as the range over which the absolute maximum value of the field's magnitude resides, have both been reduced. In fact, the absolute maximum value resides totally on the inner conductor for all values of b/a calculated for both $n = 1$ and $n = 2$. Other behavioral patterns are by now predictable, and we may refer to figures 120 through 124 without further comment.

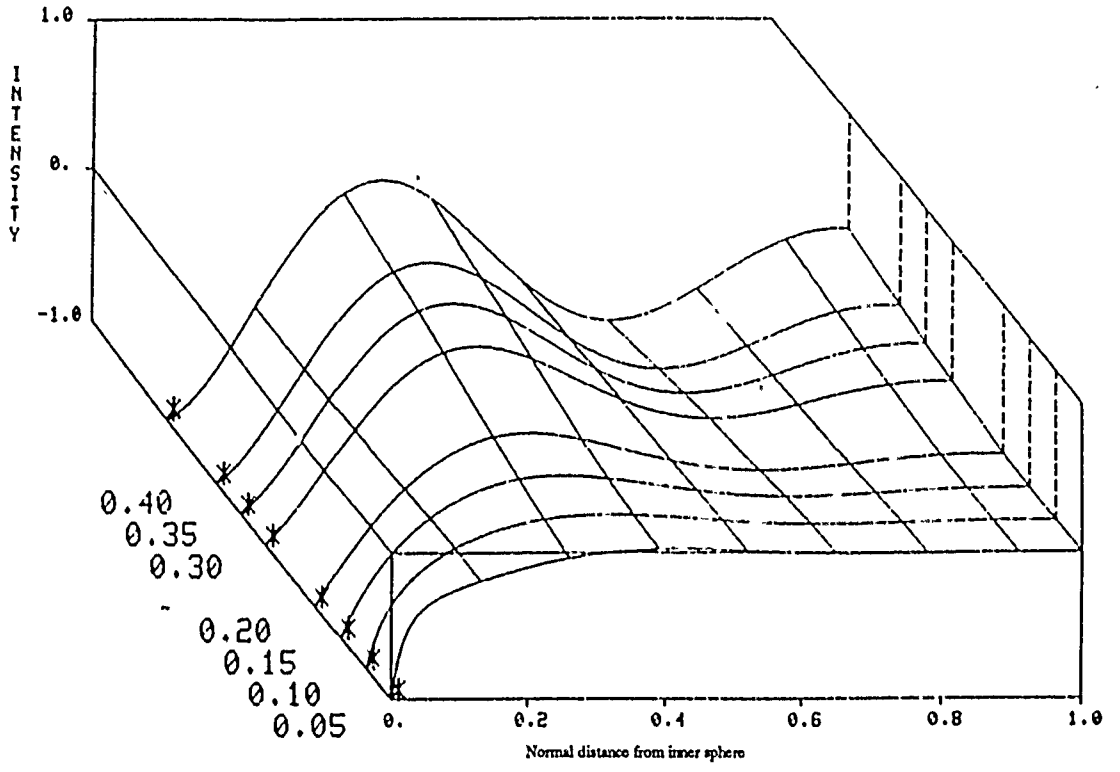

E radial

Figure 120. Distribution of the normalized radial electric field component in the concentric spherical cavity as a function of the inner to outer conductor radii, $R = b/a$, for the TM14 mode. Asterisk indicates peak value of field with d.

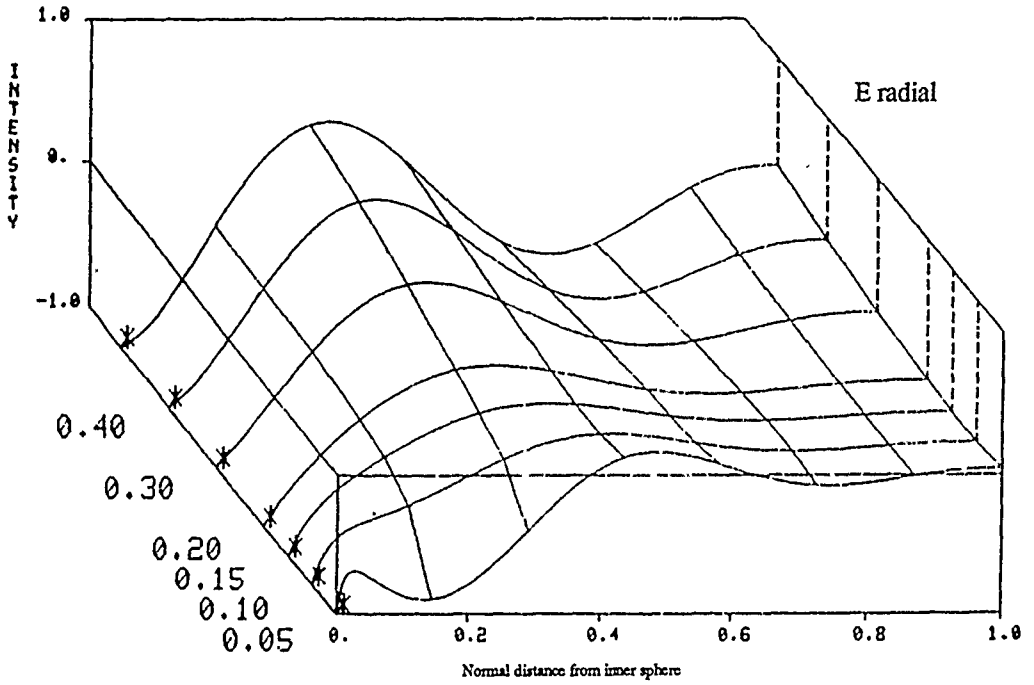

Figure 121. Distribution of the normalized radial electric field component in the concentric spherical cavity as a function of the inner to outer conductor radii, $R = b/a$, for the TM24 mode. Asterisk indicates peak value of field with d.

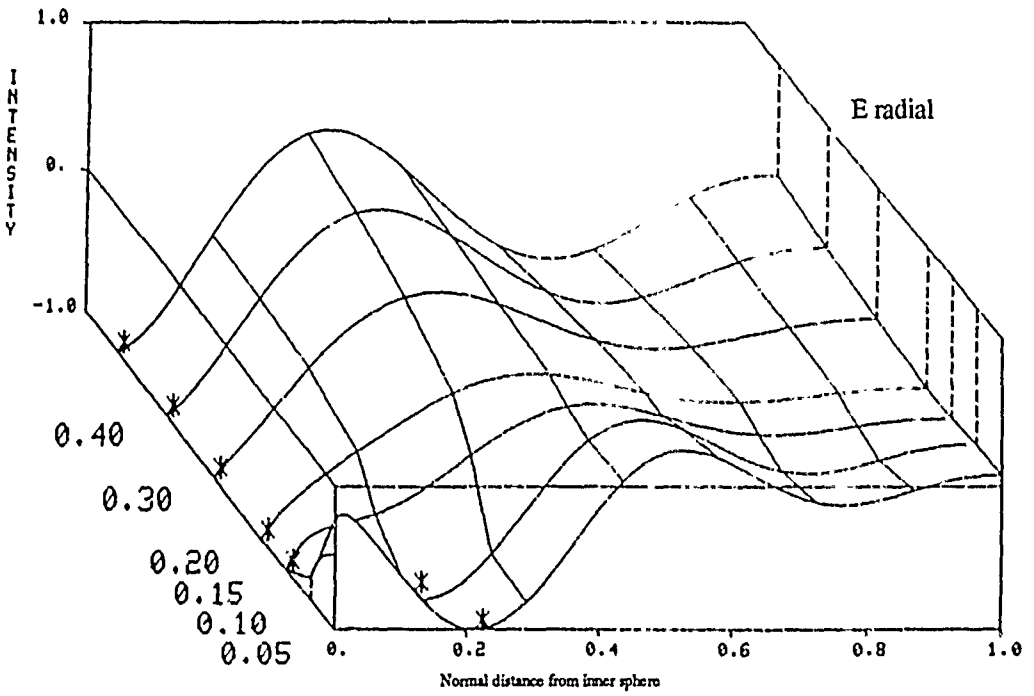

Figure 122. Distribution of the normalized radial electric field component in the concentric spherical cavity as a function of the inner to outer conductor radii, $R = b/a$, for the TM34 mode. Asterisk indicates peak value of field with d.

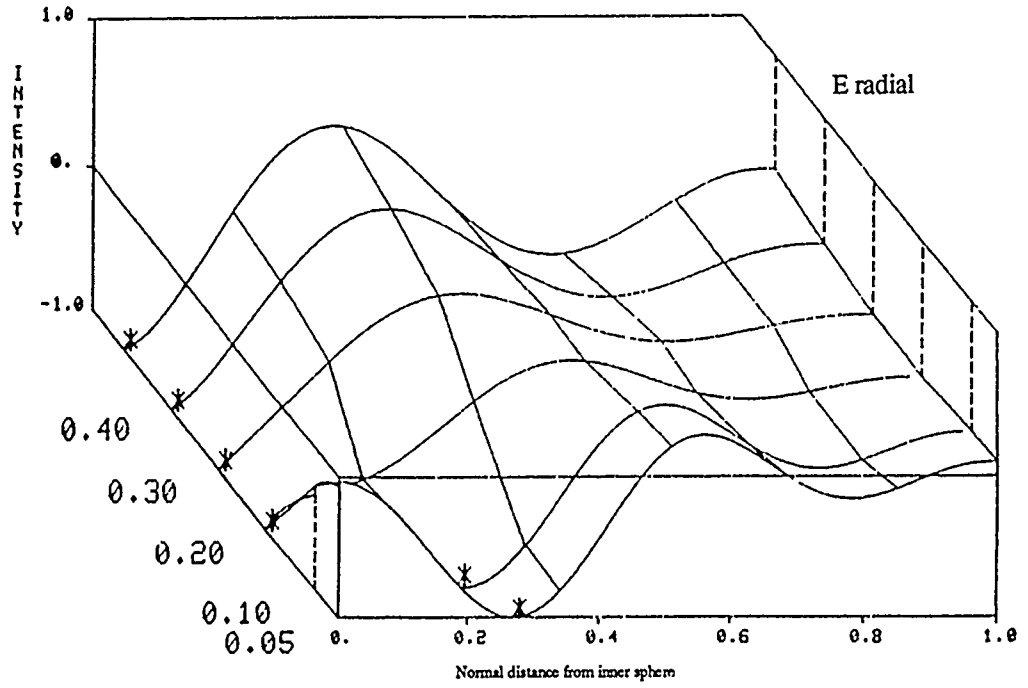

Figure 123. Distribution of the normalized radial electric field component in the concentric spherical cavity as a function of the inner to outer conductor radii, $R = b/a$, for the TM44 mode. Asterisk indicates peak value of field with d.

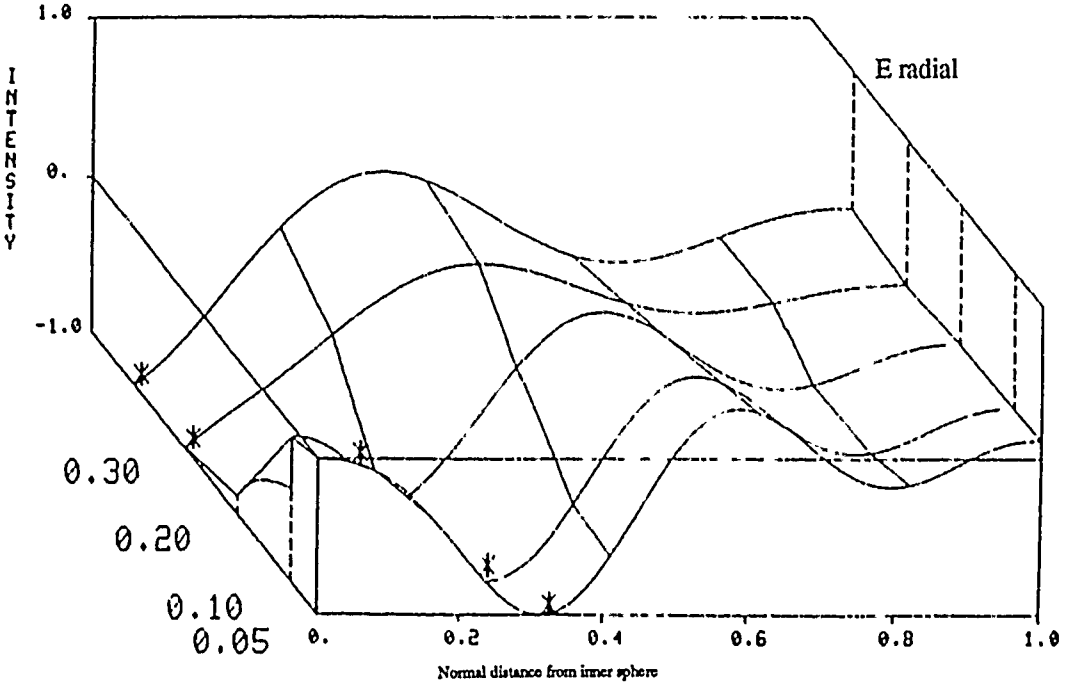

Figure 124. Distribution of the normalized radial electric field component in the concentric spherical cavity as a function of the inner to outer conductor radii, $R = b/a$, for the TM44 mode. Asterisk indicates peak value of field with d.

5. Discussion and Summary

A number of standard characteristics of electromagnetic fields are readily observed in the eigenfield components which were presented in this report. On the two conducting walls the transverse component of the electric field is always zero, whereas the normal (radial) electric field component on the walls is equal to the surface charge density. H-transverse on the walls is in general nonzero, and equal to the surface current density, whereas H-radial goes to zero on the conducting boundaries.

There are also some interesting features in these field components that are not universal to those of more generalized system geometries. Consider, for example, the higher families of modes, where there exist multiple local maxima/minima in the eigenfield distributions. These peaks vary in amplitude individually and in a continuous fashion with b/a. However, the location of the absolute maximum of the absolute value of the field variation with d is apt to change discontinuously with change in b/a. So we have observed, in sections 3 and 4, the existence of critical values in b/a at which this absolute maximum switches between the different local peaks.

The critical values may be computed, although it is sufficient to view them approximately for a good qualitative study. Figure 125 reproduces the TM mode plots for the concentric cavity that were developed in a prior report.[1] In this figure, the critical values of b/a have been marked on each trajectory for the p = 1, 2, and 3 families. The markings which belong to both a common component and family have been connected by a simple dotted line. Looking at the p = 1 family, the upper line connects the critical values in b/a for H-transverse, while the lower line connects those for E-radial. Moving to the next two higher families, the upper line connects the critical values for E-transverse, the middle line those for H-transverse, and the lower line those for the E-radial component.

[1] *L. Libelo and M. Campi, The Concentric Spherical Cavity TE and TM Eigenvalues, Harry Diamond Laboratories, HDL-TR-2034 (July 1984).*

To find some sort of a pattern in the locations of the critical values necessitates a small discussion concerning the behavior of the mode plots themselves. One observes from figure 125 that the individual trajectories begin, for small *b/a*, by exhibiting a nearly vertical form, i.e., negligible changes in the eigenvalue with *b/a*. Later, for larger *b/a*, the mode plots become markedly more curved. The $p = 1$ family for the TM modes is unique, in that the eigenvalues do not approach infinity as *b/a* approaches unity. But the trajectories do become wavy for larger *b/a*. For the higher families, the trajectories resemble sickles, with a curved drop to a minimum value, and then an increase in the eigenvalue as we increase *b/a*. It is noteworthy that the critical values occur at the part of the trajectory where its shape transitions from being near vertical to curved. One might even suggest that the change in the location in *d* of the absolute maximum of the amplitude of E-radial defines the beginning of a "transition region" of the trajectory as *b/a* is increased; and, further, that this transition between the near vertical and curved portions of the mode plot finishes at the critical value of E-transverse, where it exists, or, where it does not, at that of H-transverse. Of course, this behavioral pattern is heuristically determined, and has not been rigorously proven through mathematics for all modes. But it is worth considering seriously as a general rule because it holds true for all modes that were solved for.

It should be pointed out that for the TE modes, only one component (for all values of *b/a* we were concerned with) exhibited these critical values, namely H-transverse. Even so, this critical value seems to roughly divide the mode plots into two regions. That is, the trajectories are almost vertical for the values of *b/a* below it, and more curved for the higher values of *b/a*. See figure 126 for the lowest three families of TE modes.

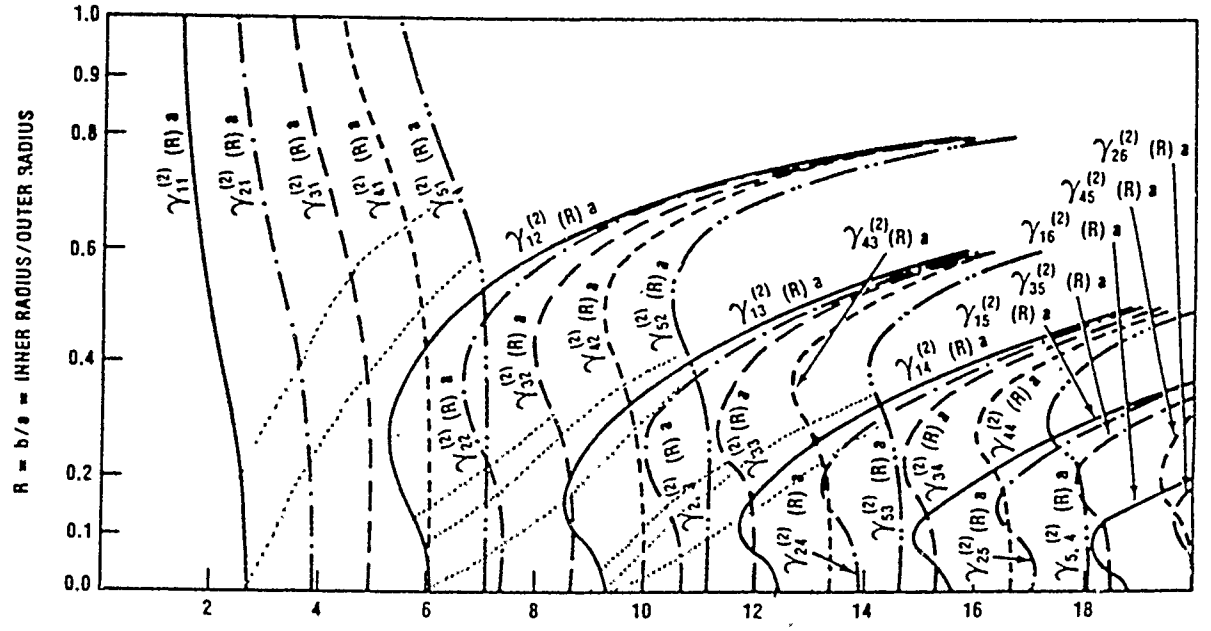

Figure 125. TM modes $\gamma_{np}^{(2)}(R)a$ for nonlossy concentric spherical cavity, with critical values of $R = b/a$ indicated for $p = 1, 2$, and 3.

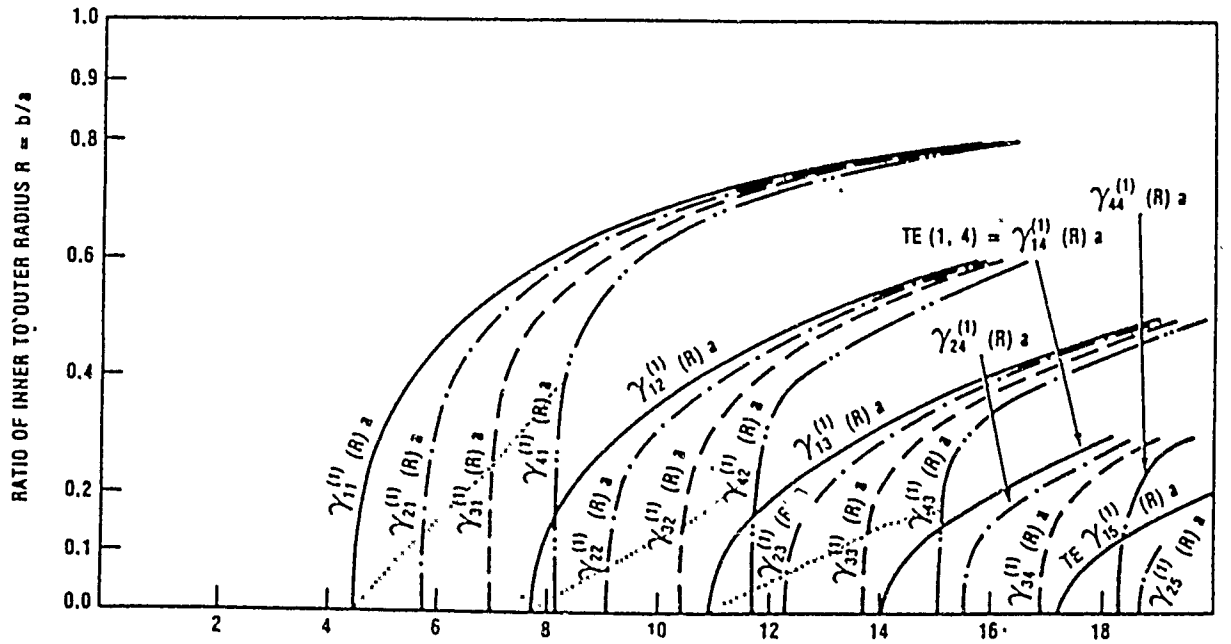

Figure 126. TM modes $\gamma_{np}^{(1)}(R)a$ for nonlossy concentric spherical cavity, with critical values of $R = b/a$ indicated for $p = 1, 2$, and 3.

We may now conclude by summarizing with certain rules of thumb. The eigenfields increase their oscillatory behavior with increased family index p. Their energy distribution is redistributed radially without substantial change in their oscillatory nature with increase in the order index n. When, as we vary b/a, the absolute maximum value of their amplitude switches (discontinuously) to another local peak, the critical value of b/a lies in a "transition" region of the eigenvalue curve, or mode plot. And, of course, E-transverse and H-radial go to zero on the conducting walls.

In future reports we will present the results of altering the interior load structure of the cavity in a number of ways, in order to see the effects of such changes on the field patterns. For example, the inner metallic sphere will be replaced by a dielectric one. Combinations of the two materials, such as a conducting inner sphere with dielectric layers, will be studied. The metal may then be made to conduct imperfectly, and the dielectric may be given loss. Thus it is hoped that the thorough exposition presented in this and the forthcoming reports of the eigenfield behavior of simply loaded spherical cavity systems may become a basis for understanding how electromagnetic energy distributes itself in more complicated cavities.

ACKNOWLEDGEMENT

The authors wish to gratefully acknowledge the contributions of Mark Thompson, a co-op student at Harry Diamond Laboratories, for plotting the eigenfields presented in this report.

DISTRIBUTION

ADMINISTRATOR
DEFENSE TECHNICAL INFORMATION CENTER
ATTN DTIC-DDA (2 COPIES)
CAMERON STATION
ALEXANDRIA, VA 22314

COMMANDER
US ARMY MATERIEL COMMAND
5001 EISENHOWER AVENUE
ALEXANDRIA, VA 22333-0001

DIRECTOR
US ARMY BALLISTIC RESEARCH LABORATORY
ATTN DRSAR-TSB-S (STINFO)
ABERDEEN PROVING GROUND, MD 21005

US ARMY ELECTRONICS TECHNOLOGY & DEVICES LABORATORY
ATTN DELET-DD
FT MONMOUTH, NJ 07703

MATERIALS TESTING DIRECTORATE
ARMY PULSE RADIATION DIV
ATTN CRAIG R. HEIMBACH
ABERDEEN PROVING GROUND, MD 21005

DIRECTOR
US ARMY MATERIEL SYSTEMS ANALYSIS ACTIVITY
ATTN DRXSY-MP
ABERDEEN PROVING GROUND, MD 21005

COMMANDER
US ARMY MISSILE & MUNITIONS CENTER & SCHOOL
ATTN ATSK-CTD-F
REDSTONE ARSENAL, AL 35809

US ARMY RESEARCH OFFICE
ATTN DR. JAMES MINK
PO BOX 12211
RESEARCH TRIANGLE, NC 27709

COMMANDER
US ARMY RSCH & STDY GP (EUR)
ATTN CHIEF, PHYSICS & MATH BRANCH
FPO, NY 09510

COMMANDER
U.S. ARMY WATERVLIET ARSENAL
AMCCOM
SOLID STATE RESEARCH LAB
ATTN MR. CLARK HOMAN
WATERVLIET, NY 12189

HQ, USAF
WASHINGTON, DC 20330

RADC/RBCT
ATTN DR. ROY F. STRATTON
GRIFFISS AFB, NY 13441

UNIVERSITY OF ARIZONA
ELECTRICAL ENGINEERING DEPT
ATTN PROF. DONALD DUDLEY
TUCSON, AZ 85721

CHAIRMAN ELECTRICAL ENGINEERING DEPT
PENN STATE UNIVERSITY
ATTN DR. KARL KUNZ
COLLEGE STATION, PA

ELECTRONICS RESEARCH LAB
COLLEGE OF ENGINEERING
UNIVERSITY OF CALIFORNIA
ATTN PROF. KEN MEI
BERKELEY, CA 94720

UNIV OF CALIFORNIA AT LOS ANGELES
ELECTRICAL ENGINEERING DEPT
ATTN PROF. CAVOUR YEH
LOS ANGELES, CA 90024

ENGINEERING SOCIETIES LIBRARY
ATTN ACQUISITIONS DEPT
345 EAST 47TH ST
NEW YORK, NY 10017

UNIVERSITY OF FLORIDA
PHYSICS DEPT
ATTN PROF. ALEX GREEN
GAINESVILLE, FL 32601

UNIV OF FLORIDA
SPACE ASTRONOMY LAB
ATTN RU T. WANG
GAINESVILLE, FL 32601

GENERAL RESEARCH CORP
ADVANCED TECHNOLOGIES DIVISION
ATTN DR. MICHAEL VON BLARICUM
5383 HOLLISTER AVENUE
SANTA BARBARA, CA 93111

CLEMSON UNIVERSITY
DEPT OF ELECTRICAL ENGINEERING
ATTN PROF. CHALMERS BUTLER
CLEMSON, SC need zip code

MASSACHUSETTS INSTITUTE OF TECHNOLOGY
DEPT OF ELECTRICAL ENGINEERING & COMPUTER SCIENCE
ATTN PROF. J. A. KONG
CAMBRIDGE, MA 02139

UNIVERSITY OF MASSACHUSETTS
DEPT OF ELECTRICAL & COMPUTER
ENGINEERING
ATTN PROF. DANIEL SCHAUBERT
AMHERST, MA 01003

UNIVERSITY OF MICHIGAN
DEPT OF ELECTRICAL & COMPUTER
ENGINEERING
ATTN PROF. VAL LIEPA
ANN ARBOR, MI 48109

McDONNELL DOUGLAS CORP
ATTN DR. W. PEARSON
ST LOUIS, MO 63166

PANAMETRICS INC
ATTN DR. NORMAN PEDERSEN
221 CRESCENT STREET
WALTHAM, MA 02254

SANDIA NATIONAL LABORATORIES
ATTN DR. MARVIN E. MORRIS
PO BOX 5800
ALBUQUERQUE, NM 87185

SYRACUSE UNIVERSITY
ELECTRICAL ENGINEERING DEPT
ATTN PROF. ROGER HARRINGTON
SYRACUSE, NY 13210

LAWRENCE LIVERMORE LABORATORY
ATTN RICHARD ZIOLKOWSKI, L-156
PO BOX 808
LIVERMORE, CA 94550

US ARMY LABORATORY COMMAND
ATTN TECHNICAL DIRECTOR,
AMSLC-CT

INSTALLATION SUPPORT ACTIVITY
ATTN LEGAL OFFICE, SLCIS-CC

USAISC
ATTN RECORD COPY, ASNC-LAB-TS
ATTN TECHNICAL REPORTS BRANCH,
ASNC-LAB-TR (3 COPIES)

HARRY DIAMOND LABORATORIES
ATTN D/DIVISION DIRECTORS
ATTN LIBRARY, SLCHD-TL (3 COPIES)
ATTN LIBRARY, SLCHD-TL (WOODBRIDGE)
ATTN CHIEF, SLCHD-NW-CS
ATTN CHIEF, SLCHD-NW-E
ATTN CHIEF, SLCHD-NW-EH
ATTN CHIEF, SLCHD-NW-EP
ATTN CHIEF, SLCHD-NW-ES
ATTN CHIEF, SLCHD-NW-R
ATTN CHIEF, SLCHD-NW-RP
ATTN CHIEF, SLCHD-NW-RS
ATTN CHIEF, SLCHD-NW-TN
ATTN CHIEF, SLCHD-NW-TS
ATTN VAULT, W. SLCHD-NW
ATTN CHASE, R. J., SLCHD-NW-E
ATTN INGRAM, SLCHD-NW-E
ATTN LUU, BRIAN, SLCHD-NW-EP
ATTN JOHNSON, T., SLCHD-ST
ATTN WALKER, P., SLCHD-ST
ATTN PISANE, G., SLCHD-ST-AB (20 COPIES)
ATTN RUTH, B., SLCHD-NW-RI
ATTN LIBELO, L., SLCHD-NW-RI (30 COPIES)